TECHNISCHE
UNIVERSITÄT
WIEN
Vienna University of Technology

DISSERTATION

A framework for the representation of the urban environment and the assessment of its microclimatic variation

ausgeführt zum Zwecke der Erlangung des akademischen Grades eines Doktors der technischen Wissenschaften

unter der Leitung von

Univ. Prof. Dipl.-Ing. Dr. techn. A. Mahdavi

E 259-3 Abteilung für Bauphysik und Bauökologie

Institut für Architekturwissenschaften

eingereicht an der

Technischen Universität Wien

Fakultät für Architektur und Raumplanung

von

DI Milena Vuckovic

Matrikelnr. 1126153

Diehlgasse 49/8, 1050 Wien

Wien, März 2015

Zusammenfassung

Im Moment steht die Forschung im Bereich der urbanen Hitzeinsel-Effekt (UHI-Phänomen) vor einer ganzen Reihe von Herausforderungen. So sind beispielsweise vertiefende Messreihen des Mikroklimas zum besseren Verständnis der beeinflussenden Faktoren erforderlich. In der bestehenden Forschung wird weitgehend konsensual davon ausgegangen, dass Veränderungen des urbanen Mikroklimas weitreichende Auswirkungen auf den thermischen Komfort der Stadtbewohner, die lokale Luftqualität, den Energiebedarf der Gebäude und sogar auf die Mortalitätsrate in Städten haben können. Das UHI-Phänomen wird als zu einem Teil anthropogen verschuldet betrachtet, vor allem durch die Veränderungen in der Nutzung von Flächen (Städtische Dichte, Versiegelung, Verringerung des Anteils and Grünflächen und freien Wasseroberflächen) und durch Emissionen (in Folge von Raumheizung, Verkehr, etc.). Problematisch ist, dass es kaum valide Daten und Studien über den Zusammenhang dieser beeinflussenden Faktoren und den Auswirkungen in Form von urbanen Hitzeinseln gibt.

In diesem Kontext befasst sich die vorliegende Arbeit mit dem Ausmaß und den Implikationen des UHI-Phänomens in der österreichischen Bundeshauptstadt Wien. Es werden die Ergebnisse von mehrjährigen Bemühungen zur Fassung und Ursachenforschung des Phänomens präsentiert. Für 5 unterschiedliche Messbereiche in Wien (vorstädtische und dicht-verbaute innerstädtische Bereiche) wurden hochauflösende Daten erhoben, strukturiert und analysiert. Aus der Datenbasis wurden methodisch Parameter identifiziert, die einen potentiellen Einfluss auf das UHI-Phänomen haben könnten. Dabei handelt es sich sowohl um geometrische (morphologische) wie auch semantische (material-bedingt) Faktoren der urbanen Umgebung. Nach der Identifikation der Parameter wurden diese auf Korrelation mit dem Auftreten von UHI-Effekten untersucht. Die Ergebnisse dieser Arbeit können für die Entwicklung von generellen Einfluss- und Vorhersagemodellen für den urbanen Hitze-Insel-Effekt verwendet werden.

Diese dieser Dissertation zugrunde liegenden Ergebnisse wurden im Rahmen eines – kürzlich abgeschlossenen – EU-Projektes (Central Europe Program, No 3CE292P3) ermittelt. Die methodische Identifikation potentieller Einflussfaktoren aud das UHI-Phänomen kann als Resultat der in dem Forschungskonsortium durchgeführten internationalen und im Team durchgeführten Bemühungen betrachtet werden.

Summary

A number of recent challenges in the realm of microclimatic studies are set on a better understanding of the Urban Heat Island (UHI) phenomenon. Particularly, UHI is believed to be a characteristic consequence of urban microclimate evolution. Changes in urban microclimate, and corresponding higher air temperatures within urban domains, are believed to have cardinal consequences on the issues such as the thermal comfort of the city dwellers, mortality rate, local air quality, and energy demand of buildings. Generally speaking, the undesired thermal circumstances in the urban environment are caused in part by human-induced changes introduced in land use and land cover (building agglomeration density, presence and extent of green areas and bodies of water), and corresponding environmental emissions (anthropogenic heat production). Currently, there is a lack of practical assessment approaches focusing on the formation of UHI while considering a relatively comprehensive range of factors of the built environment.

In this context, the present contribution summarizes the results of a multi-year effort concerned with the extent and implications of the UHI phenomena in the city of Vienna, Austria. For this purpose, high-resolution data streams across five key locations are obtained, structured, and analyzed. This allowed for an objective assessment of the location-dependent manifestations of microclimatic circumstances across distinct low-density suburban and high-density urban typologies in Vienna. Subsequently, a systematic framework is developed to identify essential properties of the urban environment that are hypothesized to influence UHI and the urban microclimate variation. These properties pertain to both geometric (morphological) and semantic (material-related) urban features. Once these features are derived, the existence and extent of the correlations between urban microclimate variation and the urban features are explored. These statistically significant correlations further provided a useful basis toward developing empirically-based predictive models. These models are expected to support the understanding and prediction of local differences in the urban climate.

The contribution presented in this dissertation was developed within the framework of a – recently completed – European project (Central Europe Program, No 3CE292P3). The framework was developed in part through extensive collaboration among the project team members and represents a valuable resource of scientific information on the links between the urban microclimate variation and essential driving factors to this variation.

Acknowledgments

Contents

List of Acronyms and Abbreviations

General

CSC	Continuous Shadow Casting
DEM	Digital Elevation Model
DN	Digital Numbers
GIS	Geographical Information System
GSR	Global solar radiation
MA22	Municipal Department of Environmental Protection in Vienna
QGIS	Quantum Geographical Information System
RH	Relative humidity
RMSE	Root Mean Square Error
SSR	Sum of squares of the regression
SST	Total sum of squares
SVF	Sky View Factor
UBL	Urban Boundary Layer
UCL	Urban Canopy Layer
UHI	Urban Heat Island
VOC	Volatile Organic Compounds
WMO	World Meteorological Organization
ZAMG	Zentralanstalt für Meteorologie und Geodynamik

Project Related

BAF	Built Area Fraction
BSF	Built Surface Fraction
CTI	Cumulative Temperature Increase
DF	Donaufeld
GD	Gaudenzdorf
HW	Hohe Warte
H/W	Aspect Ratio
IS	Innere Stadt
ISF	Impervious Surface Fraction
PSF	Pervious Surface Fraction
R	Seibersdorf
U2O	Urban Unit of Observation
UAF	Unbuilt Area Fraction

List of Symbol and Units

Theoretical Background

Symbol	Description	Units
$\Delta T_{u\text{-}r}$ or $\Delta\theta$	Urban heat island intensity	K
T_{urban}	Urban air temperature	°C
T_{rural}	Rural air temperature	°C
S_{12}	Urban canyon width	m
H_1, H_2	Building heights	m
$\overline{Z_H}$	Average building height	m
$\overline{W}$	Average distance between buildings	m
H/W	Aspect Ratio	-
SVF or ψ_{sky}	Sky View Factor	-
ΔA	Surface element at the ground level (in model for radiation exchange between the sky and surface element)	m²
R	Nominal radius of the sky hemisphere (in model for radiation exchange between the sky and surface element)	m
ΔS, dS	Surface element on the hemisphere seen from the canyon floor (in model for radiation exchange between the sky and surface element)	m²
φ	Angle between the canyon floor and the sky vault hemisphere (in model for radiation exchange between the sky and surface element)	°
Sv	Sky vault seen from the canyon floor	-
Q*	Net all-wave radiation	W·m⁻²
Q_F	Anthropogenic heat	W·m⁻²
Q_H	Turbulent flux of sensible heat	W·m⁻²
Q_E	Turbulent flux of latent heat	W·m⁻²

Symbol	Description	Units
ΔQ_S	Storage heat flux	$W \cdot m^{-2}$
ΔQ_A	Advective heat flux	$W \cdot m^{-2}$
Q_V	Heat produced by combustion of vehicle fuels	$W \cdot m^{-2}$
Q_H	Heat released from stationary sources	$W \cdot m^{-2}$
Q_M	Heat released by human activity	$W \cdot m^{-2}$

Methodology

Symbol	Description	Units
T_a	Air temperature	°C
υ	Wind speed at H = 1.1m (in model for wind profile - Hellman's exponential law)	$m \cdot s^{-1}$
υ_n	Wind speed at height Hn (in model for wind profile - Hellman's exponential law)	$m \cdot s^{-1}$
H_n	Height of the wind sensor (in model for wind profile - Hellman's exponential law)	m
H	Reference height of 1.1m (in model for wind profile - Hellman's exponential law)	m
α	Friction coefficient (Hellman exponent)	-
E	Saturation vapour pressure	Pa
e	Vapour pressure	Pa
φ	Relative humidity	%
AH	Absolute humidity	$g \cdot m^{-3}$
R	Individual gas constant of water (R = 461.52 Jkg-1K-1)	$J \cdot kg^{-1} \cdot K^{-1}$
A_b	Building plan area at ground level (building footprint) of an U2O	m^2

A_{tot}	Total ground area of an U2O	m^2
A_u	Unbuilt surface area of an U2O	m^2
$A_{u,i}$	Unbuilt impervious surface area of an U2O	m^2
$A_{u,p}$	Unbuilt pervious surface area of an U2O	m^2
A_e	Bare soil surface area of an U2O	m^2
A_g	Green surface area of an U2O	m^2
A_{H2O}	Water body surface area of an U2O	m^2
h_e	Equivalent building height	m
V_b	Building volume of an U2O	m^3
A_s	Total built surface area (walls and roofs) of an U2O	m^2
A_W	Total wall area above terrain (only the walls exposed to the outdoor environment)	m^2
A_R	Total roof area of an U2O	m^2
$A_{R,i}$	Total impervious roof area of an U2O	m^2
$A_{R,p}$	Total impervious roof area of an U2O	m^2
l_c	Effective mean compactness	m
h_{sl}	Mean sea level	m
α_{sw}	Albedo (shortwave)	-
ε_{lw}	Emissivity (longwave)	-
λ	Thermal conductivity	$W \cdot m^{-1} \cdot K^{-1}$
λ_i	Thermal conductivity, impervious surfaces	$W \cdot m^{-1} \cdot K^{-1}$
λ_p	Thermal conductivity, pervious surfaces	$W \cdot m^{-1} K^{-1}$
c	Specific heat capacity	$J \cdot kg^{-1} \cdot K^{-1}$

c_i	Specific heat capacity, impervious surfaces	$J \cdot kg^{-1} \cdot K^{-1}$
c_p	Specific heat capacity, pervious surfaces	$J \cdot kg^{-1} \cdot K^{-1}$
ρ	Density	$kg \cdot m^{-3}$
ρ_i	Density, impervious surfaces	$kg \cdot m^{-3}$
ρ_p	Density, pervious surfaces	$kg \cdot m^{-3}$
b	Thermal admittance	$J \cdot m^{-2} \cdot s^{1/2} \cdot K^{-1}$
Q_F	Anthropogenic heat output	$kW \cdot h \cdot m^{-2} \cdot a^{-1}$
Q_V	Heat produced by combustion of vehicle fuels	$kW \cdot h \cdot m^{-2} \cdot a^{-1}$
Q_H	Heat released from buildings	$kW \cdot h \cdot m^{-2} \cdot a^{-1}$
Q_M	Heat released by human activity	$kW \cdot h \cdot m^{-2} \cdot a^{-1}$
NHE_v	Net heat emission from one vehicle	$W \cdot m^{-2}$
n_v	Number of vehicles	-
E_{tot}	Annual energy consumption of a building	$kWh \cdot m^{-2} \cdot a^{-1}$
n_f	Number of floors	-
n	Population number	-
M	Average metabolic rate	$W \cdot m^{-2}$
ΔRH	Hourly deviation of relative humidity	%
CTI	Cumulative temperature increase	Kh
$\theta_{U,i}$	Urban air temperature at specific hour	°C·h
$\theta_{R,i}$	Rural air temperature at specific hour	°C·h
$\beta_0 - \beta_8$	Regression coefficients	-
Q	The sum of squared deviations	-
$f_i(x)$	Function of form $y_i = f_i(x)$	-
R^2	R-square / Coefficient of determination	-

y_i	Dependent variable (observed) in the least square regression model (in this case the CTI)	Kh
$\bar{y}_i$	Mean value of the observed dependent variable in the least square regression model	Kh
$\hat{y}_i$	Dependent variable (predicted) in the least square regression model (in this case the CTI')	Kh
n	Sample size in the least square regression model	-

1. Introduction

1.1. Objective

In recent years the general issues concerning the urban microclimate, its sources, its implications, and its variation, have raised great awareness on a global scale. One characteristic consequence of microclimatic development is the Urban Heat Island phenomenon (UHI) (Gartland 2008). Currently, UHI occupies a unique position in the realm of microclimatic studies due to its impact on the issues such as thermal comfort (heat stress), mortality, energy consumption, urban planning, etc. For these reasons, the study of UHI phenomenon is one of the prime concerns worldwide.

Thereby, this dissertation aims to develop a systematic framework for capturing street-scale climate variation while addressing a multitude of driving factors to this variation. Hence, the primary objective of this dissertation is to derive statistically meaningful relationships between morphological and physical parameters of the built environment, on one hand, and the UHI effect, on the other. The following contribution is expected to provide a better understanding of the very specifics behind the UHI phenomena and to further support the efforts towards the prediction of local differences in the urban climate.

The present contribution was conducted within the framework of the EU supported project ("Development and application of mitigation and adaptation strategies and measures for counteracting the global Urban Heat Island Phenomenon" - Central Europe Program, No 3CE292P3).

1.2. Motivation

Metropolitan areas are subjected to very diverse microclimatic circumstances influenced by different morphologies, structures, and materials of the built environment (Grimmond et al. 1991; Piringer et al. 2002; Gaffin et al. 2008; Kleerekoper et al. 2012). These factors are hypothesized to contribute to the evolution of the phenomenon called the Urban Heat Island (see, for example, Oke 1981; Voogt 2002; Arnfield 2003). Urban Heat Island (UHI) has drawn a great attention all over the world due to its implications on the issues such as thermal comfort (heat stress),

mortality, energy consumption, urban planning, etc. (Akbari 2005; Alexandri 2007; Harlan et al. 2011).

At the same time, constant urban development is bringing a radical change in land cover. As cities expand, the surrounding natural surfaces become replaced by artificial materials that might further increase the magnitude of UHI. The microclimatic implications of these changes can be subtle, but in majority of metropolitan areas the implications are found to be immense and with long-term adverse effects (Unger et al. 2000; Jenerette et al. 2007). As urbanization will continue, the undesired thermal circumstances in the urban environment can be expected to be even greater in the future.

Furthermore, the complex urban surface morphology modifies the total energy balance of the city resulting in higher heat storage in urban areas (Grimmond et al. 1991; Akbari 2005; Harlan et al. 2011). This may worsen the current situation of heat waves that are expected to be even more pronounced in the future. Heat waves have significant influence on the quality of life in metropolitan areas, increasing the mortality levels worldwide (Milojevic et al. 2010; Rosenthal 2010). The heat waves of 2003 and 2006 were exceptional in terms of duration, intensity and health impact, with a substantial loss of human life across Europe (WHO 2007). In 2007, another severe heat wave occurred in Southern Europe, stressing that even more extreme weather events might come in the future. Therefore, reducing the frequency of heat waves and people's exposure to extreme heat in urban areas should be considered as a significant health and environmental issue.

By emphasizing the far-reaching negative effects that excessive urban heat has on human health, it becomes apparent that comprehensive research efforts are needed to understand the broad impact of the UHI phenomenon. Furthermore, the potential far-reaching benefits of UHI reduction strategies must be understood and adopted to maximize their effectiveness and ensure a better quality of life for future generations.

Currently, there is a lack of practical assessment approaches available for planners, designers and developers that can analyse and evaluate the impacts of urban settlements on both the urban microclimate and the UHI. Furthermore, not many studies focused on addressing the formation of UHIs while considering a relatively comprehensive range of factors of the built environment, and their effect on the respective temporal and spatial development of urban microclimate.

In this context, this contribution introduces a novel systematic framework for a comprehensive UHI assessment that is expected to support decision-making process towards more sustainable urban design and maintenance practices.

1.3. Case study

The city of Vienna, Austria, was used as a case study to illustrate the essential aspects mentioned above. The city of Vienna experienced a vital and dynamic development of various urbanization features that are believed to influence urban climate.

Figure 1 illustrates the long-term urban development trend of the city of Vienna (Böhm 1998). The features presented within portray the course and rate of development of total urban energy consumption, woodland area, green land area (meadows, agricultural area, parks), traffic area (streets, pavements, parking lots), number of buildings, total living floor space and the number of cars, in a time range from year 1951 until year 2000.
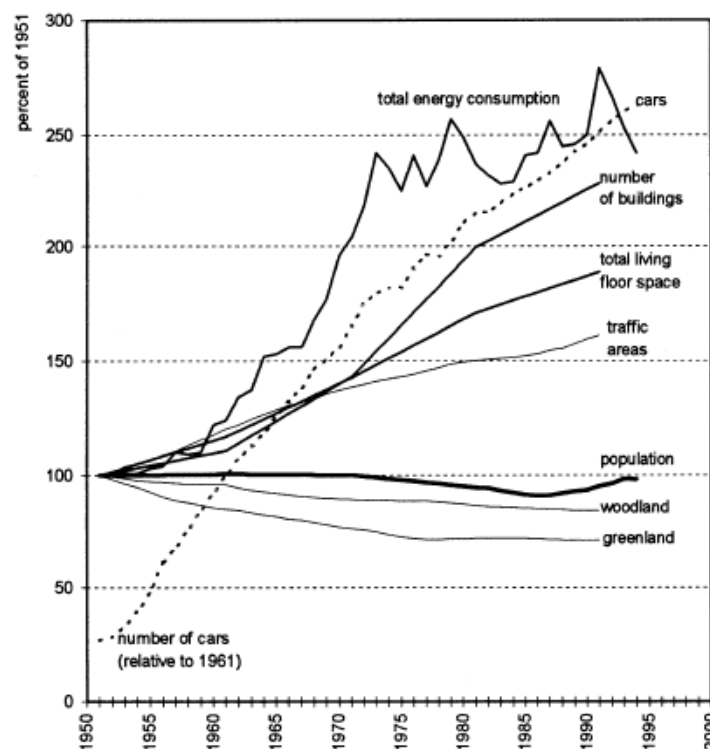
Figure 1. The urban development of Vienna since 1951 (source: Böhm 1998).

Figure 1 shows that Vienna experienced an active expansion of numerous components that may in turn influence the urban microclimate. For example, the curve representing the overall change of land use, as well as direct energy consumption, implies the higher magnitude of the UHI caused by alterations of surface energy balance, increased heat storage capacity of the ground, and direct heat input to the urban atmosphere. It can be noted that even though the number of inhabitants has not changed much over the observed period, the number of buildings in the city almost doubled. Furthermore, it can be observed that the strongest increase of all parameters is visible in the total number of cars in the city. Although Figure

1 portrays the period up to the year of 2000, the course of overall growth and amount of changes introduced into the urban environment over the years are clearly visible. The observed upward trend of nearly all of the presented features suggests a significant impact to the local microclimate. However, as the current development course might not be so intensive, it can be assumed that - based on these past trends - the slight upward trend remained, thus continuously affecting the local climate.

This can be further supported by outlining the historical temperature records of several weather stations across the city of Vienna. Figure 2 and Figure 3 provide an overview of the long-term (from 1990 to 2012) development of the (mean annual) measured air temperatures across three distinct low-density suburban and high-density urban typologies in Vienna, and a reference rural station Seibersdorf (located outside the metropolitan area). Results indicate a significant temperature deviation between the observed areas, but also an upward trend concerning both urban and rural temperatures, further stressing a plausible connection between urbanization-related thermal excess and elevated urban temperatures (Vuckovic et al. 2014).

Figure 2. Development of (mean annual) air temperatures over a period of 22 years (source: Vuckovic et al. 2014)
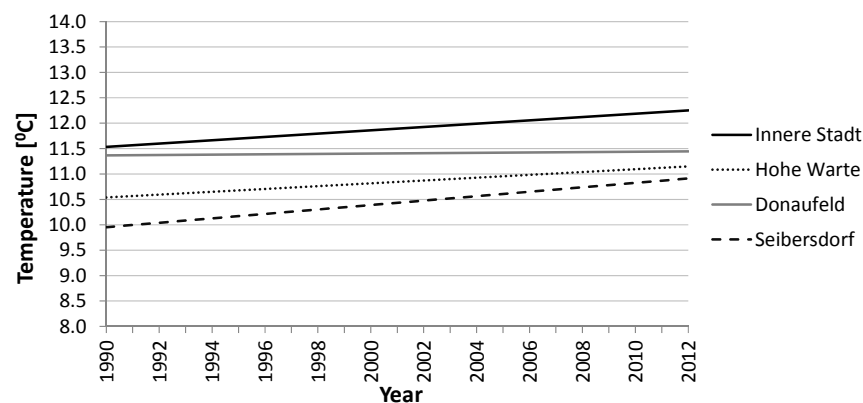
Figure 3. Trend lines for the long-term development of (mean annual) air temperatures across the four locations (source: Vuckovic et al. 2014)

1.4. **Structure**

This present contribution describes the framework for the representation of the urban environment and the assessment of its microclimatic variation. The aims of this study are many-fold:

- To quantify, evaluate and describe the street-scale microclimate variability and related UHI phenomena.

- To outline the essential driving factors to microclimatic variation - in terms of a structured set of essential geometric and physical features of the built environment.

- To demonstrate the potential of automated calculation of the urban attributes at a large (urban) scale.

- To investigate and evaluate a plausible correlation between these urban attributes and the altered thermal circumstances within the urban environment.

- To support the formulation of empirically-based predictive models for prediction of local differences in the urban climate.

To address these aims, this research is structured into five parts:

- Chapter 1 underlines the general introduction to the topic and further outlines the general objectives of the following contribution.

- Chapter 2 summarizes the definition, quantification, spatial and temporal variation, and essential influencing factors contributing to the UHI effect, by reviewing the current efforts and achievements in the field of urban climate studies.

- Chapter 3 outlines the theoretical framework and methodology underlying the dissertation, thus further explaining the process of data collection and data analysis, introducing the structured set of essential geometric and physical urban features, and presenting an operational solution for comprehensive urban form analysis.

- Chapter 4 summarizes the main results of the methodology and provides a thorough discussion of the acquired results.

- Chapter 5 summarizes the key findings and further elaborates on future research prospects.

2. Theoretical Background

2.1. Defining the Urban Heat Island

The Urban Heat Island (UHI) effect is referred to as the characteristic atmospheric warmth of the urban areas when compared to surrounding rural areas (Oke 1969; Taha 1997; Voogt 2002). The circumstance of higher temperatures is documented in all cities, large or small, in warm or cold climates (Blazejczyk et al. 2006; Alcoforado and Matzarakis 2010).

The UHI phenomenon was first addressed by Luke Howard (1833) and was defined as *'an artificial excess of heat within an urbanized area when compared with its rural area'*. Empirical observations suggest that the magnitude of the UHI effect generally falls in the range of 1 - 3.5 K. This is expected to increase by approximately 1 K per decade (Voogt 2002).

Figure 4 shows a typical profile of an UHI that illustrates distinct increase in temperature within the boundaries of the city (US EPA 2010). It is also possible to identify significant variation in temperature related to morphology, proximity to water bodies, the density of built environment, and the amount of vegetated cover.
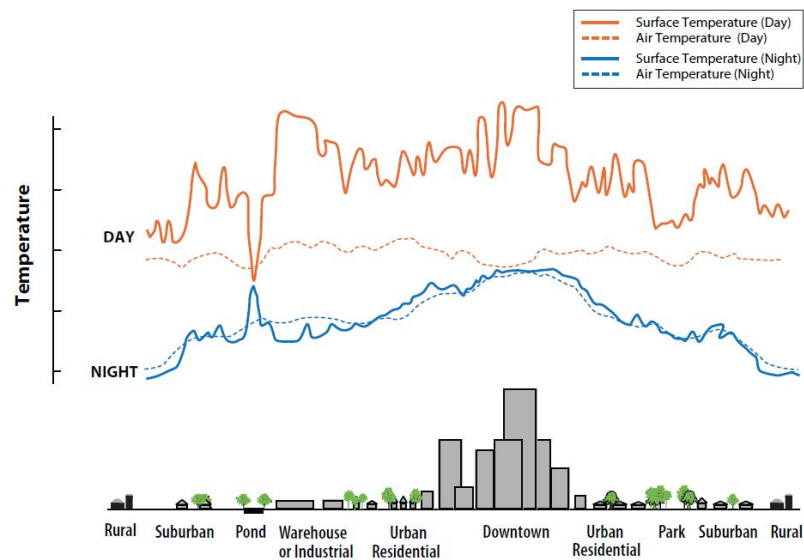

Figure 4. Sketch of a UHI profile (source: US EPA 2010)

The study of UHI phenomena embodies two essential environmental issues being reflected throughout the twentieth century – urbanization and climate change (Oke 1973; Wilby 2008).

Urbanization has an overall negative effect on the environment generally by changes introduced in land cover, the compact spatial structure of the metropolitan areas, the modification of the atmosphere, increased air pollution, etc. (Voogt 2002; Kusaka and Kimura 2004; Kleerekoper et al. 2012). The UHI effect is considered to be a cumulative effect of all the factors mentioned above. Furthermore, the UHI effect is thought as being directly related to the climate change (Corburn 2009). As discussed by Kalkstein and Green (1997), the global climate change may intensify UHIs with implications for local air quality, heat stress, mortality and energy demand.

2.2. Growth and change of Urban Heat Islands

Metropolitan areas have distinct urban morphology that implies extensive alteration of the natural landscape and atmospheric composition. These alterations are believed to lead to the formation of urban microclimates (Mills 2011). Empirical observations suggest that the microclimate can vary significantly across an area consisting of even a few streets (Kleerekoper et al. 2012). Consequently, the intensity of UHI can vary across different areas within the city (Hart and Sailor 2007). This intra-urban variation is related to a distinct thermal balance of different urban areas due to unique spatial and physical structure (Oke 1982). Additionally, observations have shown that the UHI phenomenon shows different characteristics during different seasons (Gaffin et al. 2008), and that is displayed differently during the night and day (Oke 1981).

2.2.1. Temporal development

As mentioned above, the UHI phenomena show distinct diurnal variation that arises as a result of different cooling rates between urban and rural areas (Lee 1979; Chow and Svoma 2011). Generally, UHIs are observed as nocturnal features (Voogt 2002; Wilby et al. 2011). Nocturnal heat island effect arises due to the differences in net long-wave radiation of an urban environment when compared to the rural environment (Oke 1981; Giridharan et al. 2005).

Numerous scientists have discussed the very dynamics of the UHIs (see, for example, Oke and Maxwell 1975; Lee 1979; Yow and Carbone 2006). These studies outlined that the cooling rates of simultaneously observed urban and rural areas deviate from one another several hours before sunset, emphasizing that rural areas cool more rapidly when compared to the

urban areas that have a potential to retain heat better. They further noted that the UHI effect was steadily rising to reach its maximum around midnight or 3 to 5 hours after sunset. Later on, the cooling rates of the urban and rural areas became similar and remained almost constant until sunrise. Although the UHI intensity generally increases with time from sunset, the dynamics of peak values may vary depending on weather conditions and season (Gaffin et al. 2008).

Figure 5 shows typical temporal variation of urban and rural air temperatures, cooling/warming rates and heat island magnitude under clear and calm conditions (Oke 1987).
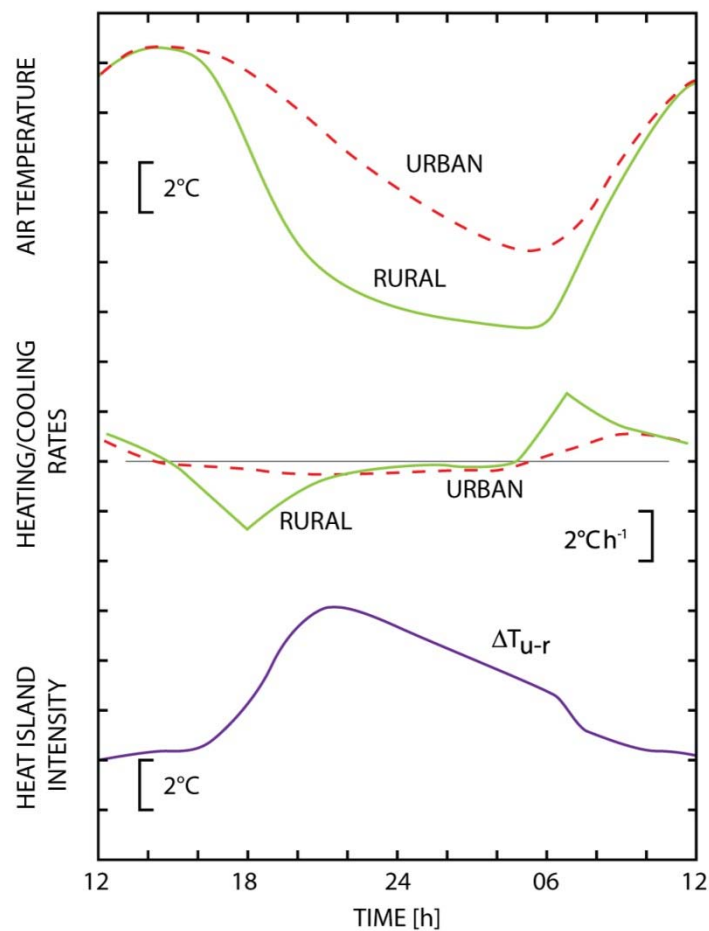
Figure 5. Typical temporal variation of urban and rural (a) air temperature and (b) cooling/warming rates and (c) the resulting heat island intensity (ΔT_{u-r}) under clear weather conditions (source: Oke 1987)

In contrast to the night-time regime, during the daytime, the net radiative input can be lower in urban areas than that of rural areas (Basara et al. 2008). This phenomenon is commonly referred to as the "Urban Cool Island". Urban Cool Islands might appear due to extensive shading by tall buildings or other structures, within an existing green area, or due to the

slower warming rate of the materials (Oke 1982; Oliveira et al. 2011). This occurrence is more prevalent for cities in semiarid and arid areas, with extreme high summer temperatures, where urban areas can provide a better urban living comfort relative to their dry desert environments (Frey et al. 2005).

2.2.2. Seasonal development

As already stated, UHI is not a static phenomenon, but displays periodic and aperiodic variations. Diurnal pattern is dominant, being more distinctive during night time, but UHI intensity changes across seasonal scale as well (Gaffin et al. 2008; Zhao et al. 2010). Corresponding monthly dynamics of temperature gradients vary with day-to-day cycles of human activity, mainly due to the contribution of anthropogenic heat to the urban energy budget (Shahmohamadi et al. 2011; Stewart 2011). Stewart (2011) further outlined that, looking at the seasonal time scale, UHI intensity fluctuates with warm and cold, or dry and wet cycles.

The fluctuation of the UHI intensity is easily observed when comparison over the heating and non-heating season is made. Considerable inter-annual UHI variability can be found in mid-latitude cities, with the greatest frequency of occurrence and highest intensities in the warmer part of the year, and specifically during the summer season (Oke 1982; Szegedi and Kircsi 2003). According to Oke (1982) this can be due to the seasonality of weather conditions (e.g. wind, cloud, air mass stability), solar influences such as angle of incidence in relation to urban canyon geometry, etc. This might not be the rule, as different studies have found either autumn or spring to be the season, second to summer, of highest UHI intensities (Morris et al. 2001). However, most papers agree that the winter time is found to be a time of year with the least intense heat islands while summer was displaying strongest UHIs.

However, in tropical regions, UHI intensity tends to be smaller than in mid-latitudes and is greatest during the dry season (Stewart 2011). Furthermore, wet-dry season contrasts have been proven to be more significant than winter–summer differences (Jauregui 1997). Jauregui further reported that daytime UHIs during the wet season are generally less intense and of shorter duration, when compared to other times of the year. However, the night-time UHI phenomena are again proven to be the most frequent and most intense in observed tropic regions.

This further outlines the overall complexity of the UHI phenomenon and its need to be explored in a broader geographical context.

2.3. Structure of the urban atmosphere

To understand how certain factors affect the formation of UHI, we must take a closer look at the very fabric of the urban atmosphere.

Oke (1976) outlined the concept of two distinct layers - one called the urban building or canopy layer (UCL) and the other called the urban boundary layer (UBL). UCL extends from the ground up to the mean roof level, like a vegetative canopy layer. This layer is mostly controlled by site-specific characteristics, more precisely surface materials and urban geometry (Arnfield 2003; Golden 2004). UBL is situated above the UCL and is affected by the thermal circumstances of the city beneath. Both layers contribute to the warming of the urban atmosphere (Oke 1976).

Voogt (2004) further defined three types of UHI: canopy layer heat island, boundary layer heat island, and surface heat island. Contrary to the UBL and UCL, the surface layer heat island refers to the warming of surfaces and is not directly linked to the layers of the urban atmosphere (Voogt, 2004).

Figure 6 illustrates the schematic representation of the main components of the urban atmosphere and the processes of the formation of UHI (Oke 1997).
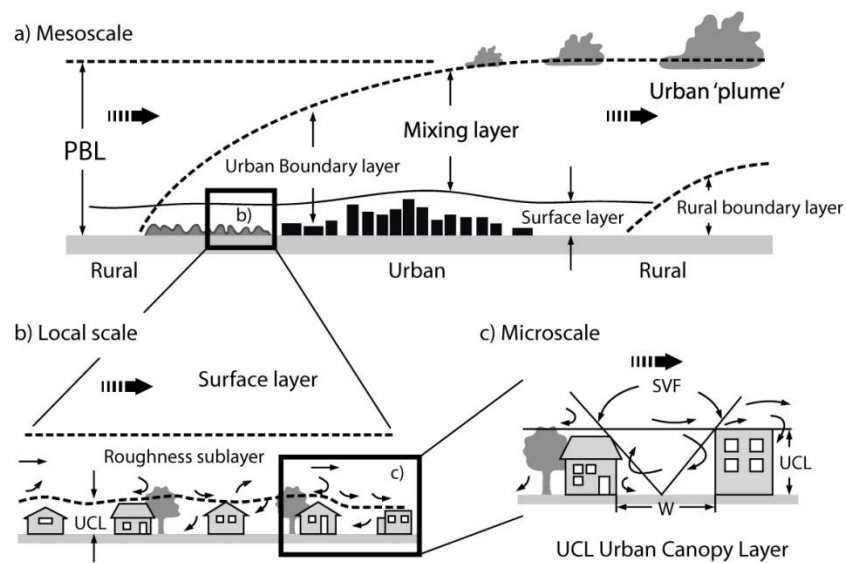

Figure 6. Horizontal scales in a city and related vertical atmospheric layers (source: Oke 1997)

2.4. Quantification of UHIs in an urban environment

2.4.1. The UHI intensity

Urban Heat Island intensity is an important indicator expressing the magnitude of the UHI effect. This term denotes the spatially-averaged temperature difference between an urban and its surrounding rural area, and is commonly represented as ΔT_{u-r} or $\Delta\theta$ (see, for example, Oke 1969; Voogt 2002; Memon et al. 2009). This difference is usually expressed in Kelvin (K). This is a commonly accepted definition of UHI intensity and has been adopted for evaluation of the UHI phenomenon worldwide.

The UHI intensity is usually determined by comparing the mean or maximum temperatures between urban and rural areas, and should be derived from weather datasets of a well-developed urban area and least developed rural area that lies outside the area of urban influence (Memon et al. 2008). It is given by:

$$\Delta\theta = T_{urban} - T_{rural} \qquad [K] \qquad\qquad \text{Eq. 1}$$

Generally, $\Delta\theta$ is reported to be of positive values, and can vary across the urban domain and between the cities (Van Hove et al. 2011). There have also been reports of occasional negative $\Delta\theta$, where the rural area temperature is higher than that of the urban area (Alonso et al. 2003). This phenomenon is referred to as the Cool Island. The time periods that are usually considered for an analysis vary and can be seasonal, monthly, annual, or in some cases within a few selected days (Gaffin et al. 2008).

2.4.2. Measuring Urban Heat Islands

As it was discussed before, there are three types of UHI: canopy layer heat island, boundary layer heat island and surface heat island (Voogt 2004). The canopy and boundary layer heat islands can be altogether referred to as the atmospheric heat islands.

To identify UHIs, scientists use direct and indirect methods. In the case of atmospheric heat islands researchers usually use the direct methods - the methods that deploy stationary monitoring stations and mobile traverses. To estimate surface heat island, researchers often use remote sensing.

2.4.2.1. Stationary stations

The most commonly used approach to investigate the UHIs is by analyzing the data obtained from stationary monitoring weather stations. Weather services usually possess the weather records with years of accumulated

information regarding the air temperatures, wind speeds, cloud cover, solar radiation, humidity, and precipitation levels. Most cities are equipped with a network of stationary weather stations that are collecting meteorological data on a daily basis, and usually in an hourly-based format.

The simplest method of analyzing a heat island effect is to compare the simultaneously measured air temperature data from representative urban and rural weather stations (Oke 1987; Böhm 1998). This difference is typically derived from the datasets obtained from one downtown station and one station situated at the airport. This comparison can be done with regard to the different time scales, allowing us to see the tendencies, trends and long-term changes of the UHI intensity (Gaffin et al. 2008). Although, it should be noted that the comparison over a larger sample of data (e.g. long-term periods of 30 years or more) might have its disadvantages. Due to repairs or malfunction, the measuring instruments can be changed over time, thus distorting the recorded data. This further stresses the importance of the thorough calibration of the new equipment by following the same standards as for the previous one, thus assuring the reliability of the results (WMO 2008; WMO 2011).

In order to quantify the magnitude of the UHI, the air temperatures are usually measured within the UCL (Gartland 2008). Standard measurements are generally made at the height of 1.5 meters above the ground. Due to the security reasons the urban weather stations are typically located on the rooftops of the buildings, which might not reflect the real street level conditions. Therefore, some data adjustments for the effects of vertical deviation in climatic parameters might be needed. A more detailed analysis of the UHI phenomenon includes datasets obtained from numerous stationary stations within and around the city. From this network, a two-dimensional contour map of the city's temperatures can be generated, as presented in Figure 7 (Voogt 2002). The study of long-term weather data retrieved from a network of weather stations can also illustrate a spatial variability of the heat island signal.
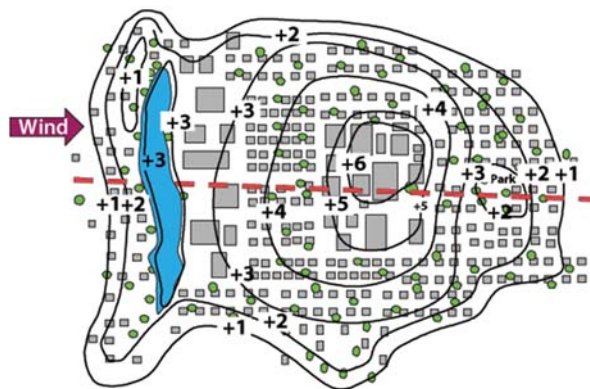

Figure 7. Isotherm map depicting an atmospheric night time UHI (source: Voogt 2002)

2.4.2.2. Mobile traverses

Extensive efforts have been made to describe the UHI effect as an extremely dynamic phenomenon with the location of the thermal maximum changing in response to the physical and geometrical variations of its surroundings (Wilby 2008; Van Hove et al. 2011; Jamei and Ossen 2012). These statistically significant variations of the microclimate can be observed and quantified by a number of mobile traverse measurements that are considered to be crucial in capturing the street-scale microclimatic conditions of the built environment (Chen et al. 2010).

Mobile traverses represent mobile transport of temperature sensors across a city and its countryside. Results have been mostly used to quantify spatial variation and intensity of the UHI within a city. Survey routes conducted across an urban-rural area are usually linear or circular, and are designed to obtain a dense sample of temperatures in a relatively short period of time (Stewart 2011). Generally, the properly equipped vehicles are used during a mobile survey (Alonso et al. 2003; Hart and Sailor 2007), although bicycles or foot traverses are often employed as well (Koomen et al. 2013). Figure 8 illustrates a vehicle-mounted sensor used in mobile temperature surveys. Figure 9 illustrates mobile weather station mounted on three-wheel E-bike (Property of Department of Building Physics and Building Ecology, Vienna University of Technology).

Figure 8. Vehicle-mounted sensors used in mobile temperature surveys (source: NOAA)

Figure 9. The mobile weather station mounted on three-wheel E- bike. Property of Department of Building Physics and Building Ecology, Vienna University of Technology. Source: https://veloviel.wordpress.com/page/7/

One should be very careful when mounting the equipment in order to avoid any external sources of heat that can influence the measurements. Therefore, temperature sensors are generally attached to roofs or bumpers of cars such that the engine or exhaust heat is avoided while traversing the city (Gartland 2008). The mobile traverses can be undertaken at any time of day or night, according to the goal and the subject of the research.

Despite this method being rather convenient, it should be noted that field measurements have several limitations (Mirzaei and Haghighat 2010). Firstly, only a limited network of mobile stations is generally used, therefore there is the inability to record simultaneous measurements at different locations. Secondly, only a small number of parameters are simultaneously measured. In addition to this, when it comes to data analysis, approximations are frequently made to account for the abundance of parameters that could influence the formation of the UHI effect.

2.4.2.3. Remote sensing

Thermal remote sensing has been widely employed to estimate surface temperatures and to assess the UHI intensity, to perform land cover classifications, and as an input for advanced models of urban surface/atmosphere exchange (Mirzaei and Haghighat 2010). This approach denotes the employment of infrared sensors, usually placed on satellites, for a comprehensive evaluation of the land surface temperature. The resultant surface temperature comprises of intertwined effects of surface radiative and thermodynamic properties, the radiative input at the surface from the sun and atmosphere, and the effects of the near surface atmosphere and its relation to turbulent transfer from the surface (Voogt and Oke 2003).

Figure 10 shows thermal infrared pictures illustrating day and night regime of an urban park with neighboring streets. The surface temperature gradients are apparent, emphasizing cooler park area during the night-time (Spronken-Smith and Oke 1998).
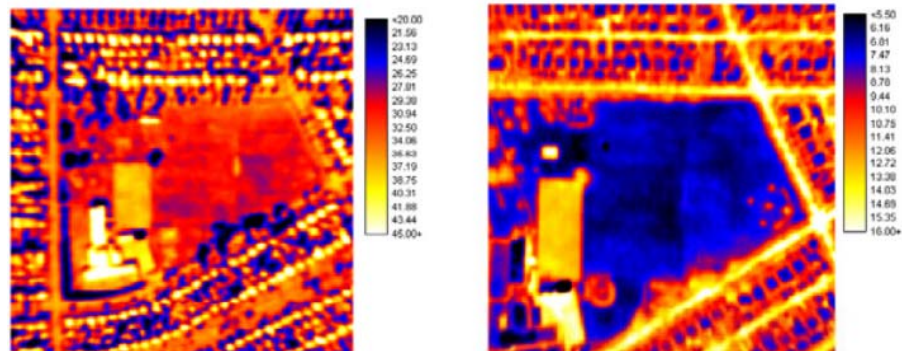
Figure 10. Thermal infrared picture illustrating day and night regime, respectively, of an urban park area (source: Spronken-Smith and Oke 1998)

It should be noted that the remote sensing has several limitations (Mirzaei and Haghighat 2010). Firstly, it is a very expensive approach. Secondly, it is not possible to have steady images from the urban surfaces due to the constant mobility of the satellites used. Additionally, satellites usually pass over an area twice a day, which prevents a profound study of the UHI phenomenon on diurnal (24-cycle) scale. Furthermore, the radiant emissions from vertical surfaces are not captured as the equipment mostly observes emissions from horizontal surfaces such as streets, rooftops, and treetops.

2.5. Influencing factors

The following section outlines the key factors that contribute to the temperature gradient detected between rural and urban areas.

The UHI phenomenon can be observed as a result of diverse responses of urban and rural areas to processes of energy (solar heating), mass and momentum transfer (airflow) (Oke 1987). These differences generate the city's unique microclimate that can be perceived as a result of mutual interactions between the atmosphere and the urban environment built by man.

Consequently, UHI phenomenon can be interpreted as a product of the synthesis of many factors, which could mainly be categorized as controllable and uncontrollable factors (Memon et al. 2008). These factors can be further divided into two main components: (1) meteorological factors (such as the cloud cover, humidity, and wind speed), and (2) urban structure factors (such as the size of city, the density of the built-up areas, aspect ratio, presence of vegetation, anthropogenic heat sources, etc.) (Givoni 1998).

Figure 11 illustrates the basic controllable and uncontrollable factors and the very process of the formation of UHIs.
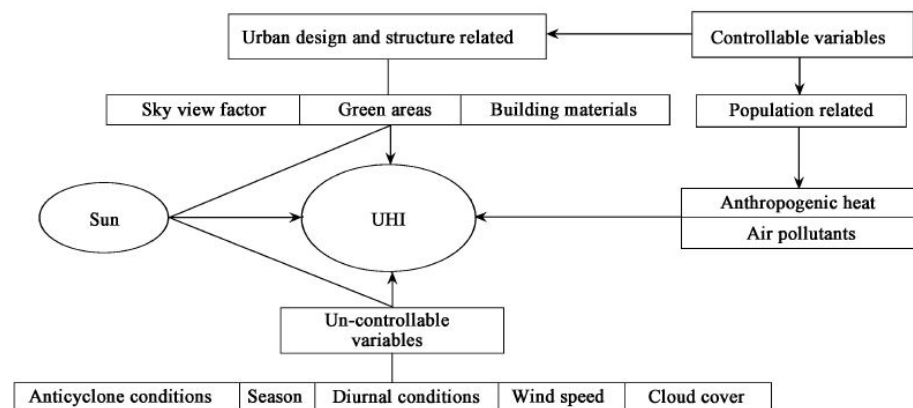

Figure 11. Generation of Urban Heat Island (source: Memon et al. 2008)

2.5.1. Atmospheric conditions - wind and cloud cover

By uncontrollable factors we are considering the main meteorological variables, of which the most significant are wind speed and cloud cover (Oke 1982; Memon et al. 2008). The cloud amount and wind speed affect the insolation and ventilation, thus affecting the radiative and turbulent exchanges within and around the urban domain (Morris et al. 2001). Together, these conditions promote high urban-rural temperature gradients that may result in higher UHI magnitudes.

Stable anticyclonic events with clear skies and calm conditions are believed to be the optimal conditions for development of UHI (Alonso et al. 2003). Alonso (2003) reported that in case of the city of Salamanca, the greatest intensity of nocturnal UHI is observed in stable weather conditions, with a mean daily wind speed of below 4 km/s and cloudiness equal to or lower than 2/8 of cloudy sky. Furthermore, when the wind surpasses the speed of 22 km/h, the nocturnal UHI tends to disappear.

Therefore, it can be concluded that the strongest UHIs develop under calm and clear weather typical of anticyclonic (high atmospheric pressure) conditions and least under windy and cloudy weather typical of cyclonic (depression or low pressure) conditions. Anticyclonic climatic conditions are characterized by clear skies, thus increasing the amount of incoming solar radiation, leading to the higher heat gain within the urban system (Szegedi and Kircsi 2003). If clouds are present, the total amount of the incoming shortwave radiation will be reduced, limiting heat stored within the urban fabric. However, it should be noted that a night-time cloud cover can present a significant obstacle to the outgoing long-wave radiation, thus affecting the nocturnal urban radiation budget (Stewart 2011).

Furthermore, the combined effects that wind and clouds have on the genesis of UHIs are found to be depended on the season as well (Morris et al. 2001). Morris (2001) stated that, during the same wind and cloud conditions, the UHI intensity was of greater magnitude during spring and summer, than autumn and winter. Furthermore, he reported that during the winter, the UHI intensity is inversely proportional to the fourth root of both the wind speed and cloud cover.

2.5.2. Urban geometry

Canyon geometry is one of the most important factors affecting the formation of the UHI (Oke 1969; Shishegar 2013). The cities are a synthesis of the variety of geometric configurations that are referred to as urban canyons. This term denotes a general urban unit combined of two typically parallel rows of buildings, a street, and the contained air volume (Nunez and Oke 1977).

The climatic circumstances within an urban canyon are referred to as the microclimate of the canopy layer and are the result of complex radiative and aerodynamic exchanges below roof-level (Oke 1969). The amount of effective urban surface area (street surface, building walls and roofs) is far greater than that of a reference rural environment. Attention is usually drawn to the difference in thermal surface properties and resulting thermal budget between the two environments, stating that cities possess greater ability to absorb, store and exchange heat (Oke 1969). This is further emphasized by the genuine configuration of urban buildings that tend to trap radiation within the city and even reduce the turbulent transport at street level (Oke 1969). Additionally, the shape of an urban canyon limits the amount of incoming solar radiation, but it may also reduce the outgoing long-wave radiation (Oke 1987).

Figure 12 illustrates the urban/atmosphere interface. Figure 13 illustrates the method of multiple reflections of incoming shortwave radiation between the adjacent steet canyon surfaces.
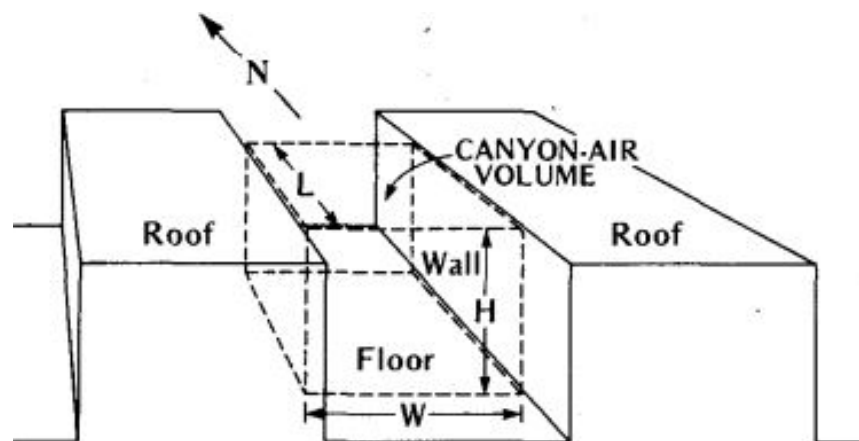

Figure 12. Schematic depiction of the urban/atmosphere interface, including an urban canyon and its canyon air volume (dashed) (source: Nunez and Oke 1977)
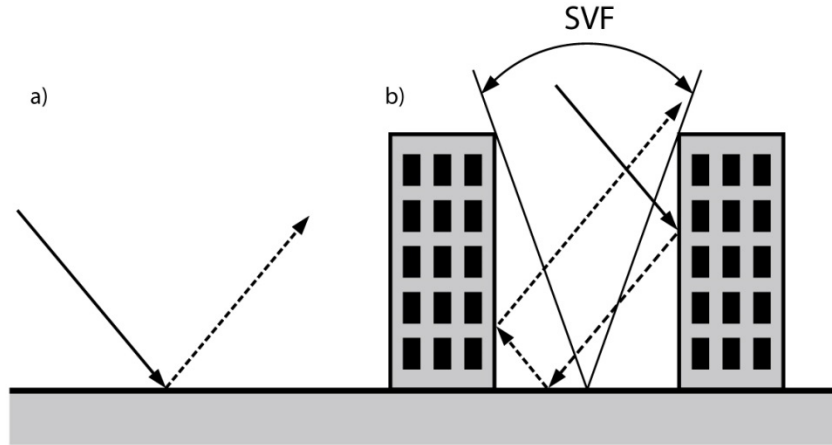
Figure 13. Schematic depiction of reflection of short-wave radiation in (a) rural setting and (b) urban setting

The geometry of the urban canyon is expressed by its aspect ratio (H/W) and the sky view factor (SVF) (Voogt and Oke 1997). From a climatic point of view, the aspect ratio and sky view factor are crucial features of an urban canyon, affecting the potential of solar access, the airflow, as well as the ability of cooling the whole urban system (Ali-Toudert and Mayer 2006).

Oke (1981) presented the relation between UHI intensity and urban geometry, as follows:

$$\Delta T_{u\text{-}r} = 7.54 + 3.97 \ln \left(\frac{H}{W}\right) \qquad\qquad \text{Eq. 2}$$

$$\Delta T_{u\text{-}r} = 15.27 - 13.88\ \psi_{sky} \qquad\qquad \text{Eq. 3}$$

where $\Delta T_{u\text{-}r}$ is the air temperature difference between urban and rural area, H and W refer to the height and width of the street canyon, and ψ_{sky} is the sky view factor.

It should be further noted that the orientation of the canyon, relative to the solar path, is another equally significant aspect affecting the heating of canyon surfaces, by determining the extent to which the canyon surfaces are exposed to the direct sunlight (Nunez and Oke 1977). This aspect may influence the thermal response of the urban canyon.

2.5.2.1. Aspect ratio

The aspect ratio is defined as the ratio of the height of the building (H) to the width of the street (W) (Burian et al. 2005). The higher aspect ratio denotes higher buildings and narrow streets and is referred to as a *deep street canyon*. The smaller aspect ratio denotes lower buildings and wider

streets and is referred to as a *shallow street canyon*. An *uniform street canyon* represents the street canyon with an aspect ratio equal to 1 (Shishegar 2013). The height-to-width ratio is calculated for two buildings by dividing the average height by the distance between the two buildings, as follows:

$$\frac{H}{W} = \frac{\frac{H1+H2}{2}}{S_{12}}$$

Eq. 4

where H_1 is the height of the upwind building, H_2 is the height of the downwind building, and S_{12} is the horizontal distance between the two buildings (i.e. the canyon width) (Burian et al. 2005). The calculation is performed for each pair of adjacent elements in a building array, which can be very tedious for complex geometries found in the city. For simplified computation, an average aspect ratio can be approximated by taking the average building height divided by the average width between buildings, as follows:

$$\frac{H}{W} = \frac{\overline{Z_H}}{\overline{W}}$$

Eq. 5

where $\overline{Z_H}$ is the average building height and $\overline{W}$ is the average distance between buildings (Grimmond and Oke 1999).

2.5.2.2. Sky View Factor

Sky view factor (SVF) is a fraction (varying between 0 and 1) used to describe to which extent the sky is obscured by the surroundings for a given point (Grimmond et al. 2001). A low SVF denotes that only a small amount of sky can be seen from a reference point, due to tall surrounding buildings. A high SVF (close to 1) can be usually found in a rural area where a large area of sky can be seen.

SVF is a very useful measure of the radiation exchange between the sky and canyon floor of a street canyon (Oke 1987). Different studies reported that the restricted SVF results in decreased surface heat loss by long-wave radiation (see, for example, Pearlmutter et al. 2005).

Many different methodologies for SVF calculation have been developed, and can be further divided into two distinct approaches: geometric or photographic (Johnson and Watson 1984; Grimmond et al. 2001; Chapman and Thornes 2003).

Johnson and Watson (1984) defined the SVF as the ratio of long-wave radiant flux reaching the sky vault from the flat floor of the canyon to that reaching the sky vault from an unobstructed flat surface. Figure 14 illustrates the model for radiation exchange between the sky and surface element (the surface element at the ground is defined as ΔA, the sky is represented as the surface of a hemisphere of radius R with its centre in ΔA, and ΔS is a surface element on the hemisphere).
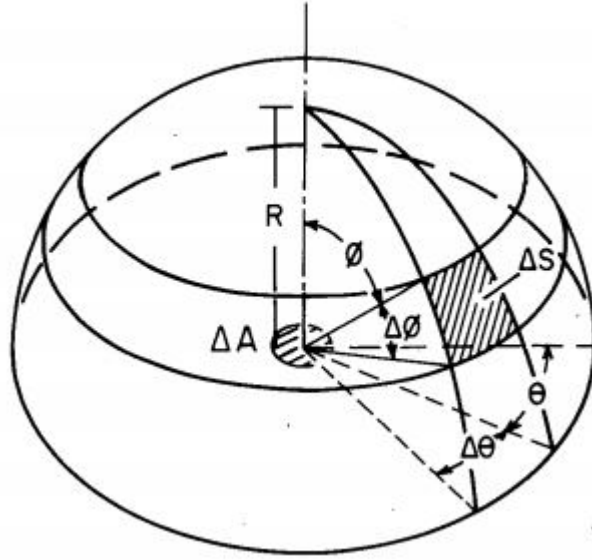

Figure 14. Model for radiation exchange between the sky and surface element (source: Johnson and Watson 1984)

The SVF for the surface element ΔA is therefore the fraction of radiant flux leaving ΔA which is intercepted by the sky. It is given by:

$$\psi_{sky} = \frac{1}{\pi R^2} \int_{Sv} cos\varphi dS \qquad \text{Eq. 6}$$

where ψ_{sky} is the sky view factor (dimensionless), R is nominal radius of the sky hemisphere [m], φ is the angle between the canyon floor and the sky vault hemisphere, dS (ΔS) is the elemental area seen from the canyon floor [m²], and Sv is the sky vault seen from the canyon floor.

Furthermore, SVF can be obtained from a hemispherical photograph. Hemispherical photographs are captured by a fish-eye lens representing the 360˚ image of the canyon. Chapman et al. (2001) suggested a method of using software called SKYVIEW in order to process the hemispherical photograph. The main input to the program is a northerly-orientated digital fish-eye JPEG. The software then converts the image into an array of greyscale digital numbers (DN) between 0 and 255, from which the

delineation of sky from non-sky is performed. Once the sky pixels have been delineated, Chapman applied specially developed algorithm for the SVF calculation. This model was adapted and further modified from the work of Steyn (1980), who first proposed the implementation of an advanced algorithm to calculate the SVF.

2.5.3. Vegetation

The impact of urban trees and parks on the city's energy balance is extensively documented in a number of research papers (Akbari et al. 1997; Nowak 2002; Alexandri 2008; Pandit and Laband 2010). From a thermal point of view, urban vegetation can be extremely beneficial for the city. Vegetation can mitigate UHIs directly by shading heat-absorbing surfaces, and indirectly through evapotranspiration cooling. Increasing urban vegetation holds a great potential for reducing urban summertime air temperatures and saving cooling energy use in buildings.

The presence of trees and vegetation in urban canyon can affect the urban ecosystem in different ways. Given the right conditions, shade provided by trees can reduce energy use for cooling, thus decreasing anthropogenic heat released into the atmosphere and lowering the ambient air temperature (Akbari et al. 1997; Taha 1997). Furthermore, evapotranspiration processes can help reduce peak summer air temperatures. Taha (1997) reported that an increase in vegetation in urban areas can result in some 2°C decrease in air temperatures. Additionally, decrease in air temperatures can affect the ground-level smog formation by reducing its concentration (Akbari 2002). Likewise, the reduction in near-surface temperatures can reduce the ground level ozone (Piety 2007). It can be concluded that trees can potentially reduce energy consumption in a city and improve air quality and comfort (Akbari 2002).

Urban parks, on the other hand, can mitigate the UHI effect only at its micro- or mesoscale, rather than the citywide (Alexandri 2008). Although the air temperature inside the park can be reduced significantly, only a few buildings in the neighboring area of the park benefit from this air temperature reduction. Alexandri (2008) stressed that the presence of the park will not affect the rest of the city from a thermal point of view.

Figure 15 illustrates the daytime energy exchanges between an isolated tree and its street canyon environment.
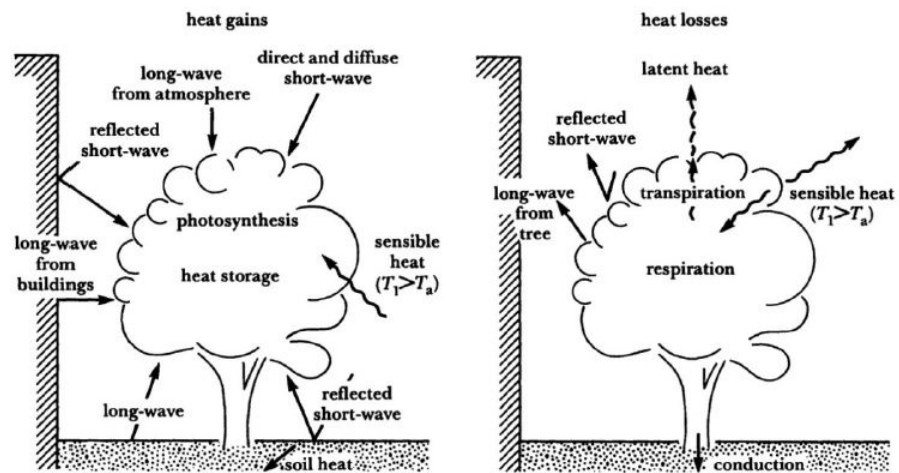
Figure 15. Scheme of the daytime energy exchanges between an isolated tree and its street canyon environment (source: Oke 1989)

It should be noted that trees can have some negative features as well. As it was already mentioned that trees contribute to the air quality, their presence can also contribute to smog problems by emitting volatile organic compounds (VOCs) (Chameides et al. 1988). The work performed by Donovan et al. (2006) stressed the importance of planting trees that are low-VOC emitters. In this research, trees were analyzed and ranked accordingly to their potential to impact air quality. The least favorable trees were the genera poplar - willow and oak, while the most beneficial were maples - hawthorns and pines. Another study conducted by Beckett et al. (2000) came to the conclusion that conifers species – such as pines and cypresses - may be the best choice for pollution-control plantings. This study revealed that species with rough leaf surfaces are most efficient at capturing particles. These studies stressed the importance of careful selection of tree species so that low-emitting trees could be considered when planning an urban reforestation.

Another concern regarding the presence of urban trees is that vegetation may act as an obstacle limiting the air circulation and pollutant removal processes at the pedestrian zone of some shallow urban canyons (Ng and Chau 2011). Results from this study revealed that tree crowns may block ventilation processes inside deep canyons, thus letting the pollutants stay trapped at the pedestrian zone. Nevertheless, the conclusion of this study was that strategically planned urban vegetation can improve air quality and maximize the positive features of vegetation within the urban canyon.

2.5.4. Surface thermal properties

Given the complexity of an urban environment, it is recognized that the heat storage in urban areas will be more significant than at simpler bare soil or agricultural sites (Grimmond and Oke 1998; Piringer et al. 2002). The densely built urban areas result in higher amount of total built surface area with its unique physical mechanisms that are believed to be responsible for the modifications of the local climate. Most urban materials possess thermal properties which make them good conductors with greater heat storage abilities (Landsberg 1981). In this sense, it is crucial to understand the mechanisms of the heat storage uptake and release within an urban system for their role in the daily urban energy balance.

If we take a closer look at the three-dimensional nature of an urban canopy, we will observe two essential units of this system (Nunez and Oke 1977): we can recognize the urban canyon as the basic surface unit, followed by the canyon air volume (Figure 16). The thermal properties of active canyon surfaces (walls and floor) are responsible for the storage of heat during the day and its slow release at night, thus changing the net energy status of the air volume. Therefore, the urban surface energy balance is a key component in estimating the implications of total heat storage within an urban area in formation of UHI. It can be written as (Pearlmutter et al. 2005):

$$Q^* + Q_F = Q_H + Q_E + \Delta Q_S + \Delta Q_A \qquad [Wm^{-2}] \qquad \text{Eq. 7}$$

where Q^* denotes the net all-wave radiation, Q_F is anthropogenic heat, Q_H and Q_E are the respective turbulent fluxes of sensible and latent heat, ΔQ_S the storage heat flux, and ΔQ_A is the net advective heat flux.

Net radiation is a direct function of the shortwave absorption and long-wave emission characteristics of the surface. These features are dependent upon the material, as well as geometric properties typical of urban areas (Pearlmutter et al. 2005).
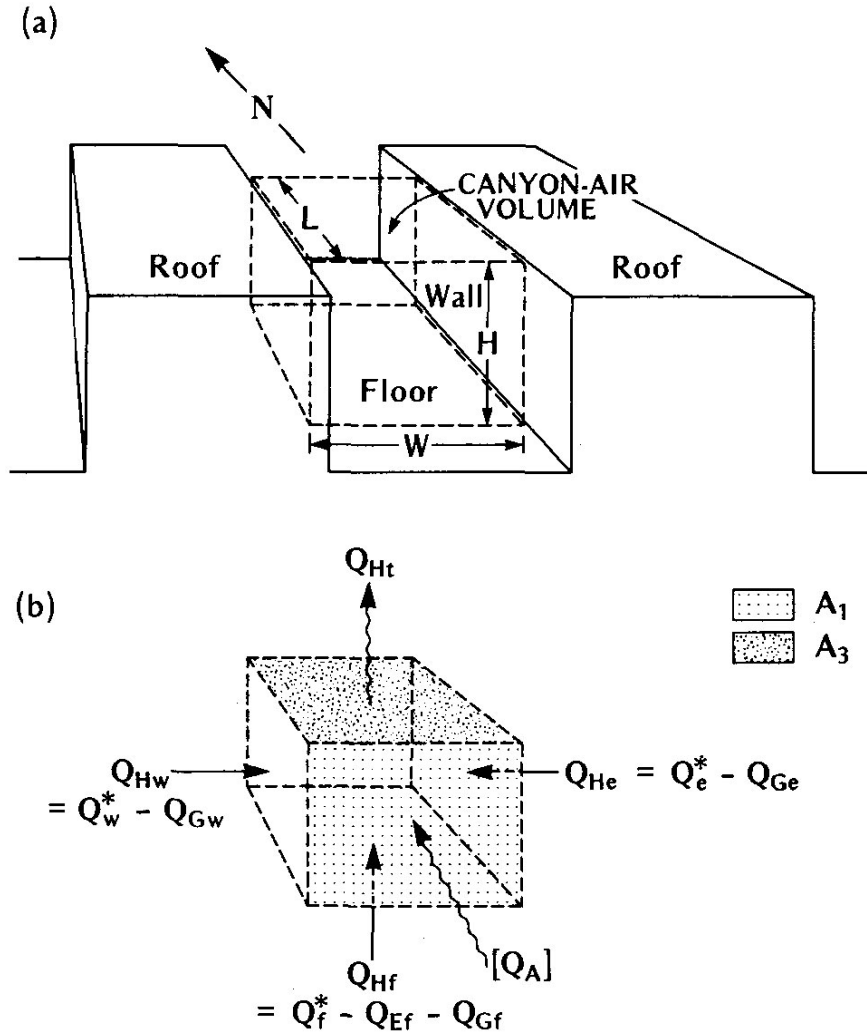
(a)

(b)

Figure 16. Schematic representation of a) the urban/atmosphere interface, including an urban canyon and its canyon air volume (dashed), and b) sensible heat exchanges into and out of the canyon air volume (source: Nunez and Oke 1977)

When the energy balance is empirically obtained, the above equation must be modified (Masson et al. 2002):

$$Q^* = Q_H + Q_E + \Delta Q_S \qquad [Wm^{-2}] \qquad \text{Eq. 8}$$

Anthropogenic heat is often omitted from the measured urban energy balance because it is assumed to be embedded in other fluxes. Furthermore, if the source area where the sensor is positioned is homogeneous, the net advective heat flux is minimized and can be neglected.

This approach allows most of the physical effects associated with the urban energy balance to be reproduced, including radiative trapping (long-wave

and shortwave), the momentum flux, the turbulent sensible and latent heat fluxes, heat storage uptake and release, and water and snow interception.

Furthermore, it should be noted that the sensitivity of the surface energy balance strongly depends on material's albedo and emissivity (Taha et al. 1992). High-albedo materials can effectively reduce the heat gain through the building`s envelope by reflecting the incoming shortwave radiation, but can also affect the air temperature in the near surrounding of the building. Simulations performed by Taha et al. (1988) showed that a change of 0.01 in albedo can lower the air temperatures for some 0.2 – 0.25 K.

Emissivity is equally important as the albedo. As the emissivity is the ability of material to emit thermal radiation, the higher emissivity means that the materials are capable of emitting longwave radiation readily, thus allowing the building system to cool faster (Sailor 2006). Table 1 gives an overview of albedo and emissivity of some common materials.

Table 1. Albedo and emissivity of some common materials (Oke 1987)

	SURFACES	**ALBEDO**	**EMISSIVITY**
ROAD	Asphalt	0.05 – 0.20	0.95
WALL	Concrete	0.10 – 0.35	0.71 – 0.90
	Brick	0.20 – 0.40	0.90 – 0.92
	Stone	0.20 – 0.35	0.85 – 0.95
ROOF	Tar and gravel	0.08 – 0.18	0.92
	Tile	0.10 – 0.35	0.90
WINDOW	Clear glass	0.09 – 0.52	0.87 – 0.94
PAINT	White, whitewash	0.50 – 0.90	0.85 – 0.95
	Black	0.02 – 0.15	0.90 – 0.98

2.5.5. Anthropogenic heat

UHI can be intensified by the anthropogenic heat output (Q_F) (Shahmohamadi et al. 2011). Sources of anthropogenic heat include heat generated by the combustion process in vehicles, heat created by industrial processes, the conduction of heat through building walls or emitted directly into the atmosphere by air-conditioning systems, and the metabolic heat produced by humans (Sugawara and Narita 2009). The energy released by human activities is often regarded as negligible, especially when compared to the other sources, although it is usually incorporated into the energy balance equation for its completeness (Grimmond 1992).

Q_F can be subdivided into three components (Sailor and Lu 2004):

$$Q_F = Q_V + Q_H + Q_M \qquad [Wm^{-2}] \qquad\qquad Eq. 9$$

where Q_V is the heat produced by combustion of vehicle fuels, Q_H is released from stationary sources (primarily within buildings), and Q_M is the heat released by human activity.

Sailor and Lu (2004) demonstrated a representative summer and winter diurnal energy consumption profiles for 6 large US cities, conducting a city-scale analysis. The largest wintertime anthropogenic heating was in the range of 70–75 Wm^{-2} (averaged over the entire city). During the summer, the total energy consumption by buildings was usually in the range of 30–60 Wm^{-2}. The significant winter heating loads during the winter peak in the anthropogenic heating profile are in some cases nearly twice as large as the summer peaks. They also reported that all profiles displayed the dual peak shape with the morning peaks generally being a little larger than the evening peaks. Furthermore, heating from vehicles was the dominant term for every city during the summer, making up between 47% and 62% of the total value. During the winter, the relative importance of heating fuels increased substantially in the cold climate cities, making up to 57% of the total value. Metabolic heat release was consistently the least important component in these profiles making up from 2 to 3% of the total heating for all cities studied. This study provided an insight into how spatial and temporal variability in anthropogenic heat output affects the development of the UHI and its resultant impact on air quality and other features of the urban climate. Additional study conducted by Sailor and Fan (2004) further portrayed the importance of capturing the anthropogenic heating profiles with respect to the different spatial resolutions. They reported that anthropogenic heating can be around 10 Wm^{-2} when averaged over a large metropolitan area, 100 Wm^{-2} when averaged over a city, and can as high as the peak solar load when averaged over just the central business district of a large city.

2.6. Statistical Analysis of Urban Heat Islands

Statistical methods and analysis are statistical tools for estimating, quantifying and exploring spatial patterns and relationships. These statistics have been used extensively in UHI studies, especially for predicting future occurrences (Unger et al. 2000; Chen et al. 2010).

For a reliable analysis of climate data, homogenized datasets should be used. Hence, during the data processing it is highly advisable to maintain observing practices and instruments unchanged, to avoid any changes in the collection, handling, transmission, and processing of the data (WMO 2008; Syrakova and Stefanova 2009; WMO 2011).

Table 2 summarizes numerous studies using statistical models for prediction of the UHI phenomenon.

Table 2. Survey of some studies using statistical models for prediction of UHI (source: Bottyán et al. 2003)

Predicted Variable	Employed Parameters	Reference
UHI intensity	wind speed, cloudiness	*Sundborg (1950)*
UHI intensity	population, wind speed	*Oke (1973)*
UHI intensity	wind speed, cloudiness, atmospheric stability, traffic flow, energy consumption, temperature	*Nkemdirim (1978)*
UHI intensity in four different air levels	lapse rate, wind speed, ratio of lapse rate to wind speed	*Nkemdirim (1980)*
max UHI intensity	sky view factor, height/width ratio	*Oke (1981)*
UHI intensity	wind speed, land-use type ratios	*Park (1986)*
max UHI intensity	population, sky view factor, impermeable surface	*Park (1987)*
UHI intensity	wind speed, cloudiness, temperature, humidity mixing ratio	*Goldreich (1992)*
UHI intensity	wind speed, cloudiness, air pressure	*Moreno-Garcia (1994)*
surface UHI intensity	solar radiation, wind speed, cloudiness	*Chow et al. (1994)*
UHI intensity	built-up area, height, wind speed, time, temperature amplitude	*Kuttler et al. (1996)*
UHI intensity for T_{avg}, T_{max}, T_{min}	NDVI, surface temperature (satellite-based)	*Gallo and Owen (1999)*
UHI intensity	distance from the city centre, built-up ratio	*Unger et al. (2000) Unger et al. (2001b)*
UHI intensity	wind speed, cloudiness	*Morris et al. (2001)*
max UHI intensity	max UHI intensity of the previous day, wind speed, cloudiness, relative humidity	*Kim and Baik (2002)*

A standard technique used for analyzing data sets is regression analysis (WMO 2011). Regression analysis is a powerful tool for modelling target element as a function of one or a set of variables, allowing for a description of relationships and the construction of tests of the strength of the relationships, in the case of this dissertation - the UHI intensity and a set of geometric and surface/material properties of an urban domain.

Memon et al. (2009) used linear regression technique to compare the UHI intensity with mean hourly relative humidity difference (ΔRH) in order to assess the possible impact of the ocean on the UHI intensity in the city of Hong Kong. They believed that the presence of the ocean was the primary reason of the higher humidity for most hours of the diurnal cycle, which will eventually lead to higher UHI. They defined the mean hourly relative humidity difference (ΔRH) as the difference between the mean hourly RH of the rural area and that of the urban and suburban areas. This analysis clearly demonstrated the influence of the RH on UHI intensity in the urban and suburban areas of Hong Kong.

Another statistical model was deployed in the study performed by Bottyán et al. (2003). In order to assess the extent of the relationships between the mean maximum UHI intensity and various urban surface factors in the city of Szeged, Hungary, they applied a set of multiple correlation and regression analysis methods. They also captured a seasonal variation by using two linear statistical model equations - one for the heating and one for non-heating season. The results suggested a strong linear relationship between mean UHI intensity values and selected urban parameters such as SVF, building height, built-up ratio, water surface ratio and their areal extensions in both seasons.

The above mentioned studies stress the potential and versatility of using statistical models in intra-urban relationship assessment.

3.   Methodology

3.1. Overview

The overall goal of this study is to introduce a systematic framework for the representation of the urban environment and the assessment of its microclimatic variation. For this purpose, several locations have been selected and analyzed in order to identify the spatial and temporal features of the microclimate in the city of Vienna. The objective of this analysis was to capture the existing UHI intensity in selected study areas and to obtain an in-depth understanding of intra-city climate variability.

Furthermore, a structured set of geometric and physical properties has been derived in order to accurately address the main principles by which the UHI is formed. Once the specifics of the envisioned variables are determined, a quantitative assessment of their impact on the development and intensity of UHI was estimated based on appropriate statistical methods and analysis.

3.2. Selected areas

As already discussed, the UHI phenomenon is not a constant, but varies according to the location and time. In this context, several study areas have been observed and analyzed in order to capture significant urban climate differences across the city of Vienna.

3.2.1. Definition of an Urban Unit of Observation

The notion of "Urban Unit of Observation" (U2O) is introduced to systematically address the existing local variation of the UHI effect across the city of Vienna (Mahdavi et al. 2013; Mahdavi et al. 2014a; Mahdavi et al. 2014b). U2Os represent clearly bounded segments of the urban domain. These areas represent typical urban and suburban building domains, providing thus a good basis to explore how variation in urban parameters can lead to microclimatic variation in the built environment. Hence, the selected U2Os are chosen to be representative in terms of surface morphology, land cover, and human activity.

Due to temporal changes in stability of microclimatic conditions, the dimensions of a U2O should be estimated with caution. In order for measured microclimatic parameters (e.g. air temperature, wind speed, humidity) to be spatially representative, the size of a sample area should not exceed a few hundred meters in radius (Stewart and Oke 2012). Stewart and Oke (2012) suggested that in order for any potential micro-scale advection from the immediate environs to be reduced to a minimum, the observed area should be defined within the radius of 200 to 500 meters. For the purpose of this study, a radius of approximately 400 meters was chosen as most adequate for capturing the most representative climatic conditions of the urban domain (Mahdavi et al. 2013).

In order for the dynamics of climatic changes to be monitored over time, the most suitable U2O is the one with existing stationary meteorological station. Therefore, the radius of every U2O was carefully drawn starting from the point where a stationary meteorological station is positioned. This allowed for a representative temperature signal to be recorded and further analyzed.

3.2.2. Selected U2Os in the city of Vienna

The specific aim of this chapter is to identify and evaluate the extent of the UHI effect and its variation across the city of Vienna. In this context, four distinct locations were selected to represent typical urban and suburban areas. The selected sites include both low-density suburban and high-density urban typologies in Vienna. Additionally, a rural location outside the metropolitan area was selected as a reference. The variety of locations, in terms of morphological and physical features, will address their role in modifying the local climate according to the location specifics.

Figure 17 shows the position of selected U2Os within the city of Vienna. Used abbreviations - IS, GD, HW, and DF - stand for Innere Stadt, Gaudenzdorf, Hohe Warte, and Donaufeld, respectively. Additionally, this figure shows the position of the reference rural station Seibersdorf (R) with regard to the boundaries of the metropolitan area.
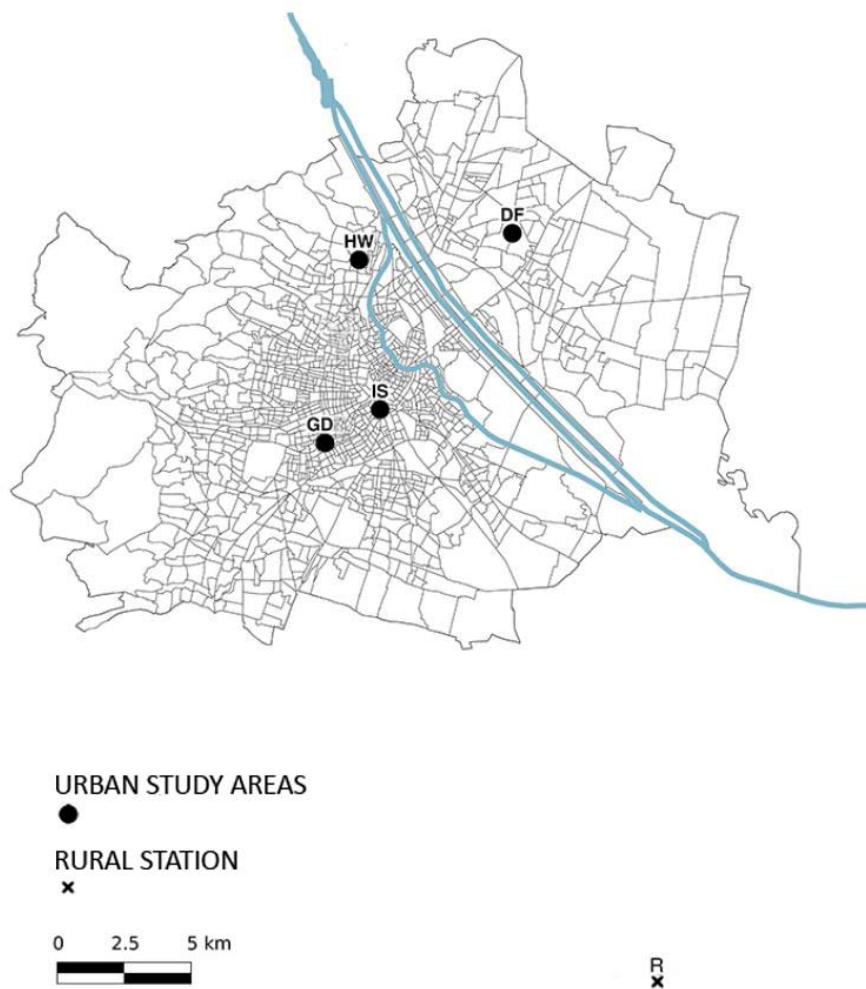
Figure 17. The position of U2Os in the city of Vienna (courtesy of K. Hammerberg)

3.2.2.1. Innere Stadt

The location Innere Stadt is situated in the city center of Vienna. The area is representative for a typical urban Viennese setting. The area is intersected by narrow streets of medium to high traffic rate. Innere Stadt presents densely built area of highly compact built environment. The surrounding buildings are of almost the same height, typically around 5-6 stories with pitched and tiled roofs. The average height is approximately 25 to 30 meters. The prevailing materials of the built structures are brick, in the case of older buildings, and concrete, steel, and glass, in the case of the newly built forms. This area represents a mix-use development, where residential, retail and business premises can be found. Most of the buildings in this area are occupied by the Technical University of Vienna. A central city square called Karlsplatz, with rich green segments, occupies one part of the Innere Stadt area. The terrain is rather flat, with average sea level of 169 meters.

Figure 18 shows the spatial map of Innere Stadt area with spatial boundary (in red). Red dot marks the position of the stationary weather station.
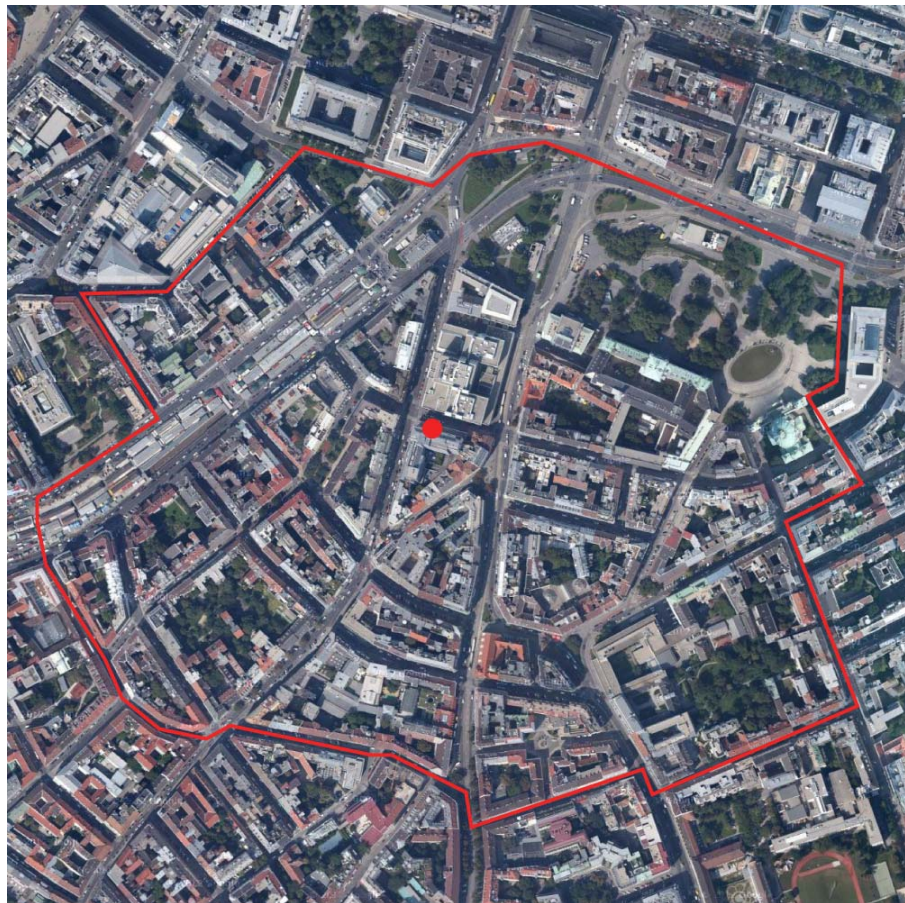

Figure 18. Innere Stadt U2O (source: Google Maps)

3.2.2.2. Gaudenzdorf

The location Gaudenzdorf is situated in the outer ring of the city center of Vienna. The area is bounded by a wide city ring road called the Gürtel, of substantial high traffic volume, especially during the rush hours. Gaudenzdorf presents densely built area of more compact built environment. The surrounding buildings are of almost the same height, typically around 4-5 stories with pitched and tiled roofs. The average height is approximately 20 to 25 meters. The prevailing materials of the built structures are concrete, steel and glass. This area represents a mix-use development, where residential, retail and industrial buildings can be found. One part of this area is occupied by vast open green area with just a few scattered trees. The terrain is rather flat, with average sea level of 177 meters.

Figure 19 shows the spatial map of Gaudenzdorf area with spatial boundary (in red). Red dot marks the position of the stationary weather station.
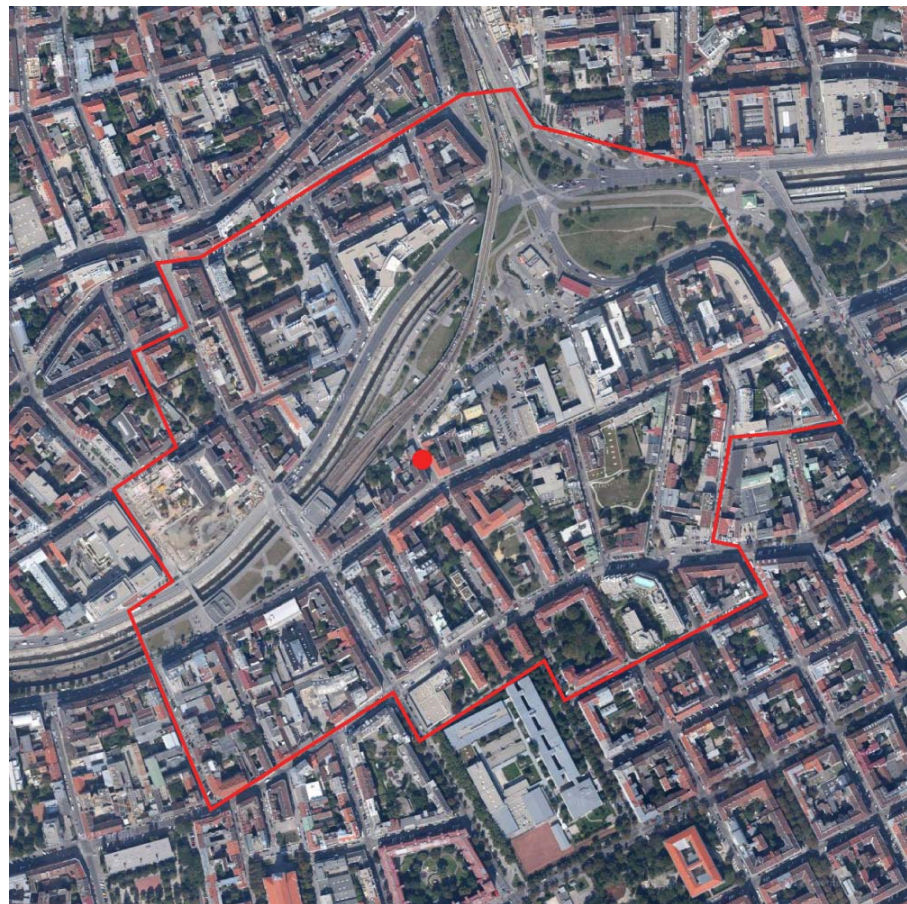

Figure 19. Gaudenzdorf U2O (source: Google Maps)

3.2.2.3. Hohe Warte

The location Hohe Warte is situated in the suburban area of the city of Vienna. Hohe Warte presents sparsely buildup area of individual houses and abundant green spaces. The average height of surrounding buildings is 10 to 15 meters, being of 1 to 3 stories high and with pitched roofs. The exception is The Central Institution for Meteorology and Geodynamics complex (Zentralanstalt für Meteorologie und Geodynamik, ZAMG) that alter the surrounding built environment. This public building exceeds the average height recognized across the area, being of 5 stories high and with flat roofs. The prevailing material of the individual housing units is brick, while, in the case of ZAMG, solid concrete construction intersected with glazed surfaces can be recognized. The area consists of few streets with medium to low traffic rate. Abundance of pervious land cover can be identified within the study area. The terrain is slightly elevated, with sea level in the range of 195 to 210 meters.

Figure 20 shows the spatial map of Hohe Warte area with spatial boundary (in red). Red dot marks the position of the stationary weather station.

Figure 20. Hohe Warte U2O (source: Google Maps)

3.2.2.4. Donaufeld

The location Donaufeld is situated in the suburban area of the city of Vienna. Donaufeld presents sparsely build up area of individual houses and a significant portion of flat green area within inner courtyards. The average height of surrounding buildings is 10 to 15 meters, being of 1 to 3 stories high and with pitched roofs. The exception is the central building complex of University of Veterinary Medicine that presents a group of scattered buildings of higher volume. The average height of this complex ranges from 15 to 25 meters, being of 2 to 5 stories high. The prevailing material of the individual housing units is brick, while in the case of University we can find solid concrete construction. The surrounding area consists of narrow streets with low traffic rate while the central area is intercepted by wider road of higher traffic volume. The terrain is rather flat, with average sea level of 160 meters.

Figure 21 shows the spatial map of Donaufeld area with spatial boundary (in red). Red dot marks the position of the stationary weather station.

Figure 21. Donaufeld U2O (source: Google Maps)

3.2.2.5. Seibersdorf

The location Seibersdorf is situated in a rural area in Lower Austria close to the city of Vienna, and outside the metropolitan area. It is mostly surrounded by farming land. A research campus is located nearby, and the next village is approximately two kilometers away. The research campus is composed of numerous hangars with average height of around 5 meters, and several research buildings with average height of around 10 meters, being of 1 to 3 stories high.

Figure 22 shows the spatial map of Seibersdorf area with spatial boundary (in red). Red dot marks the position of the stationary weather station.

Figure 22. Seibersdorf U2O (source: Google Maps)

3.3. Measurements

A city's microclimate, and the effects of the city on its microclimate, is influenced by various factors whose unthoughtful application can contribute to the severe environmental conditions, with negative implications pertaining to human comfort, health and productivity (Tomlinson et al. 2011; Moonen et al. 2012). Therefore, the attention of this dissertation is focused on capturing and investigating the spatial variation and implications of urban microclimate, by employing a set of stationary weather stations located in different locations in the city of Vienna.

3.3.1. Stationary stations

The weather data used for this analysis was collected at several stationary weather stations positioned in five observed locations throughout Vienna. Each of the selected urban locations is representative for individually different surroundings. Four stations are monitored and operated by The Central Institution for Meteorology and Geodynamics (Zentralanstalt für Meteorologie und Geodynamik, ZAMG), while station called Gaudenzdorf (GD) is monitored by Municipal Department of Environmental Protection in Vienna (MA22). The data sets acquired provided weather information pertaining to air temperature, humidity, global solar radiation, precipitation and wind speed.

Table 3 provides an overview of used stationary weather stations.

Table 4 gives an overview of the height of the measuring instruments (measured from the ground level) for used stationary weather stations.

Table 3. Description of the weather stations with information regarding type, latitude, longitude and elevation of study area [m]

	NAME	TYPE	COORDINATES	ELEVATION [m]
IS	Innere Stadt	Urban (central)	LAT 48° 11' 54.00''	177
			LONG 16° 22' 1.00''	
GD	Gaudenzdorf	Urban	LAT 48° 11' 15.53''	179
			LONG 16° 20' 25.91''	
HW	Hohe Warte	Urban (peripheral)	LAT 48° 14' 55.00''	198
			LONG 16° 21' 23.00''	
DF	Donaufeld	Suburban	LAT 48° 15' 27.00''	161
			LONG 16° 26' 0.00''	
R	Seibersdorf	Rural	LAT 47° 58' 35''	185
			LONG 16° 30' 18''	

Table 4. Height [m] of the measuring instruments (from the ground level) for selected weather stations: air temperature (T_a), wind speed (υ), global solar radiation (GSR), relative humidity (RH)

NAME	T_a	υ	GSR	RH
Innere Stadt	9.3	59	9.3	9.3
Gaudenzdorf	3.5	-	-	3.5
Hohe Warte	1.9	35	15	1.9
Donaufeld	2	13	4.5	2
Seibersdorf	2.1	15	13.5	2.1

The specifics of measuring instruments monitoring atmospheric conditions are defined by the WMO standards and guidelines (WMO 2008). This guide proposes a set of requirements that should be met to acquire a representative data sample. For instance, the essential meteorological requirements are discussed, such as the exposure and sitting of the instruments, as well as a range, resolution and accuracy of data acquired.

That being said, certain inconsistency in selected weather stations was observed, especially in terms of the height of the monitoring sensors. The height of the sensors monitoring air temperature and humidity conditions vary as follows: Innere Stadt - 9.3 meters, Gaudenzdorf - 3.5 meters, Hohe Warte - 1.9 meters, Donaufeld - 2 meters, Seibersdorf - 2.1 meters. It can be observed that the elevation of measuring instruments is not uniform. Therefore, the additional set of measurements was performed to account for possible vertical spatial variation. This method was applied in the case of Innere Stadt (IS) area. More about this method will be discussed in the following section.

Figures 23 to 26 show the corresponding used weather stations: Innere Stadt, Donaufeld, Gaudenzdorf, and Hohe Warte, respectively.

Figure 23. Weather Station Innere Stadt (image provided by ZAMG)

Figure 24. Weather Station Donaufeld (image by Fabienne Muriset)

Figure 25. Weather Station Gaudenzdorf (image provided by MA22)

Figure 26. Weather Station Hohe Warte (image provided by ZAMG)

3.4. Vertical profile of air temperature

The analysis of vertical air temperature profile of an urban canyon aims at better understanding of the micro-scale circulation of air mass due to factors such as building density, anthropogenic heat production, traffic intensity, surface properties, etc. (Kanda et al. 2005; Georgakis et al. 2010). Furthermore, the knowledge of how the temperature is distributed within an urban canyon is crucial for the validity of acquired data. In this sense, the additional set of measurements was conducted to illustrate the vertical air temperature profile. This step was essential for estimating possible vertical temperature deviation and if the adjustment of weather data was necessary.

This validation process was performed in IS study area only. As the WMO standards (WMO 2008) recommend the average height of measuring instruments to be of around 2 meters, in the case of stationary weather station IS some inconsistencies were observed. Both temperature and humidity sensors are mounted at the height of 9.3 meters above the ground level. This could lead to some erroneous conclusions when comparing the data, as in the case of other weather stations the sensors are set to mean elevation of around 2 meters above ground level.

The additional set of 10 minute-based measurements was conducted on a calm and sunny day in September 2013, from morning hours until mid-afternoon. This was performed using the mobile weather station mounted on regular two-wheel bicycle (Figure 27), the property of the Department of Building Physics and Building Ecology, Vienna University of Technology. A number of carefully selected sensors were employed to collect the necessary data. They were mounted at the same height of about 1.6 meters, thus being compatible with a mean height of the other stationary weather stations. As already mentioned, this is believed to be the ideal height to measure urban climate (Gartland 2008). The bicycle was equipped with temperature and humidity sensor, a low power anemometer for wind speed (Vector Instruments Type A100L2) and a pyranometer for solar radiation (Skye Instruments), all connected to the same logger (Weatherstation DK-Stat1, Driesen + Kern GmbH). Additionally, the bicycle was equipped with Telaire 7001 CO_2 / temperature monitors connected to two Synotech Onset HOBO data loggers. The overall measurement period covered a sequence of 9 hours, which was assumed to be adequate to assess the vertical temperature profile trend.

Both temperature and relative humidity records from employed mobile weather station were compared to that of stationary weather station IS to assess the extent of possible time-dependent vertical temperature variation and to question if the correction factors should be applied.

Figure 27. The mobile weather station mounted on regular two-wheel bike (image by M. Vuckovic)

3.5. Data analysis

Once the data compatibility is investigated, the assessment of existing UHI intensity in study areas can be performed. Diurnal and seasonal variation has been derived from data sets obtained from stationary weather stations. Data was recorded on an hourly basis.

3.5.1. Data selection for evaluation

The annual weather records representing the year 2012 were used to determine the most suitable datasets for further analysis. The study area IS was chosen as the most appropriate for this evaluation, as it is believed that central urban areas are usually prone to the most extreme microclimatic circumstances, as being the most developed parts of a city (Oke 1987; Saaroni et al. 2000; Voogt 2004).

Given the far-reaching implications of excess urban heat for energy use and human requirements pertaining to health and comfort, the necessity to attenuate microclimatic extremes is essential to maintain environmental quality. Therefore, a comprehensive statistical analysis was applied to define the time frame that reflects the most representative and, in case of summer and winter, the most extreme conditions of the season. The results suggested a time span of three weeks as the most representative for each season.

Figures 28 to 31 illustrate the process of data selection for further analysis. Table 5 summarizes the data range used for seasonal analysis.
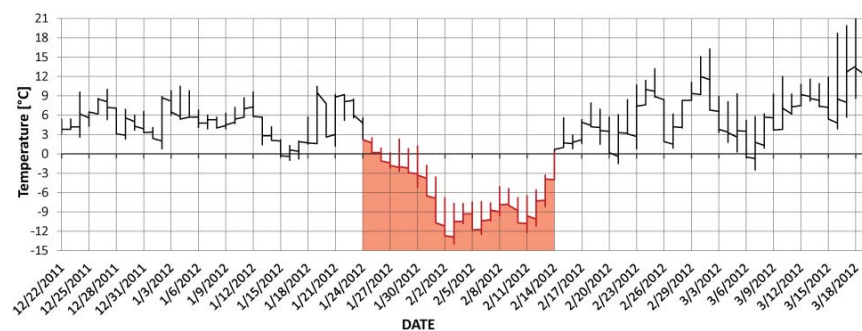
Figure 28. Mean hourly temperature distribution for winter season 2012
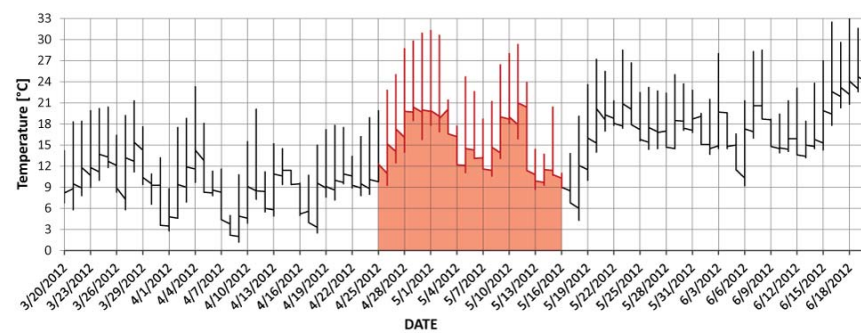
Figure 29. Mean hourly temperature distribution for spring season 2012
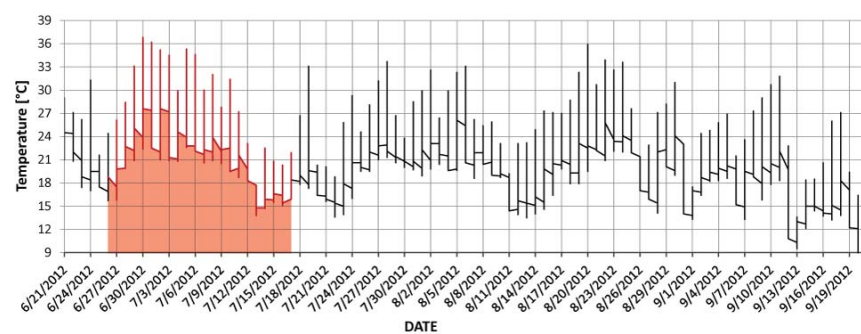
Figure 30. Mean hourly temperature distribution for summer season 2012
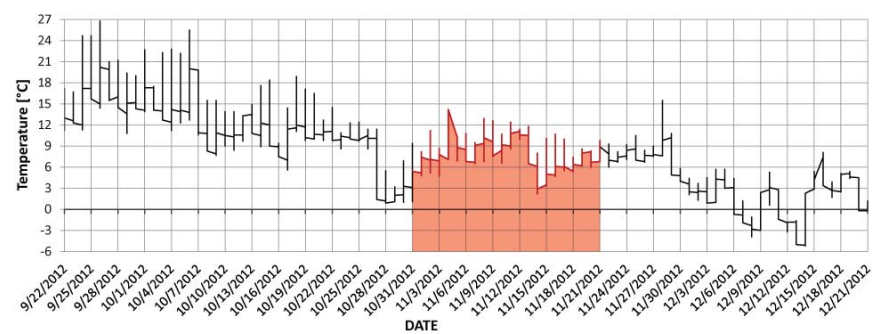
Figure 31. Mean hourly temperature distribution for autumn season 2012

Table 5. Overview of the data sets used for analysis

SEASON	Reference time range	Duration
Winter	25.01.2012 – 14.02.2012	Three-week period
Spring	26.04.2012 – 16.05.2012	Three-week period
Summer	27.06.2012 – 17.07.2012	Three-week period
Autumn	01.11.2012 – 21.11.2012	Three-week period

3.5.2. Seasonal variation

In order to explore the seasonal thermal transitions over different locations, the mean seasonal UHI values were derived for a period of year 2012. As already mentioned, the records from five stationary weather stations operated by ZAMG and MA22 were used for this analysis. The representative time span of three weeks was defined for each season. From these data sets the mean daily hourly data was generated and represented in the course of a reference day, summarizing both characteristic and extreme microclimatic conditions of observed seasons. The calculated reference day represents an hourly-based distribution of climatic circumstances, which is expected to provide an insight into day-night trends, along with seasonal variation of both microclimatic conditions and UHI. This method was then repeated for four representative seasons (winter, spring, summer, and autumn) in order to derive the seasonal patterns from the entire data set.

3.5.3. Diurnal variation

For a more detailed comparison of UHI effects in each of the study areas, UHI intensity values for selected reference week were analyzed. The reference week, representing a hot summer period, was chosen in order to provide an impression of the extent of the UHI effect in the city of Vienna. For this purpose, a period of 7 consecutive hot days in the summer of 2012 (from 29th June to 5th July) was chosen as the most suitable for the analysis of UHI intensity (Figure 32).
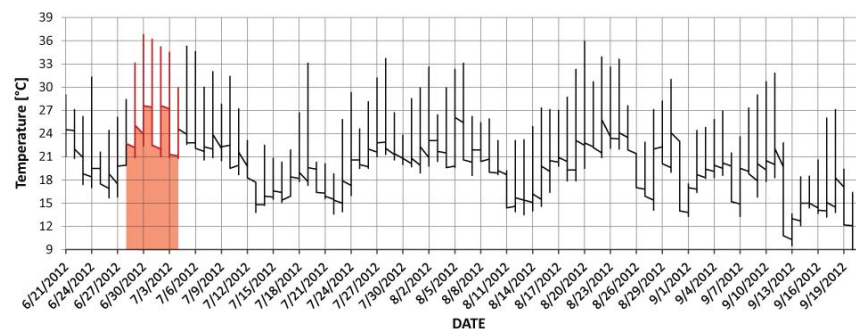
Figure 32. Mean hourly temperature distribution for summer season 2012, representing one-week summer period

First phase of the analysis was focusing on air temperature distribution only, in order to estimate and verify the existence and extent of the UHI effect in different parts of the city. The magnitude of the UHI effect was expressed in terms of Urban Heat Island Intensity ($\Delta\theta$). It should be noted that the Urban Heat Island Intensity is defined in terms of air temperature difference (expressed in K) between simultaneously measured urban and rural temperatures. From the hourly UHI intensity values the cumulative

frequency distribution for the reference week period was calculated. Furthermore, the week-long data sets for each location were processed to present the mean hourly urban temperature and UHI values distribution thus representing the microclimatic conditions for a reference day.

Subsequently, the analysis included the representation of other essential climatic parameters (wind speed, absolute humidity, and global solar radiation). It should be noted that a set of additional formula was applied to further adjust the data, thus making them suitable for a comprehensive comparative analysis.

Firstly, as the height of wind sensors differ across study areas, the data needed to be recalculated at a height relevant for the representation of the street level conditions. For this purpose the wind speed data was recalculated to the height of 1.1 m above ground surface, using Hellman's exponential law (Bañuelos-Ruedas et al. 2011; Urban and Kyselý 2014):

$$\frac{v}{v_{n}} = \left(\frac{H}{H_{n}}\right)\alpha \qquad \text{Eq. 10}$$

where v is the wind speed at height H = 1.1 m, v_{n} is the wind speed at height H_{n}, and α is the friction coefficient (Hellman exponent). Table shows the friction coefficients of various terrains (Sen et al. 2012). For the purpose of this study, the coefficient of 0.25 was used for the rural area (R), 0.30 was used for suburban (DF), and 0.40 for urban areas (IS and HW).

Table 6. Friction coefficient α for a variety of terrains

TERRAIN TYPE	Friction coefficient α
Lake, ocean, and smooth-hard ground	0.10
Foot-high grass on level ground	0.15
Tall crops, hedges, and shrubs	0.20
Heavily forested land	0.25
Small town with some trees and shrubs	0.30
City area with tall buildings	0.40

Secondly, the monitored temperature and relative humidity data were used to derive the absolute humidity values. A set of equations was applied to assess this parameter.

First the saturation vapor pressure was calculated using the following formula:

$$E = 611.2 * \exp\left(17.08085 * T_{a} / (234.175 + T_{a})\right) \ [Pa] \qquad \text{Eq. 11}$$

where E is the saturation vapor pressure and T_a is the air temperature in °C.

These results were then used to derive the vapor pressure following this formula:

$$e = \varphi * E / 100 \qquad\qquad\qquad [Pa] \qquad\qquad Eq.\ 12$$

where φ is the relative humidity, and e is the vapour pressure.

Lastly, the vapor pressure was used to calculate the absolute humidity:

$$AH = e / (R * (273.15 + T_a)) \qquad\qquad [kg/m^3] \qquad\qquad Eq.\ 13$$

where AH is the absolute humidity, R is individual gas constant of water (R=461.52 [J/kg·K]), and T_a is the air temperature expressed in °C.

Additionally, it should be noted that the values of absolute humidity were further multiplied by 1000 in order to translate kilograms into grams, thus having the g/m^3 as the final unit.

3.6. Definition of aggregate variables

To understand the very complexity behind the UHI phenomenon, manifold mutual interactions between urbanization and climatic factors should be explored. It is believed that the UHI and its manifestation within the urban environment are intensified by the geometric and thermal properties of an urban domain (e.g. SVF, H/W, building density, albedo, emissivity, etc.) (Taha 1997; Ali-Toudert and Mayer 2006; Jenerette et al. 2007). Furthermore, it is likely that the factors which might cause higher urban temperatures can in turn display certain spatial variability. The combination, spatial distribution and quantity of these factors determine the way in which the heat is absorbed, stored, released and dispersed within the urban environment. This will be further expressed as a temperature increase in an urban area.

In this light, the first step was to define a complete set of salient variables in order to accurately describe the urban topographic, surface cover characteristics and physical properties of an area. Second step was to provide a numeric description of these variables, thus making them easily comparable and accessible for further analysis.

Figure 33 illustrates the main processes affecting the energy balance of an urban area and thus contributing to the UHI phenomenon.
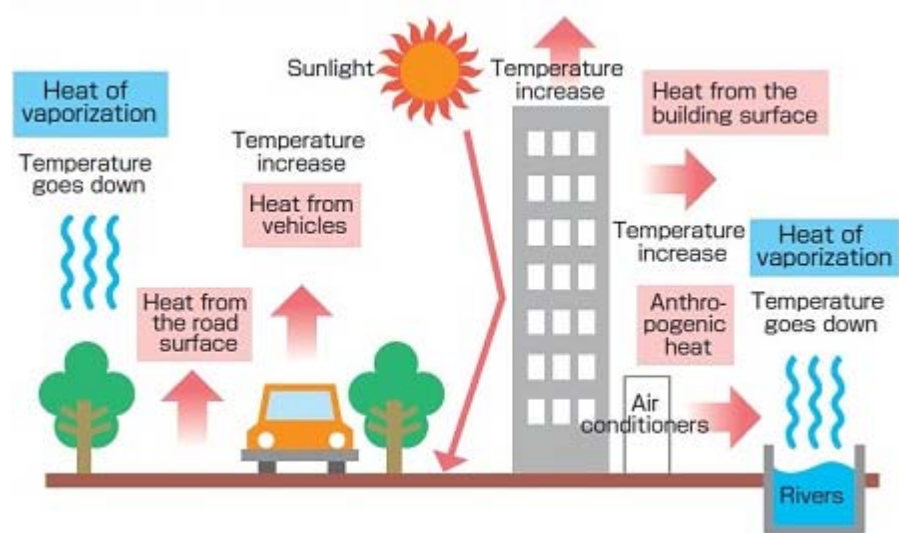
Figure 33. Schematic depiction of the main processes affecting the energy balance of an urban area (source: http://www.gardinergreenribbon.com)

3.6.1. Geometric features of urban environment

The urban geometric parameters were defined and computed for the process of a complete specification and identification of urban morphology of an U2O. Parameters include sky view factor, aspect ratio, built area fraction, unbuilt are fraction, impervious surface fraction, pervious surface fraction, equivalent building height, effective mean compactness, built surface fraction, and mean sea level. These parameters are likely to differ across the city in a very variable manner.

The following table summarizes the general list of derived variables with explanatory specifications, including information regarding the unit, symbol used, and expected value range.

Table 7. Variables to capture the geometric properties of an U2O

GEOMETRIC PROPERTIES	UNIT	SYMBOL	RANGE
Sky View Factor	-	ψ_{sky}	0-1
Aspect ratio	-	H/W	0-3+
Built area fraction	-	$BAF = A_b / A_{tot}$ $A_{tot} = A_b + A_u$	0-1
Unbuilt area fraction	-	$UAF = 1 - BAF$	0-1
Impervious surface fraction	-	ISF	0-1
Pervious surface fraction	-	$PSF = (A_e + A_g + A_{H2O}) / A_{tot}$	0-1
Bare soil fraction	-	A_e / A_{tot}	-
Green area fraction	-	A_g / A_{tot}	-
Water bodies fraction	-	A_{H2O} / A_{tot}	-
Equivalent building height	m	$h_e = V_b / A_{tot}$	-
Built surface fraction	-	$BSF = A_s / A_b$ $A_s = A_w + A_R$	>1
Wall fraction	-	A_W / A_b	>1
Roof fraction	-	A_R / A_b $A_R = A_{R,i} + A_{R,p}$	~1
Impervious roof fraction	-	$A_{R,i} / A_b$	~1
Pervious roof fraction	-	$A_{R,p} / A_b$	~1
Effective mean compactness	m	$l_c = V_b / (A_s + A_u)$	-
Mean sea level	m	h_{sl}	-

3.6.2. Physical features of urban environment

The physical properties describe the thermal characteristics of urban surfaces. Parameters include albedo, emissivity, heat capacity, thermal conductivity, and density. In addition to this, the anthropogenic heat output was introduced as a principal factor affecting the energy balance of the urban environment.

The following table summarizes the general list of derived variables with explanatory specifications, including information regarding the unit, symbol used and value range. It should be noted that, besides the semantic (material-related) urban features, the anthropogenic heat output is presented within the same table.

Table 8. Variables to capture surface/material properties of an U2O

SURFACE PROPERTIES	UNIT	SYMBOL	RANGE
Reflectance/Albedo	-	α_{sw}	0-1
Emissivity	-	ε_{lw}	0-1
Thermal conductivity		$\lambda = (\lambda_i, \lambda_p)$	-
Impervious surface	$W \cdot m^{-1} \cdot K^{-1}$	λ_i	-
Pervious surface		λ_p	-
Specific heat capacity		$c = (c_i, c_p)$	-
Impervious surface	$J \cdot kg^{-1} \cdot K^{-1}$	c_i	-
Pervious surface		c_p	-
Density		$\rho = (\rho_i, \rho_p)$	-
Impervious surface	$kg \cdot m^{-3}$	ρ_i	-
Pervious surface		ρ_p	-
Anthropogenic heat output		$Q_F = Q_V + Q_H + Q_M$	-
Vehicles		Q_V	-
Buildings	$kWh \cdot m^{-2} \cdot a^{-1}$	Q_H	-
Human activity		Q_M	-

3.7. GIS-supported values extraction

In this chapter, the emerging GIS technology is presented as an operational solution for comprehensive urban form analysis. Extensive collaborative efforts have been made to develop a Python-based framework incorporated into the GIS tool for the automated calculation of the salient geometric and physical features of an urban environment (Glawischnig et al. 2014a; Glawischnig et al. 2014b; Hammerberg 2014).

3.7.1. Application of QGIS software

A Geographical Information System (GIS) is advanced software that allows users to create, visualize, query and analyse geospatial data (Campbell and Shin 2011). Quantum GIS (QGIS) is an Open Source Geographic Information System. The results of the analysis may be shown on a map, making them easy to visualize, but are also tabulated into a report to support management decisions (Figure 34).
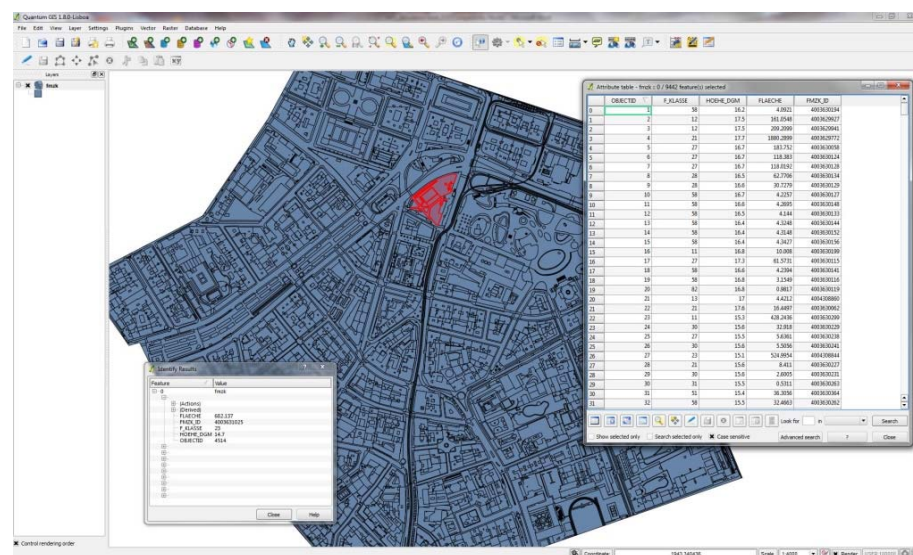
Figure 34. QGIS user interface, example of U2O Innere Stadt (image extracted from the data provided by MA22)

Li et al. (2004) tested the potential of a GIS environment to visually represent links between the climatic factors and urban geometry. SVF is utilized here as an indicator of urban form performance for supporting climatic design decision making. The case study illustrated the advantages of precision and speed of SVF computation, which can be achieved through the development of GIS-based spatial analysis tools.

Another study focused on calculations of building morphological parameters as a function of land use type (Burian et al. 2005). This research revealed a comprehensive method to efficiently compute building

morphological parameters for mesoscale meteorological and air quality modeling applications. Synthesis of their results indicated that the urban morphological parameters vary significantly between different land uses.

Skelhorn et al. (2012) went one step further and presented results of their research based on developing an urban canopy layer (UCL) model that will integrate the urban microclimate and related impacts on building energy consumption. They introduced the GIS environment as the suitable tool that allows a very accurate representation of urban geometry and integrated GIS with object-oriented programming languages that are able to represent and manipulate 2.5D or 3D objects. Furthermore, the selected object-oriented scripting language is then utilized to perform the dynamic routines required for determining changes over time.

It can be concluded that the primary benefit of GIS is the ability to interrelate spatially multiple types of information assembled from a range of sources. Furthermore, GIS allows the user to automate a certain process, thus making the analysis easier, faster, and more accurate.

3.7.2. Calculation methods

Comprehensive data sets provided by the city of Vienna were used to derive the specific values of the abovementioned variables (Glawischnig et al. 2014a; Glawischnig et al. 2014b; Vuckovic et al. 2014). The data was provided in the form of a base map, referred here as the Vienna base map.

3.7.3. Vienna base map

Vienna base map represents a collection of polygons with associated building height data (which indicates the height of the building eaves) and combined with text-based attribute information. It should be noted that used base map represents a simplified urban surface made up of flat-roofed buildings only. The text-based attribute information represents the essential non-spatial information (Figure 35). This collection of information is stored in a table as an attribute and linked to the each entity of the base map by a unique identifier, making them easily distinguished and combined using specific land use type or classes (e.g. building, street, water bodies, vegetation, etc.), geometric features (e.g. area, length, volume, etc.), and semantic features (e.g. number of building storeys, building age, building type, etc.). The essential U2O variables were calculated by combining all necessary classes of Vienna base map within a Python Script Module and producing the final value.
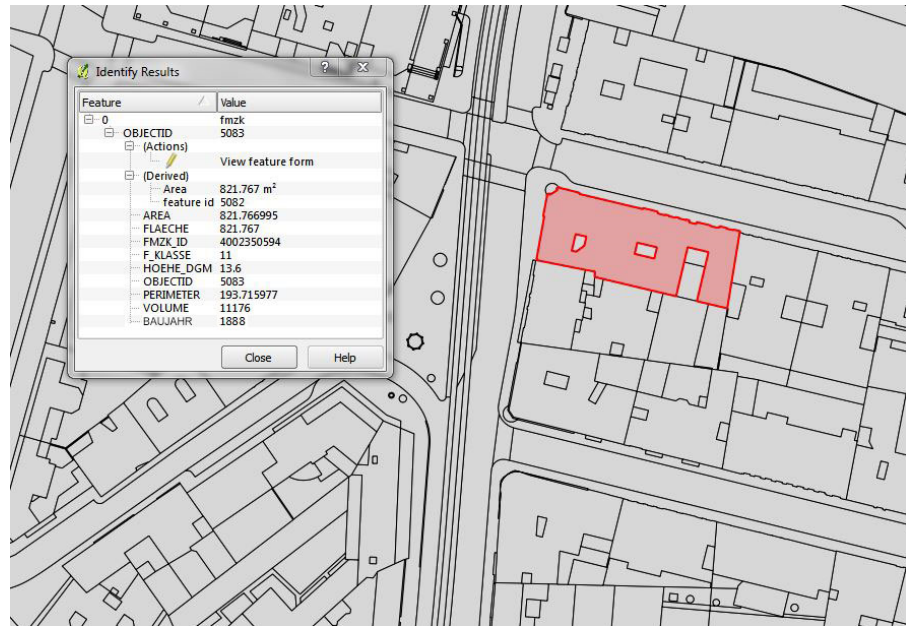
Figure 35. Vienna base map with selected building entity and essential non-spatial information (image extracted from the data provided by MA22)

3.7.4. Geometric features

Following sections discuss the advanced methods used to calculate geometric attributes of an U2O. As the urban structure is believed to be an essential aspect in the process of the formation of UHI, the essential information regarding the urban morphology can be considered crucial when explaining and parameterizing its intensity.

3.7.4.1. Sky View factor

In order to calculate the SVF for the selected areas in the city of Vienna, the method of continuous shadow casting (CSC) introduced by Richens (1997) was used (Glawischnig et al. 2014b; Hammerberg 2014; Hammerberg and Mahdavi 2014). For this purpose, a Digital Elevation Model (DEM), including all buildings, trees and obstructions, was used as the input. Richens's central algorithm computes the shadow volume created from a hypothetical light source vector by continuously offsetting and decreasing the height of a DEM along the vector. To compute the areal SVF, 1000 new light sources across the sky hemisphere were defined, and the described method was repeated. Finally, the SVF was computed as the ratio of a number of times that a certain pixel is lit to the total number of light sources.

Although this method has been validated in several occasions (Brown et al. 2001; Lindberg 2005), a case of overestimation of SVF was still detected in applied algorithm. This error was namely present due to the missing spatial

information beyond the boundary of the DEMs used, thus creating the false areas of high SVF values. Therefore, the applied algorithm was slightly modified to avoid the erroneous information along the boundary line of the DEM (namely by introducing the buffer zone along the perimeter of DEM), and to better suit the used GIS environment (Hammerberg 2014; Hammerberg and Mahdavi 2014).

3.7.4.2. Aspect ratio

To derive the aspect ratio values for the observed areas in the city of Vienna, a principle based on a well-established spatial concept was used. This concept namely implies the introduction of Delaunay triangulation method (Glawischnig et al. 2014a; Glawischnig et al. 2014b). A Delaunay triangulation considers generation of a polygonal mesh that simplifies the geometric domain. In this case, centroids of building blocks are connected to form triangulated network from which the aspect ratio will be derived (Figure 36). A building block is defined as a spatial enclosure consisting of a number of buildings that are logically and spatially enclosed by streets. Furthermore, the buildings facing the streets are identified within each triangle, and for each pair of facing buildings both the distance (street canyon width) and average building height are computed. Having in mind the non-uniform composition of an urban area, especially in terms of the varying widths of street segments, the aspect ratio can be computed using either the minimum, mean or median width of street canyons.

Figure 36. Delaunay triangulation with building blocks centroids computed for the Innere Stadt area (source: Glawischnig et al. 2014a)

3.7.4.3. Built and unbuilt area fraction

Built area (A_b) and Unbuilt area (A_u), both expressed in m², together make the total ground area of the area of interest (A_{tot}):

$$A_{tot} = A_b + A_u \qquad\qquad \text{[m}^2\text{]} \qquad\qquad \text{Eq. 14}$$

Built area fraction (BAF) is referred to as the ratio of building plan area to total ground area. More precisely, built area fraction presents the fraction of the ground surface with building cover. It can be expressed as follows:

$$BAF = \frac{\sum A_b}{A_{tot}} \qquad\qquad\qquad \text{Eq. 15}$$

where A_b [m²] represents building plan area at ground level (the footprint of a building) and A_{tot} [m²] represents total ground area of the area of interest. The computed value of the built area fraction is dependent on the size of the area and heterogeneous nature of the urban landscape. This value was derived for the observed area in a form of a factor, as a dimensionless number.

Unbuilt area fraction (UAF or 1-BAF) is defined as the ratio of unbuilt surface area to total ground area. More precisely, it is a fraction of the ground surface without building cover, as follows:

$$UAF = 1 - \frac{\sum A_b}{A_{tot}} = 1 - BAF \qquad\qquad \text{Eq. 16}$$

UAF is further divided into Impervious and Pervious surface fraction, in order to account for different types of surfaces that are fundamental in the processes of evaporation, as well as for their thermal properties.

These variables can be calculated using two distinct methods. One method requires the employment of the Analysis Tools – Basic statistics functionality provided in GIS. By selecting the appropriate land use class, the basic computation (e.g. calculating the area) can be performed on the selected polygons only, by defining the target field (in this case AREA information associated with each polygon). This procedure will result in listing the essential statistical information, such as the mean value, standard deviation, the total sum, the minimum value, the maximum value, etc. This process was further repeated to derive the total ground area (by selecting all polygons of base map), and subsequently, the total unbuilt area values. Figure 37 illustrates the selection process and output for the Built

area (A_b) variable. The final product of this method is a number (e.g. total built area, total ground area, total unbuilt area, etc.). Therefore, additional manual calculations must be performed to assess the final value of a specific U2O variable (e.g. $\frac{A_b}{A_{tot}}$).

Figure 37. The selection process and output of the Built area U2O variable (image extracted from the data provided by MA22)

The second method introduces the specific set of geometry-based spatial algorithms developed within the Python Script Module (Glawischnig et al. 2014a; Glawischnig et al. 2014b). These algorithms follow the defined formula for each geometric feature and further combine all necessary classes of polygons of Vienna base map to calculate the final value. The end result is the complete U2O variable (e.g. Built area fraction). Therefore, this method requires minimal user interaction and supports the automated calculation of the microclimatic attributes of an U2O.

Both methods were employed to derive all essential geometric features of a U2O, which allowed for a comparison and validation of developed algorithms.

3.7.4.4. Impervious and pervious surface fraction

Impervious surface fraction (ISF) is defined as the ratio of unbuilt impervious surface area (e.g. paved, sealed) to total ground area, as follows:

$$ISF = \frac{\sum A_{u(i)}}{A_{tot}} \qquad \text{Eq. 17}$$

where $A_{u(i)}$ [m²] represents the unbuilt impervious surface area. This value was derived for the observed area in the form of a factor, as a dimensionless number.

Pervious surface fraction (PSF) is defined as the ratio of unbuilt pervious surface area to total ground area:

$$PSF = \frac{\sum A_{u(p)}}{A_{tot}}$$

Eq. 18

where $A_{u(p)}$ [m²] represents the unbuilt pervious surface area. It summarizes the total amount of surfaces covered with bare soil, vegetation, and water bodies within the observed location, as follows:

$$A_{u(p)} = (A_e + A_g + A_{H2O}) / A_{tot}$$

Eq. 19

where A_e represents the bare soil surface area, A_g represents the green surface area, and A_{H2O} represents the water body surface area, all expressed in m². This value was derived for the observed area in the form of a factor, as a dimensionless number.

As the UAF is a function of ISF and PSF, an additional validation of accuracy of the calculated values can be performed using the following equation, which will in turn determine if the calculation error is present:

$$UAF = A_{u(i)} + A_{u(p)}$$

Eq. 20

The same calculation principle, as described in the previous section, was used to derive total unbuilt pervious and impervious area values. Figure 38 illustrates selection process and output for unbuilt pervious green area variable.

Figure 38. The selection process and output of the Unbuilt pervious green area U2O variable (image extracted from the data provided by MA22)

3.7.4.5. Equivalent building height

Equivalent building height (h_e) is referred to as the ratio of built volume (more precisely, the total volume of built structures above terrain) to total built area, as follows:

$$h_e = \frac{\sum V_b}{A_{tot}} \qquad\qquad [m] \qquad\qquad Eq. 21$$

where V_b [m³] represents the building volume. This parameter is expressed in meters. The same principle, as described in previous sections, was used to derive the total built volume value.

3.7.4.6. Built surface fraction

As materials applied to the exposed surfaces of the buildings (outer walls and rooftops) define specific physical properties (such as reflectance, emissivity, thermal conductivity, etc.), built surface fraction will further demonstrate to what extent the surrounding environment can be affected by material's ability to absorb and release thermal energy.

Built surface fraction (BSF) is defined as the ratio of total built surface area (considering only horizontal and vertical surfaces above terrain - facades and roofs) to total built area. BSF can be expressed as follows:

$$BSF = \frac{\sum A_s}{A_b} \qquad\qquad Eq. 22$$

where A_s [m^2] represents the total built surface area, and A_b [m^2] represents building plan area at ground level. This value was derived for the observed area in the form of a factor, as a dimensionless number.

The A_s summarizes the total amount of horizontal surfaces (walls) and vertical surfaces (roofs), wherein roofs are observed as being flat throughout the area of interest, as follows:

$$A_s = (A_w + A_{R,i} + A_{R,p}) / A_b \qquad \text{Eq. 23}$$

where A_w [m^2] represents the total wall area above terrain (only surfaces exposed to the outdoor environment were taken into account), $A_{R,i}$ [m^2] represents total impervious roof area, and $A_{R,p}$ [m^2] represents total pervious roof area.

To derive these factors all building polygons within base map were separated into distinct line features. This method allowed for adjacent walls (shared between two buildings) to be identified and excluded from the calculation as the focus was set on capturing the exterior walls only. Once the wall surface is calculated, the roof area is added to the calculation (Glawischnig et al. 2014a; Glawischnig et al. 2014b).

3.7.4.7. Effective mean compactness

Effective mean compactness (l_c) is referred to as the ratio of built volume (more precisely, the total volume of built structures above terrain) to total surface skin of the U2O (the sum of exposed surfaces of the buildings - outer walls and rooftops, and the unbuilt surface area - streets, pavements, etc.), as follows:

$$l_c = \frac{\Sigma V_b}{A_s + A_u} \qquad\qquad \text{[m]} \qquad\qquad \text{Eq. 24}$$

3.7.4.8. Mean sea level

Mean sea level (h_{sl}) represents the average height of the ocean's surface used as a standard in evaluating land elevation. This parameter is expressed in meters. This information was acquired from features included within base map and their respective attributes (absolute height feature).

3.7.5. Physical features

The information pertaining to A_b, $A_{u(i)}$, $A_{u(p)}$, and A_s, was used as a basis for calculation of physical properties of an U2O. The information about material's specific physical features (albedo, emissivity, heat capacity, thermal conductivity and density) was linked to the representative area information (e.g. wall area, roof area, green area, etc.).

The general method used to derive these variables was based on the concept of a weighted average. The first step was to assess the total effective surface area (only surfaces exposed to the outdoor environment were taken into account) for each type of surfaces/materials in the U2O. Once these values are derived, the coverage percentage was then obtained in regard to the total built and unbuilt surface area (A_s, $A_{u(i)}$, and $A_{u(p)}$). This information was used as a respective weight for further calculation. Lastly, the total value is then obtained for each surface by multiplying the surface area weight (expressed in percentage) by the value of respective physical property, and summarizing the values for all pervious and impervious surfaces. The detailed information regarding the respective physical properties was obtained from the literature.

3.7.5.1. Albedo

Albedo (α_{sw}), or reflection coefficient, is the diffuse reflectivity or reflecting power of a surface (Oke 1987). Generally, albedo is associated with colour, with lighter colours being more reflective. Albedo is expressed as a percentage and is measured on a scale from zero (for no reflection of a perfectly black surface) to 1 (for perfect reflection of a white surface). It is a dimensionless parameter.

The information from the table of thermal properties of typical urban materials defined by Arnfield (1982) and Oke (1987) was used as a basis for this estimation (Table 9). Additionally, Table 9 provides information pertaining to the exact albedo values used for this study. These values were namely adopted from the work of Arnfield (1982) to simplify the computation process. Arnfield provided the mean albedo values for each material, while Oke (1987) provided a range of albedo values that represents the respective albedo values of both sunny and shaded materials. However, in case where the data was not provided, the respective value was adopted from the work of Oke (1987). It should be noted that in case of vegetation, and especially trees, the information related to the respective albedo value was acquired from the work of Akbari (2009).

Table 9. Albedo values of typical urban materials

SURFACE	MATERIAL	ALBEDO		USED
		Oke (1987)	*Arnfield (1982)*	
Ground	Asphalt	0.05 - 0.20	0.10	0.10
	Soil	0.35	-	0.35
Wall	Concrete	0.10 - 0.35	0.27	0.27
	Brick	0.20 - 0.40	0.32	0.32
Roof	Tar and gravel	0.08 - 0.18	0.14	0.14
	Tile	0.10 - 0.35	-	0.3
Window	Zenith angle less than 40°	0.08	0.09	0.09
	Zenith angle 40 to 80°	0.09 – 0.52	0.09	0.09
Vegetation	Trees	-	-	0.18
Urban area	Range	0.10 – 0.27	-	-
	Mean	0.15	-	-

3.7.5.2. Emissivity

The emittance of a material (ε_{lw}) refers to its ability to release absorbed heat (Oke 1987; Hens 2012). Thus, the emissivity is the ability of a surface to emit energy by radiation (longwave). It is common to discuss the predefined emissivity of a certain material, which means that materials usually have the emissivity values defined account of their nature. Emissivity ranges from 0 to 1 and is a dimensionless parameter.

The information from the table of thermal properties of typical urban materials defined by Oke (1987) was used as a basis for this estimation (Table 10). Additionally, Table 10 provides information pertaining to the exact emissivity values used for this study. It should be noted that in the case where the value was presented in the form of a range (illustrating emissivity values of both sunny and shaded materials), the middle value was adopted.

Table 10. Emissivity values of typical urban materials

SURFACE	MATERIAL	EMISSIVITY Oke (1987)	USED
Ground	Asphalt	0.95	0.95
	Soil	0.92	0.92
Wall	Concrete	0.71 – 0.90	0.80
	Brick	0.90 - 0.92	0.90
Roof	Tar and gravel	0.92	0.92
	Tile	0.90	0.90
Window	Zenith angle less than 40°	0.87 – 0.94	0.92
	Zenith angle 40 to 80°	0.87 – 0.94	0.92
Vegetation	Trees	-	-
Urban area	Range	0.85 – 0.96	-
	Mean	~0.95	-

3.7.5.3. Thermal admittance

Thermal conductivity (λ) is the property of a material's ability to conduct heat (Hens 2012). Heat transfer occurs at a higher rate across materials of high thermal conductivity than across materials of low thermal conductivity. The unit of thermal conductivity is $Wm^{-1}K^{-1}$.

Specific heat capacity (c) is a measurable physical quantity that characterizes the amount of heat required to change the body's temperature by a given quantity (Hens 2012). The unit of specific heat capacity is $Jkg^{-1}K^{-1}$.

Density (ρ) of the material is a quantitative expression of the amount of mass contained per unit volume (Hens 2012). The unit of density is kgm^{-3}.

These values are dependent upon the nature of the material. For the purpose of this research, materials were divided into two groups: pervious and impervious, and for both the values were determined. The standard values obtained from the 2009 ASHRAE Handbook - Fundamentals were used for this calculation (ASHRAE 2009).

Table 11 provides a summary of standard values obtained from the 2009 ASHRAE Handbook - Fundamentals.

Table 11. λ, c, and ρ values of typical urban materials

SURFACE	MATERIAL	λ	c	ρ
Ground	Asphalt	0.74	920	2110
	Soil	0.064	800	1500
Wall	Concrete	0.93	653	2300
	Brick	0.70	800	1970
Roof	Tar and gravel	0.88	2500	1100
	Tile	0.84	800	1900
Window	Zenith angle less than 40°	1.05	840	2600
	Zenith angle 40 to 80°	1.05	840	2600

Together, thermal conductivity, specific heat capacity and density form a quantity called Thermal Admittance (b). Thermal admittance illustrates to what extent built assemblies absorb and release heat (Hens 2012). The higher the value, the larger is the absorption under fluctuating surface temperature conditions. Admittance is expressed in $Jm^{-2}s^{1/2}K^{-1}$. It can be calculated as follows:

$$b = \sqrt{\lambda c \rho} \qquad\qquad [Jm^{-2}s^{1/2}K^{-1}] \qquad\qquad Eq.\ 25$$

3.7.5.4. Anthropogenic heat output

As it was mentioned before, the anthropogenic heat (Q_F) denotes the heat released inside the structure either intentionally as space heating (e.g. heaters, furnace heated air, etc.), as a by-product of other activities (e.g. cooking, lighting, electrical appliances, etc.), by vehicles, and including the metabolic release of the human occupants (Smith et al. 2009). For the purpose of this research, the anthropogenic heat was further divided into three components: the heat produced by combustion of vehicle fuels (Q_V), followed by the Q_H that denotes the heat released from stationary sources (primarily within buildings), and Q_M as the heat released by human activity. For each component, the mean values were derived. The final parameter is expressed as the sum of the components presented above.

Q_V was defined as the annual average heat emitted by one car multiplied by the number of vehicles circulating within the source area. Due to lack of precise information regarding the total heat emitted by numerous vehicle types (diesel vehicles, gasoline, natural gas, etc.), the annual average heat emitted by one car was adopted from the literature (Grimmond 1992; Sailor 2009). The information regarding the car ownership rate was obtained from the Statistics Austria website (Statistics Austria). The general form of the equation is as follows:

$$Q_V = \frac{\sum(NHE_v \, n_v \, A_r \, 365 days)}{A_{tot}} \qquad \text{[kWh m}^{-2}\text{a}^{-1}\text{]} \qquad \text{Eq. 26}$$

where NHE_v is the net heat emission from one vehicle per m² (the cumulative heat emission for a 24-hour cycle), n_v is the number of vehicles, A_r is the effective road area, A_{tot} is the source area (area of an U2O).

A range of data was used to calculate Q_H. The used parameters pertain to the average energy consumption according to the construction age of the building, the total number of floors of a building, the building floor area (building footprint), and the total U2O ground area. The general form of the equation is as follows:

$$Q_H = \frac{\sum(E_{tot} \, n_f \, A_b)}{A_{tot}} \qquad \text{[kWh m}^{-2}\text{a}^{-1}\text{]} \qquad \text{Eq. 27}$$

where E_{tot} is the energy consumption of a building, n_f is the number of floors, A_b is the floor area, and A_{tot} is the source area (area of an U2O). The necessary information regarding the buildings' energy consumption (Table 12) was acquired from the Energy Certificate Standards for Austria (Vonkilch 2009).

Table 12. Overview of energy consumption of certain types of buildings according to the construction age

CONSTRUCTION TYPE	YEAR	ENERGY EFFICIENCY RATING	REQUIREMENTS [kWh/m²a]
Old construction	1900	D,E,F,G	120 - 350
Post war construction	1950	F,G	200 - 400
1970th buildings	1970	D,E,F,G	100 - 300
1990th buildings	1990	C	75 - 100
New construction	2009	A,B	25 - 75

To calculate Q_M the information from the table of metabolic rates defined by Fanger (1970) was used, along with the total number of people within the study area, distributed across the area of the observed U2O. It can be expressed as follows:

$$Q_M = \frac{n\,M\,365days}{A_{tot}} \qquad [\text{kWh m}^{-2}\,\text{a}^{-1}] \qquad \text{Eq. 28}$$

where n represents the population number (information acquired from the Statistics of Austria), M is the average metabolic rate, and A_{tot} is the source area (area of an U2O). The necessary information regarding the adult human metabolic heat production at different levels of activity is presented in Table 13.

Table 13. Adult human metabolic heat production (Q_M), at different levels of activity (after Fanger 1970)

ACTIVITY	APPROXIMATE METABOLIC RATE	
	W	W m⁻²
Resting		
Sleeping	70	40
Seated, quiet	100	60
Standing, relaxed	120	70
Walking		
Level, 3.2 km h⁻¹	200	120
Level, 5.6 km h⁻¹	320	190
Level, 8.0 km h⁻¹	570	340
Occupational		
Office work	90 – 120	50 – 70
Driving	100 – 200	60 – 120
Domestic work	160 - 350	90 - 200

3.8. Statistical Modelling of UHI

Regression analysis was used to explore the relationship between each U2O variable and respective seasonal UHI. Furthermore, Least-Squares Fitting method was used to estimate the cumulative effect of a number of U2O variables on respective UHI intensity.

3.8.1. Correlation analysis

Once U2O's respective geometric (morphological) and semantic (material-related) variables are derived, possible relationships between these factors and the UHI intensity are investigated. For the statistical analysis, the MS Excel Analysis ToolPak was used to estimate the degree of agreement between the observed variables. Firstly, the same hourly-based datasets as for the seasonal variation analysis were used. To further investigate the temporal nature of UHI, additional factors were introduced. In this sense, the notion of Cumulative Temperature Increase (CTI) is applied to systematically address the relationships between the variables and UHI effect (Musco 2015). CTI can be understood as an original measure of "overheating". CTI is computed as the cumulative sum of all positive $\Delta\theta$ values in the course of a reference day. It can be calculated as follows:

$$CTI = \sum_{i=1}^{24} (\theta_{U,i} - \theta_{R,i}), \text{ subject to: } \theta_{U,i} > \theta_{R,I} \qquad \text{[Kh]} \qquad \text{Eq. 29}$$

where $\theta_{U,i}$ is the urban temperature at specific hour, and $\theta_{R,i}$ is the rural temperature at specific hour. The unit is [Kh]. The CTI factors are further computed for all four seasons. This method was chosen as the most suitable to capture the amplitude of positive $\Delta\theta$ values in a single factor.

In general, the CTI values are expected to outline the total heat retained within an urban system, thus providing a comprehensive understanding of distinctive link between the salient variables and their role in the formation of UHIs. Once the seasonal CTI factors are derived, the relation between these factors and predetermined variables of built environment is assessed, in order to prove or disprove hypotheses about correlational relationships. For this purpose, the regression analysis was employed, and data was plotted on scatter plots, which allowed for the degree of correlation to be displayed.

3.8.2. Predictive model

Once the correlation analysis was performed, the cumulative effect of a number of U2O variables on respective CTI values was investigated. These variables were chosen based on their relevance, degree of correlation with the CTI values, and to avoid the redundancy of U2O variables. To find appropriate parameters for the predictive model, a simple linear regression between U2O variables and respective UHI intensity is computed. The parameters were estimated with the Least-Squares Fitting method. This method was documented in numerous occasions as suitable for solving similar kind of computational challenges (Hoffmann et al. 2012; Szymanowski and Kryza 2012; László and Szegedi 2014). Data fitting was performed using the MATLAB® software (MathWorks®).

The general form of the model is given by:

$$CTI = \beta_0 + \beta_1 \cdot \psi_{sky} + \beta_2 \cdot H/W + \beta_3 \cdot ISF + \beta_4 \cdot PSF + \beta_5 \cdot h_e +$$
$$\beta_6 \cdot BSF + \beta_7 \cdot l_c + \beta_8 \cdot \alpha_{sw} \qquad [Kh] \qquad\qquad \text{Eq. 30}$$

where CTI is the computed seasonal measure of overheating, β_0 to β_8 are regression coefficients, and ψ_{sky}, H/W, ISF, PSF, h_e, BSF, l_c and α_{sw} are the mean spatial values of the selected U2O variables for the U2O in question.

In general, the Least-Squares method aims at minimizing the sum of squared deviations of the measured values (expressed as a function of dependent variables - in this case the U2O variables) from those predicted by the model (Hill and Lewicki 2005). Specifically, it can be express as follows:

$$Q = \sum [\hat{y}_i - f_i(x)]^2 \qquad\qquad\qquad \text{Eq. 31}$$

where Q represents the sum of squared deviations, $\hat{y}_i$ is the predicted value, and $f_i(x)$ is a known function of form $y_i = f_i(x)$.

The MATLAB® function lsqr(A,b,tol,maxit) was used as the core solver to solve the system of linear equations with specified tolerance (set to default) and maximum number of iterations (set to 100). The MATLAB® code is provided within the Appendix.

In addition, the statistical significance of the computed model is calculated numerically, by the means of R-square (Coefficient of determination) and Root Mean Square Error (RMSE). Both measures are included into the developed MATLAB® code. First indicator defines the ratio of the sum of squares of the regression (SSR) and the total sum of squares (SST) (Rawlings et al. 1998). R-square ranges from zero to one, indicating how close the

data are to the fitted regression line (value of 1 indicates a perfect fit). It is given by:

$$R^2 = \frac{SSR}{SST} = \frac{\sum(\hat{y}_i - \bar{y}_i)}{\sum(y_i - \bar{y}_i)}$$

Eq. 32

where $\hat{y}_i$ is the predicted dependent variable, $\bar{y}_i$ is the mean value of the measured dependent variable, and y_i is the measured dependent variable. The second indicator is the square root of the variance of the residuals, where lower values indicate a better fit. While the R-square can be understood as the measure of fit between the observed and the predicted values, the RMSE is the measure of the goodness-of-fit of the model (Lewis-Beck 2004). It is given by:

$$RMSE = \sqrt{\frac{\sum(y_i - \hat{y}_i)^2}{n}}$$

Eq. 33

where n is the sample size.

4.   Results and Discussion

4.1.   Overview

The following chapter summarizes the results of the methodology that was developed and discussed in the previous section. Furthermore, this chapter offers a thorough discussion of the issues related to the urban microclimate and its temporal and spatial variation. Hence, the potential to observe and understand microclimatic processes and associated variation across a range of urban domains, while reflecting on the main driving factors to this variation, was explored.

4.2.   Vertical profile of air temperature

Figure 39 shows the simultaneously measured temperature values for mobile and stationary (IS) weather stations, obtained on 25th of September, in an urban canyon within the U2O area Innere Stadt. Figure 40 shows, for the same period, the simultaneously measured humidity values for mobile and stationary weather station. For the ease of comparison between two profiles, the hourly deviation ($\Delta\theta$/ΔRH) was plotted within the same graph.
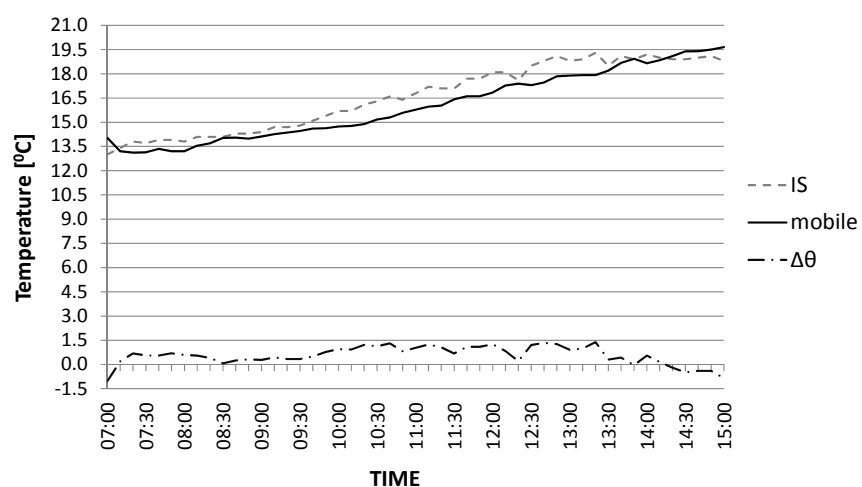
Figure 39. Vertical profile of air temperature in urban canyon (Innere Stadt)
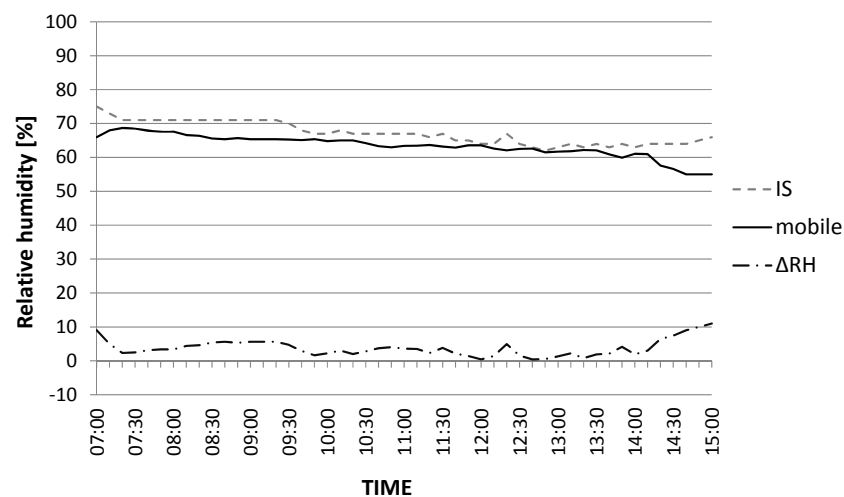
Figure 40. Vertical profile of humidity in urban canyon (Innere Stadt)

The results show that the existing difference between the two profiles is not significant and results in a little change within a 7.5 meter vertical profile. In case of air temperature, it did not exceed 1 K of difference, having an average deviation of around 0.4 K. Therefore, it can be argued that the obtained temperature values from stationary weather station are adequate for on-going study, thus not affecting the accuracy of final results. The same argument can be applied in case of humidity distribution as the average deviation was found to be of around 4%.

4.3. Variation of UHI effect in the city of Vienna

This section focuses on temporal and spatial variation of microclimatic conditions across the city of Vienna. For this purpose results are structured in terms of seasonal temperature and UHI intensity distribution across the city, representing the year of 2012. Additionally, time-dependency (diurnal and nocturnal) of numerous climatic parameters was portrayed in the course of a reference summer day.

4.3.1. Seasonal variation

Figure 41 to Figure 44 show the mean hourly air temperature distribution across observed areas, for four seasons, from winter to autumn, respectively. Figure 45 to Figure 48 show the mean hourly UHI intensity distribution across observed areas for four seasons, from winter to autumn, respectively. The abbreviations IS, GD, HW, DF, and R stand for Innere Stadt, Gaudenzdorf, Hohe Warte, Donaufeld, and Seibersdorf, respectively. These results (Figure 41 to Figure 48) suggest that the extent of both temperature and UHI intensity differ considerably in time (day, season) and space (location).
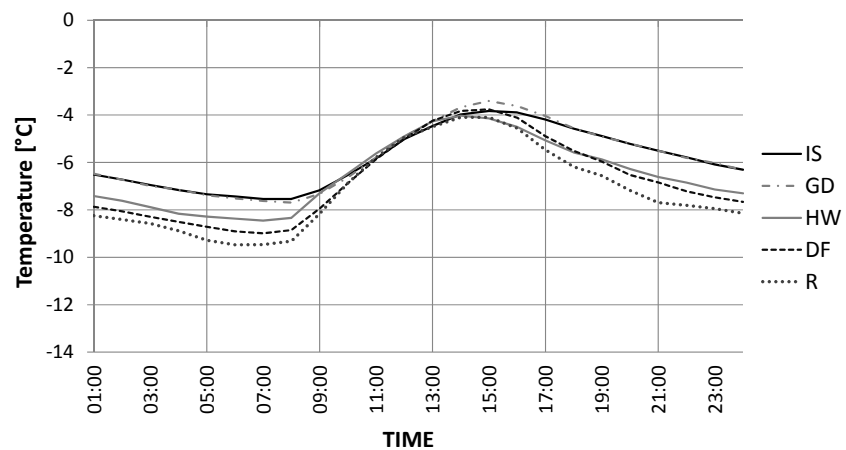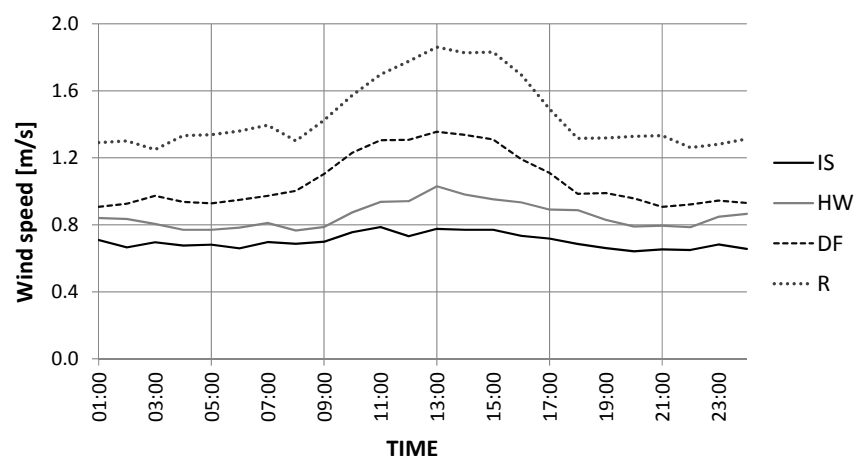
Figure 41. Mean hourly temperature distribution for the reference day, winter season
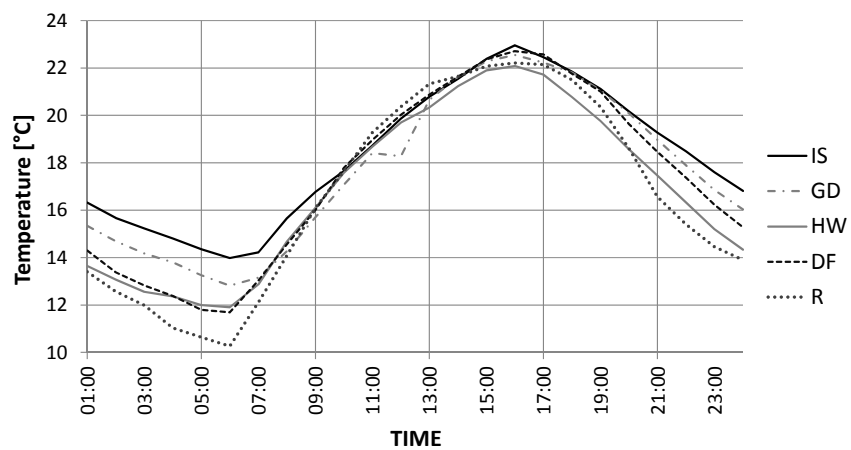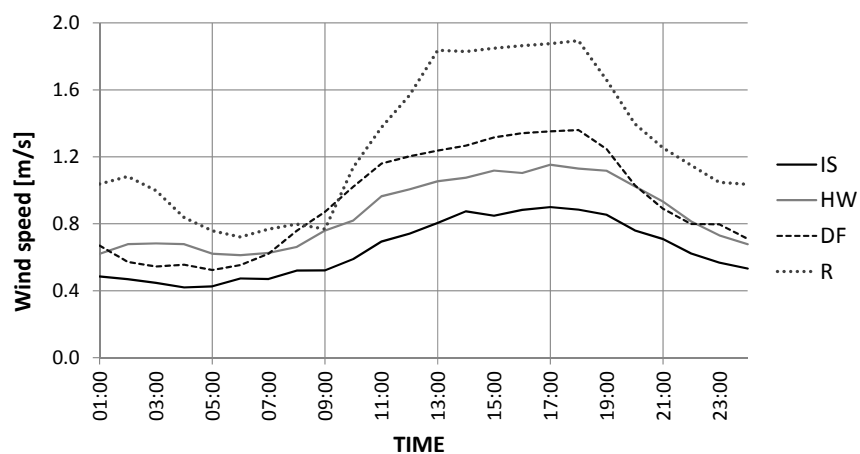

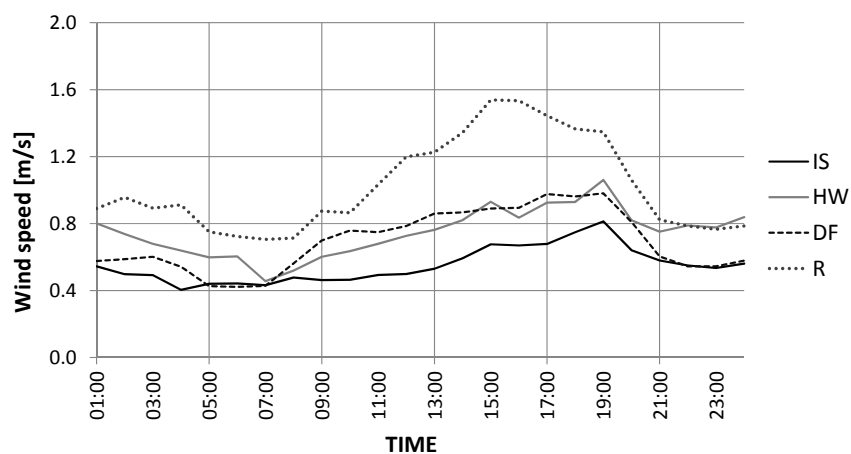*Figure 42. Mean hourly temperature distribution for the reference day, spring season*
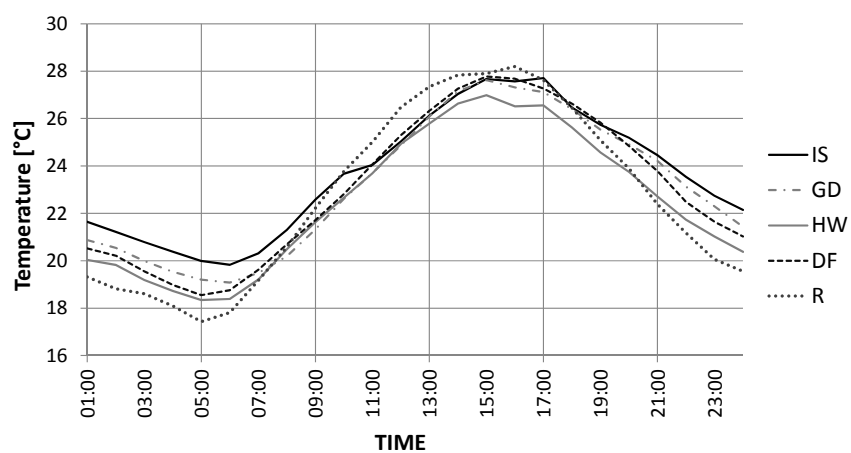
*Figure 43. Mean hourly temperature distribution for the reference day, summer season*
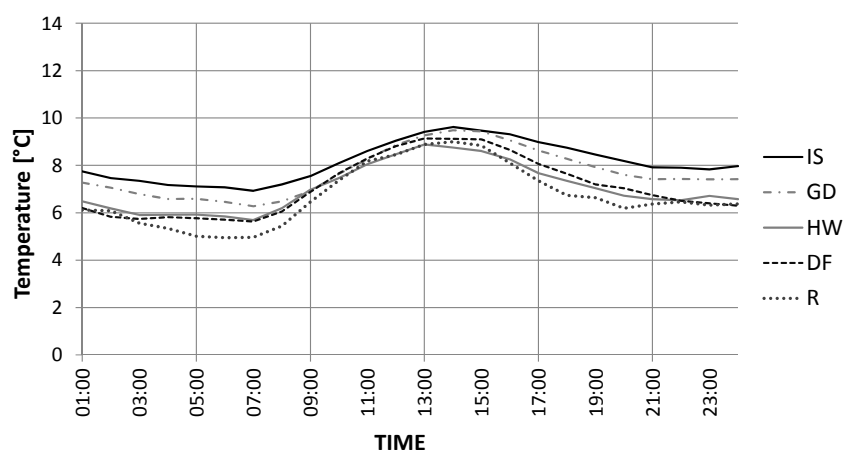
Figure 44. Mean hourly temperature distribution for the reference day, autumn season

Results pertaining to the air temperature distribution clearly demonstrate a significant difference between the observed areas. This deviation was observed not only with respect to diurnal scale, but with regard to seasonal scale as well. Furthermore, the results suggest more pronounced temperature deviation between the locations during night hours, which was further observed during all four seasons. This deviation was generally found to be in the range of 2 to 3 K, and may be discussed as the consequence of a number of factors, but namely different nocturnal urban versus rural cooling.

During the day, temperature curves corresponding to different areas come closer together revealing that urban, suburban and rural areas tend to heat up at relatively similar rate. The only discrepancy from this trend was observed during summer season (Figure 43), when the rural area was experiencing the highest temperature. This might be due to the higher solar gain, which will be further discussed at the end of this paragraph, when reflecting on the seasonal solar radiation distribution.

It can be observed that central urban station IS was generally displaying the highest air temperature during each season, and especially during night hours, revealing how variations in morphology, land-use and land cover may be the key aspects in affecting the temperatures across a city.
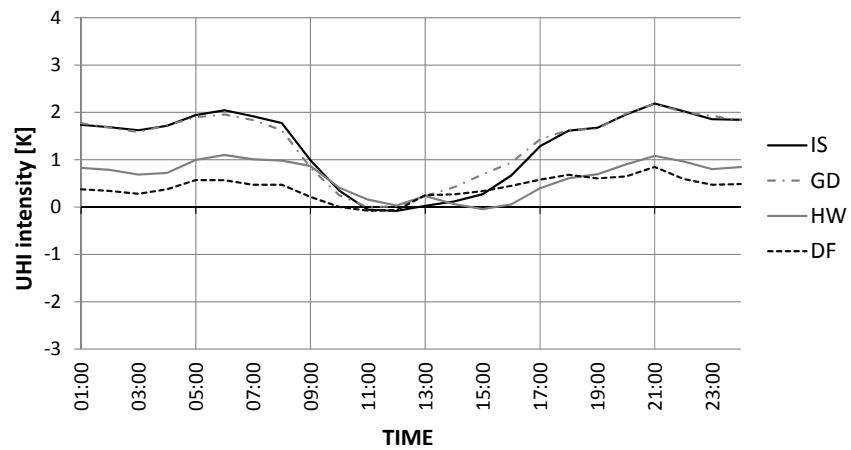
Figure 45. Mean hourly UHI intensity distribution for the reference day, winter season
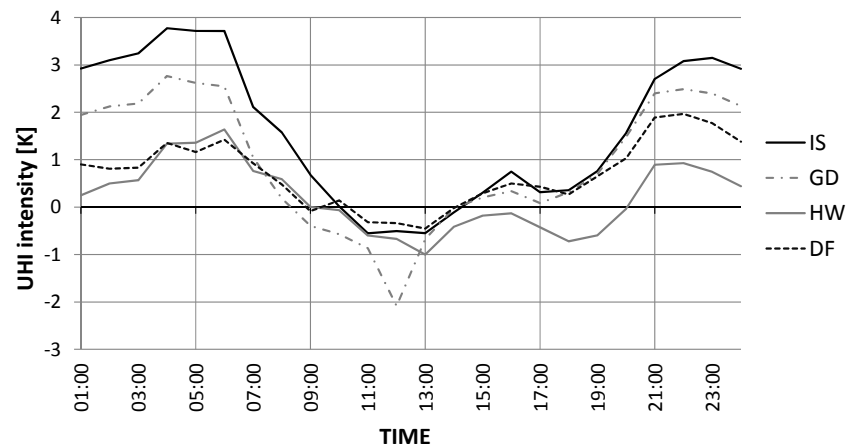
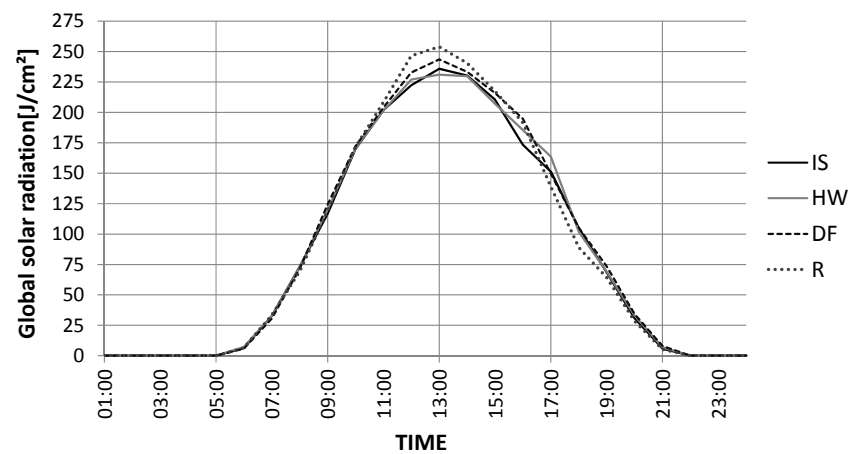*Figure 46. Mean hourly UHI intensity distribution for the reference day, spring season*
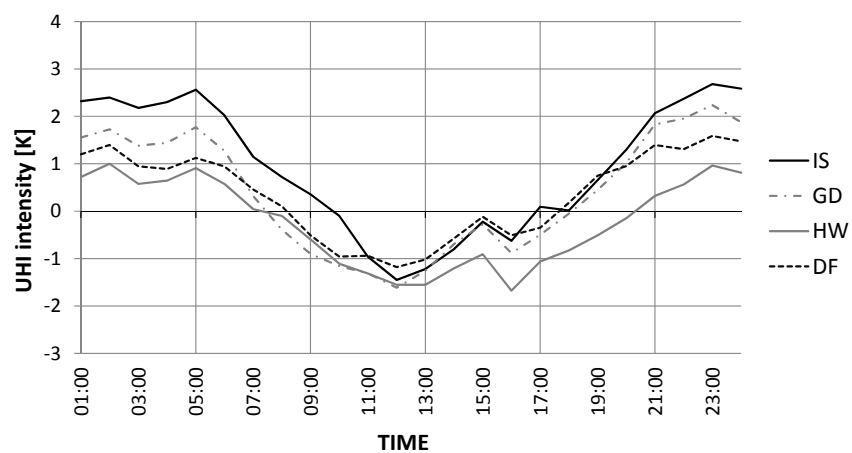
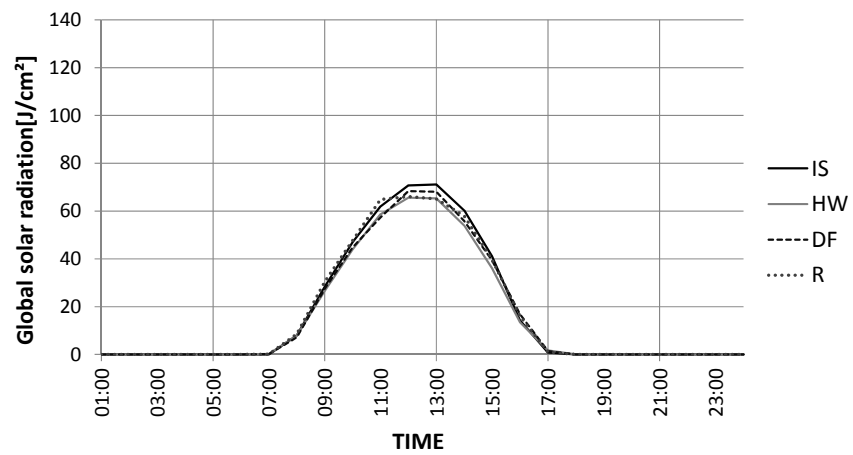*Figure 47. Mean hourly UHI intensity distribution for the reference day, summer season*
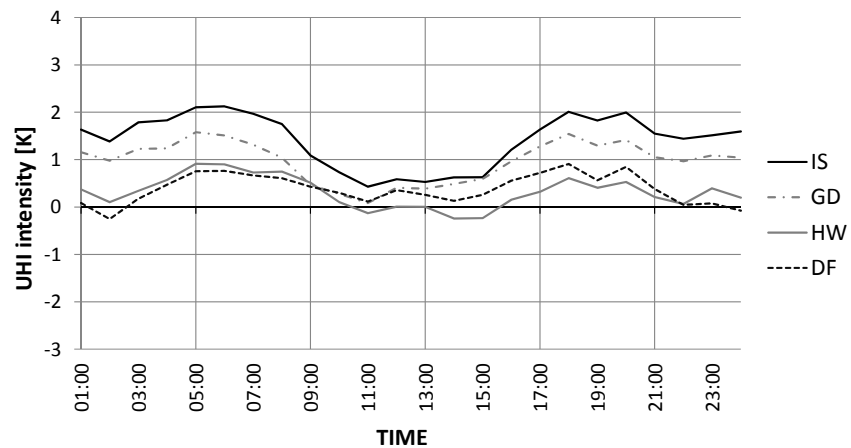
Figure 48. Mean hourly UHI intensity distribution for the reference day, autumn season

Results pertaining to UHI intensity distribution (Figure 45 to Figure 48) clearly demonstrate the existence and significant magnitude of the UHI effect in all study areas. A number of distinct circumstances were observed. First, the UHI was documented during all seasons, being of the highest intensity during spring and summer, and especially within the central urban area IS. Second, the distinct temporal pattern was revealed, which implies larger UHI intensities during the night hours. The UHI intensity maxima lie in the range between 2 K to almost 4 K, depending on the season. The highest magnitude of the UHI phenomenon was revealed to occur during the spring and summer. Third, results suggest the highest UHI intensity occurring with the highest diurnal amplitude of air temperature. Spring and summer seasons (Figure 42 and Figure 43) reveal large diurnal air temperature fluctuations, up to 12 K, while during winter and autumn (Figure 41 and Figure 44) mean deviation of the temperature fluctuations was around 5 K.

Additionally, it should be noted that during midday a negative UHI is probable to appear, revealing the presence of Cool Island. This circumstance was predominant during two seasons - spring and summer. In general, the UHI phenomena can be outlined as considerably dynamic phenomenon with distinct variation with regard to both location and time.

Additionally, the seasonal distribution of wind speed and global solar radiation were derived from the same dataset (Figure 49 to Figure 56). It should be noted that the following figures illustrate the data collected only at four out of five areas observed, due to the lack of both wind and global solar radiation sensors at the location GD.

Figure 49 to Figure 52 show the mean hourly wind speed distribution across observed areas for four seasons, from winter to autumn, respectively. Unsurprisingly, the rural area measured consistently higher wind speeds, with the greatest deviation occurring at midday. Wind speed was notably lower within the urban and suburban areas. This may explain in part the higher urban air temperature, noted previously, due to the obstructed air flow by densely built volume. Furthermore, temporal variation of the mean hourly rural wind speed, with maxima occurring around midday, may offer a plausible explanation why the Cool Island is likely to occur. With the stronger rural winds, a tendency toward faster surface cooling is evident. Therefore, the potential for significant temperature difference between the areas is revealed.

Figure 49. Mean hourly wind speed distribution for the reference day, winter season

Figure 50. Mean hourly wind speed distribution for the reference day, spring season

Figure 51. Mean hourly wind speed distribution for the reference day, summer season
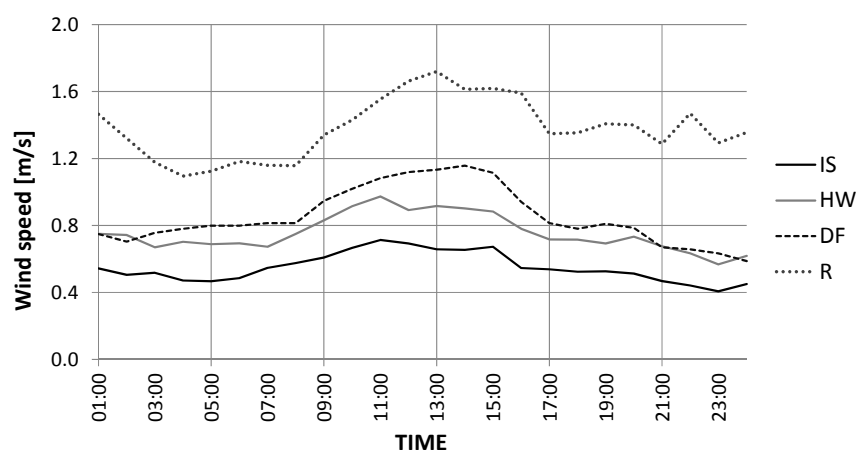
Figure 52. Mean hourly wind speed distribution for the reference day, autumn season

Figure 53 to Figure 56 show the global solar radiation distribution across observed areas for four seasons, from winter to autumn, respectively. These results suggest that the overall solar intensity received was relatively consistent throughout the observed areas during morning and late afternoon hours. The highest offset was recorded during midday. Generally, rural and suburban areas were receiving more solar radiation, and therefore a higher energy input. This is namely due to the dense and more compact building stock of the central urban areas resulting in reduced solar input. The only discrepancy from this trend was observed during autumn, when the highest solar input was recorded within the central urban area. This occurrence may be explained in part by a sudden interruption of incoming direct solar radiation by cloud cover forming over rural area, as until 11:00 rural area was displaying continuously higher solar intensity.
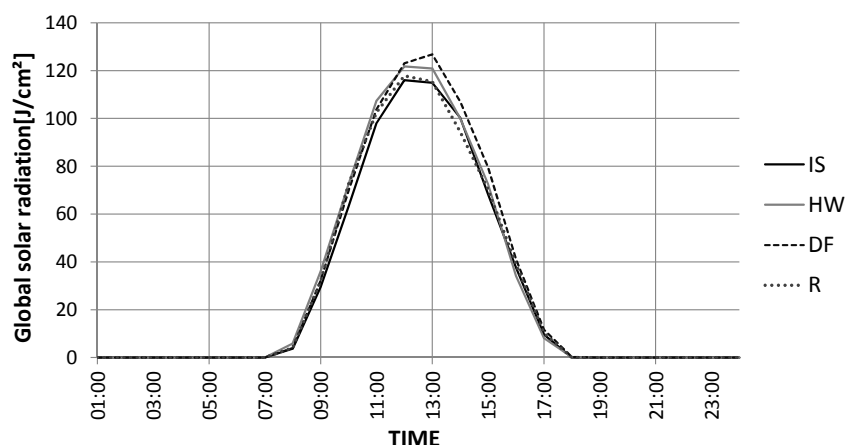
Figure 53. Mean hourly global solar radiation distribution for the reference day, winter season
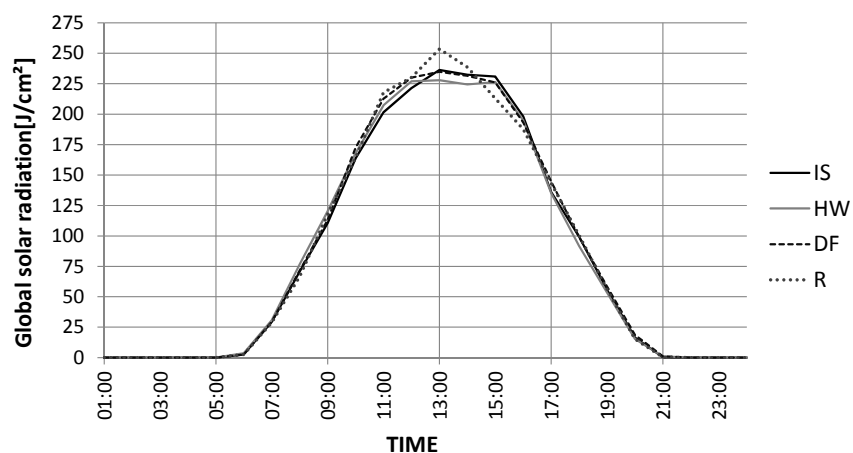
Figure 54. Mean hourly global solar radiation distribution for the reference day, spring season

Figure 55. Mean hourly global solar radiation distribution for the reference day, summer season

Figure 56. Mean hourly global solar radiation distribution for the reference day, autumn season

4.3.2. Diurnal variation

Figure 57 and Figure 58 show the mean hourly distribution of both temperature and UHI intensity for the reference summer day, representing the period from 29th June to 5th July 2012 (two-week period). Figure 59 shows the results in terms of cumulative frequency UHI intensity distribution, representing the same period. The results clearly demonstrate considerable variability of climatic parameters between observed areas. Additionally, Figure 60 to Figure 62 show the mean hourly wind speed, global solar radiation, and absolute humidity distribution, respectively. These results are expected to further outline the causative relation between urban design and thermal overheating of urban domains.
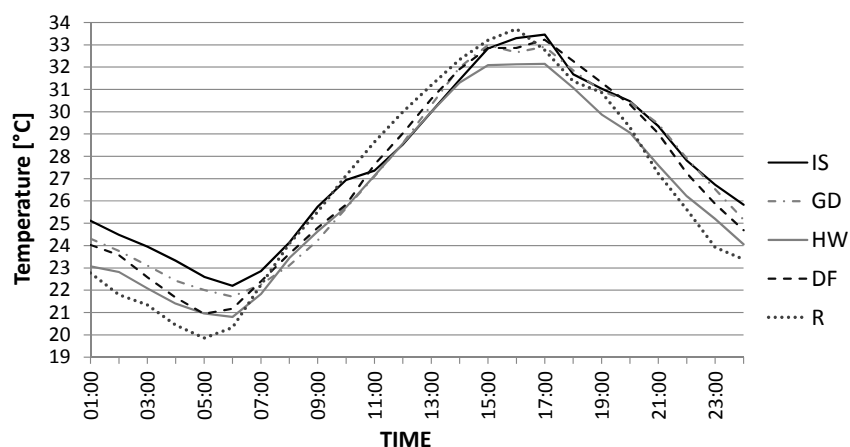
Figure 57. Mean hourly temperature distribution for a reference summer day
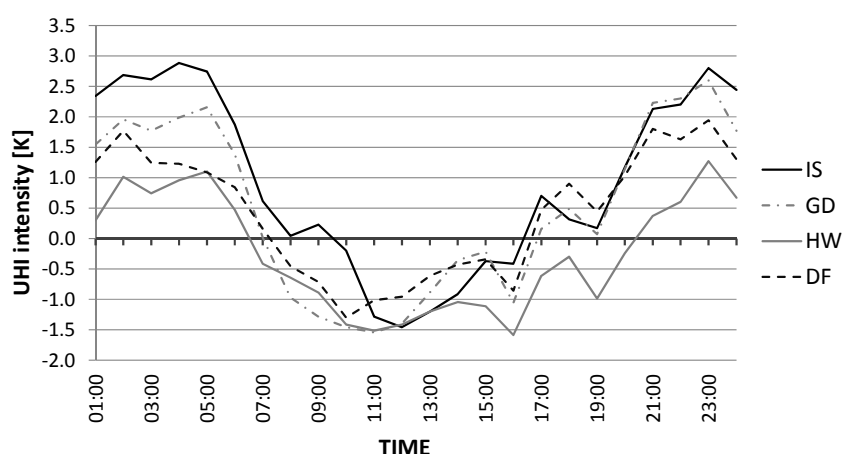
Figure 58. Mean hourly UHI distribution for a reference summer day
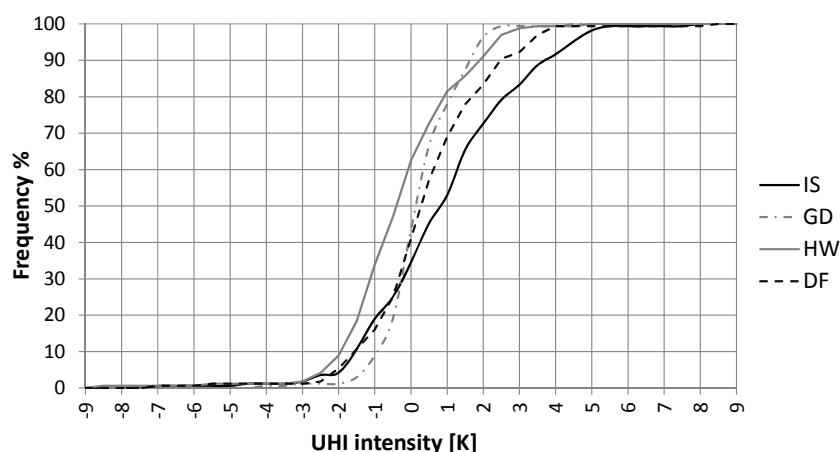
Figure 59. Cumulative frequency distribution of UHI intensity for two-week summer period

As already noted, intra-urban temperature variations are evident and of significant magnitude (Figure 57). During night-time, intra-urban areas were consistently displaying higher temperatures when compared to the rural environment, with central urban area being the hottest. Daytime warming trend is apparent, with rural area experiencing the highest temperature.

Consistent with previous findings, the predominant nocturnal nature of UHI phenomenon is evident (Figure 58). It can be observed that the magnitude of summertime UHI is rising from the hour before sunset, reaching its peak around midnight, and starting to descend an hour after sunrise (lasting in total from 19:00 to 06:00). However, these hourly based observations show a significant variation in UHI intensity, especially in terms of peak values. The central urban location IS clearly displays the highest UHI level, particularly during the night hours. Suburban stations HW and DF display the lowest UHI intensity during the night hours.

Furthermore, it can be observed that during the daytime, differences between the urban and the reference rural stations were altered, and a negative heat island (cool island) became apparent. The intensity of this phenomenon was lower and its duration shorter than that of the nocturnal heat island.

Figure 59 shows the cumulative frequency distribution of UHI intensity over two-week summer period. The frequency distribution clearly demonstrates the predominance of positive UHI values, where a clear shift to the right denotes higher values. However, the degree to which the UHI effect characterizes observed areas varies significantly. The data reveal that the central urban area IS was experiencing the UHI almost 75% of the time, while peripheral urban area HW expresses the lowest periods of UHI, having the UHI present around 40% of the time during two week summer

period. Given the multitude of different urban environments, a number of factors may have contributed to this occurrence, but namely existing morphological contrasts of the urban environments (especially the factors related to density, abundance of impervious surfaces, reduction of night-time back radiation, etc.) that might have affected the total heat exchange, solar access and radiative cooling rates.

To further explore the issues and concerns related to the undesired thermal circumstances in the urban environment, additional climatic parameters were analysed. Figure 60 to Figure 62 illustrate, for the reference summer day, the mean hourly wind speed, global solar radiation, and absolute humidity distribution, respectively.
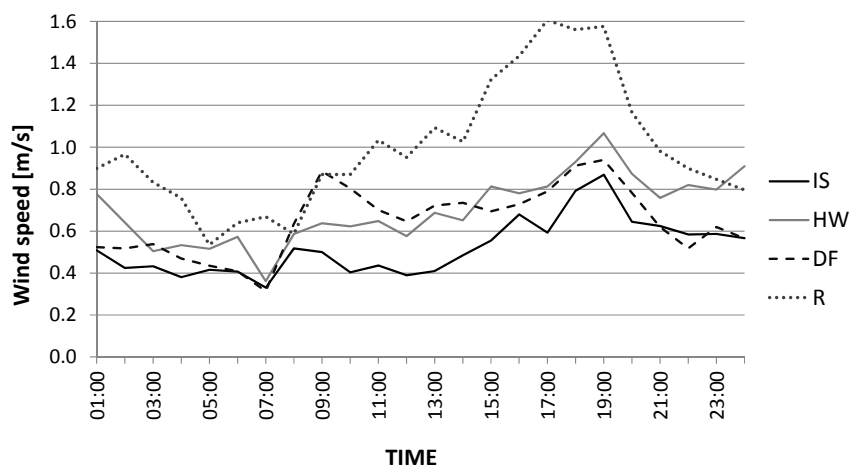
Figure 60. Mean hourly wind speed distribution for the reference summer day
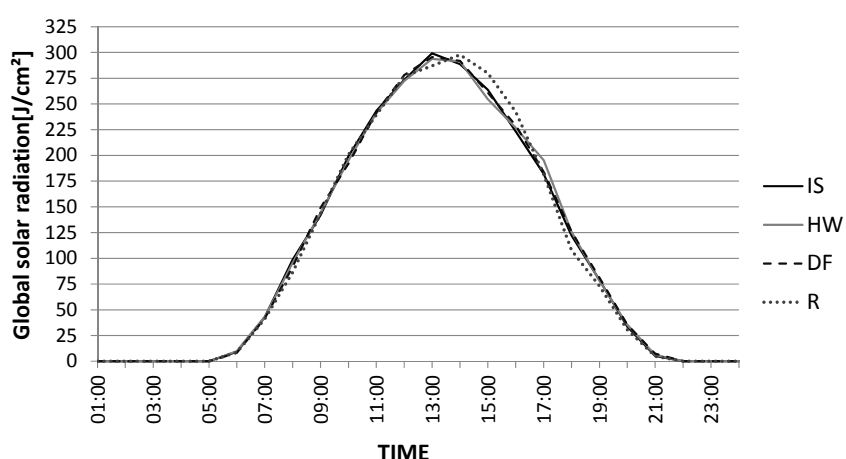
Figure 61. Mean hourly global solar radiation distribution for the reference summer day
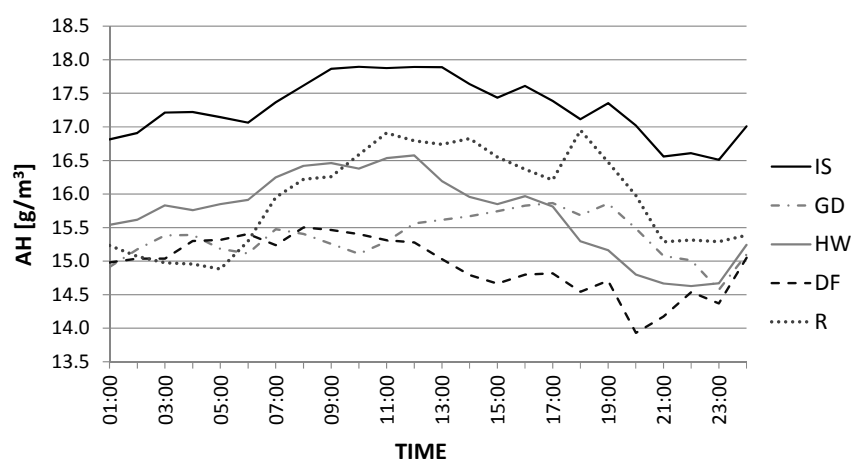
Figure 62. Mean hourly absolute humidity distribution for the reference summer day

Consistent with seasonal trends already discussed, the rural area measured consistently higher wind speeds, with somewhat lower wind speeds within the urban and suburban areas (Figure 60). The only discrepancy from this trend was observed from 08:00 to 09:00 when curves came closer together. Additionally, morning and midday differences appeared to be of lesser extent. The rural wind curve displayed a dramatic rise starting from 16:00. This may explain in part the drop of rural air temperature noted at the same time, due to stronger winds, followed by a tendency towards faster surface cooling. This circumstance is consistent with the occurrence of heat island, noted at the same time.

Figure 61 reveals that the overall solar intensity received was relatively consistent throughout the day. The shift in rural curve was observed starting from 14:00 until 17:00, revealing a higher energy input of the rural area. This circumstance may be attributed to the aspect of the unobstructed sky view of the rural environment and the shade effect of tall urban buildings. Furthermore, this occurrence is consistent with Figure 57, where the rural area measured continuously higher temperature, observed during the same time period. A clear descend of both urban and suburban solar intensity curves were observed starting from 15:00, stressing the decreased solar input. However, Figure 57 reveals a steady progression of air temperature in these areas, even after the total solar input had decreased. A distinct descend of air temperature was observed starting from 17:00. This occurrence may be related to the factors such as thermal inertia of building masses, abundance of impervious surfaces with high absorbing potential, and reduced skyward longwave radiation, stressing that high structure urban systems have a potential to absorb, trap and

reradiate more radiation than respective nonurban plains, leading to the more intense UHIs.

Additionally, Figure 62 shows that absolute humidity was significantly and constantly higher at central urban area IS. This occurrence may be attributed to the substantially higher anthropogenic sources of heat and air pollution within the area, especially due to the traffic emissions and emissions from urban structures. Somewhat higher humidity levels are also noted within the rural area, which might be attributed to the abundance of pervious cover and the related processes of evapotranspiration.

4.4. Numeric description of aggregate variable

To further evaluate the cumulative effect of both urban morphology and surface thermal properties on the urban microclimate variation, a set of salient geometric (morphological) and semantic (material-related) variables was derived for all study areas. A complete overview of the results can be found in the Appendix.

4.4.1. Geometric features

Table 14 provides a concise summary of derived geometric variables that capture the complex geometry of urban domains. The abbreviations IS, GD, HW, DF, and R stand for Innere Stadt, Gaudenzdorf, Hohe Warte, Donaufeld, and Seibersdorf, respectively.

Table 14. Summary of the geometric properties of Vienna U2Os

GEOMETRIC PROPERTIES	IS	GD	HW	DF	R
Sky View Factor	0.47	0.51	0.59	0.75	0.87
Aspect ratio	1.63	1.54	0.92	0.73	0.28
Built area fraction	0.41	0.40	0.18	0.20	0.08
Unbuilt area fraction	0.59	0.60	0.82	0.80	0.92
Impervious surface fraction	0.45	0.46	0.34	0.31	0.09
Pervious surface fraction	0.14	0.14	0.48	0.49	0.83
Bare soil fraction	0.00	0.00	0.00	0.04	0.00
Green area fraction	0.14	0.14	0.48	0.45	0.83
Water bodies fraction	0.00	0.00	0.00	0.00	0.00
Equivalent building height	9.18	5.46	1.43	1.20	0.45
Built surface fraction	3.85	3.46	3.04	2.74	2.04
Wall fraction	2.85	2.46	2.04	1.74	1.04
Roof fraction	1.00	1.00	1.00	1.00	1.00
Impervious roof fraction	0.99	0.99	0.99	1.00	1.00
Pervious roof fraction	0.01	0.01	0.01	0.00	0.00
Effective mean compactness	4.23	2.74	1.05	0.72	0.41
Mean sea level	169	177	202	160	182

4.4.2. Physical features

Table 15 provides a concise summary of derived surface/material variables that namely describe the thermal characteristics of urban surfaces. The abbreviations IS, GD, HW, DF, and R stand for Innere Stadt, Gaudenzdorf, Hohe Warte, Donaufeld, and Seibersdorf, respectively.

Table 15. Summary of the surface/material properties of Vienna U2Os

SURFACE PROPERTIES	IS	GD	HW	DF	R
Reflectance/Albedo	0.15	0.19	0.22	0.22	0.32
Emissivity	0.93	0.93	0.93	0.93	0.92
Thermal conductivity					
Impervious surface	0.80	0.80	0.78	0.77	0.85
Pervious surface	1.1	1.1	1.1	1.1	1.1
Specific heat capacity					
Impervious surface	784	790	822	826	766
Pervious surface	800	800	800	800	800
Density					
Impervious surface	2082	2078	2065	2045	2125
Pervious surface	1000	1000	1000	1000	1000
Thermal Admittance					
Impervious surface	1146	1148	1152	1144	1176
Pervious surface	938	938	938	938	938
Anthropogenic heat	350	430	177	89	67
Vehicles	35	51	17	11	7
Buildings	315	379	160	78	60
Human activity	0.02	0.01	0.01	0.01	0.00

4.4.3. Semantic representation

To further illustrate the application of the aforementioned procedures, Figure 63 depicts computed values of a selected set of geometric and semantic variables for five locations across Vienna in a novel profile format (Vuckovic et al. 2014; Musco 2015). These variables were chosen based on their degree of variation within the observed U2Os. Given the specific arrangement of the respective scales in this representation (descending versus ascending order of the scale numbers), an apparent trend can be observed: a clear shift to the left denotes a more suburban and rural character, while the shift to the right denotes a more urban character. Furthermore, three distinct clusters support the notion of highly developed and denser urban areas toward less developed suburban and rural areas. This is an effective way to visualize the characteristics of specific urban locations and highlight their differences.
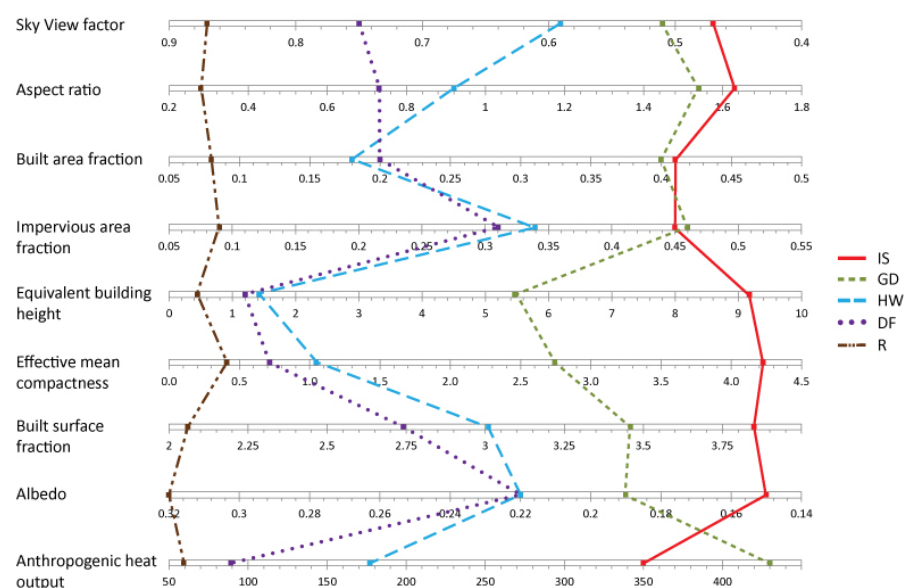
Figure 63. The computed values of a number of U2O variables for five selected U2Os

4.5. Statistical Analysis Results

Once the U2O variables are calculated, statistically significant correlations between these variables and CTI factors are derived to investigate the sensitivity of microclimatic quantities against the urban geometry parameters and related thermal properties.

4.5.1. Correlation analysis

Table 16 gives an overview of calculated seasonal CTI values for all study areas.

Table 16. Summary of seasonal CTI values for all study areas

SEASON	IS	GD	HW	DF
Winter	31.31	32.10	15.22	9.90
Spring	40.75	27.97	10.01	18.21
Summer	27.76	18.82	7.13	14.70
Autumn	33.98	23.40	8.20	9.47

Figure 64 to Figure 73 illustrate the respective relationships between fundamental features of the urban setting (morphology, materials) and basic microclimatic variables (seasonal CTIs). It should be noted that correlation pertaining to all four seasons is presented within the same graph, always displayed in the upper corner of the graph.
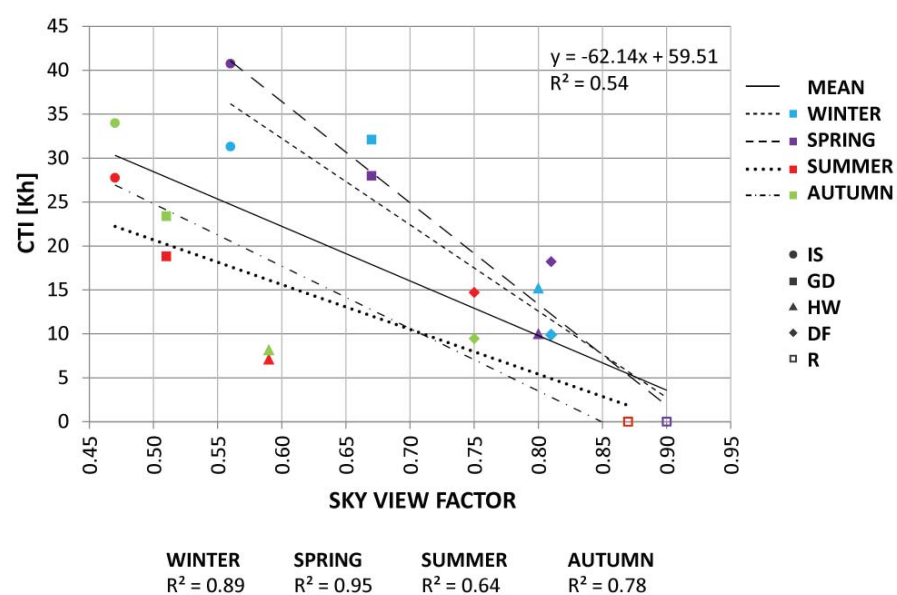
Figure 64. CTI as a function of SVF
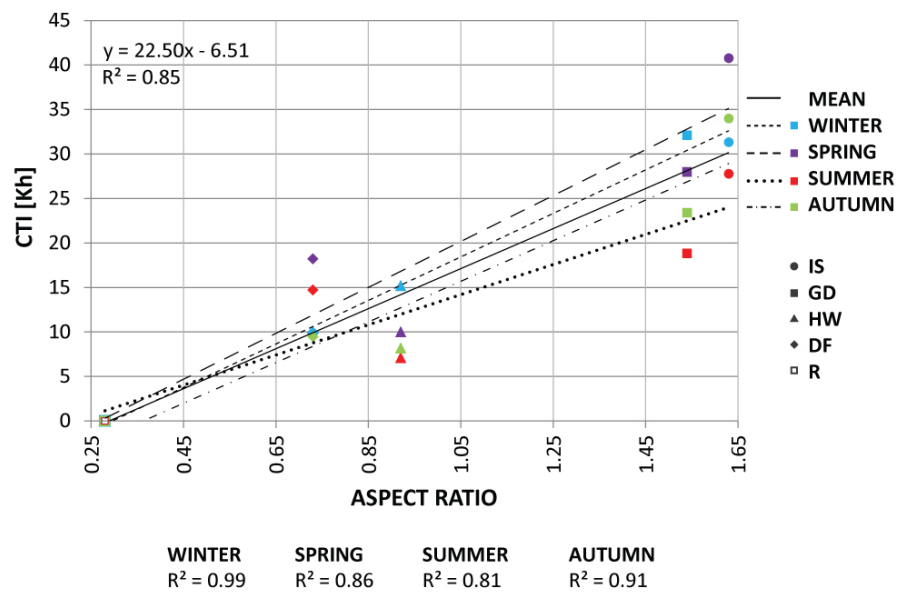
Figure 65. CTI as a function of Aspect Ratio
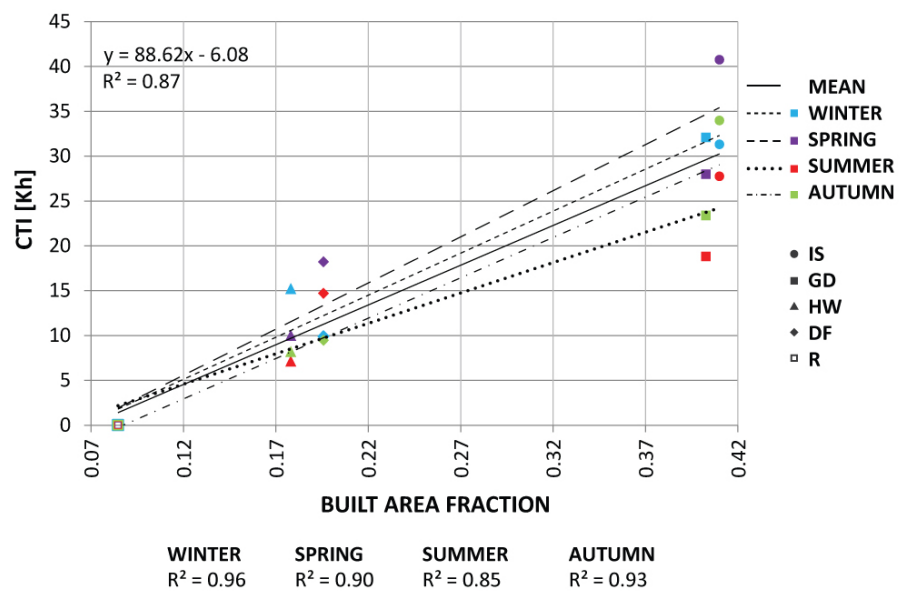
Figure 66. CTI as a function of Built Area Fraction
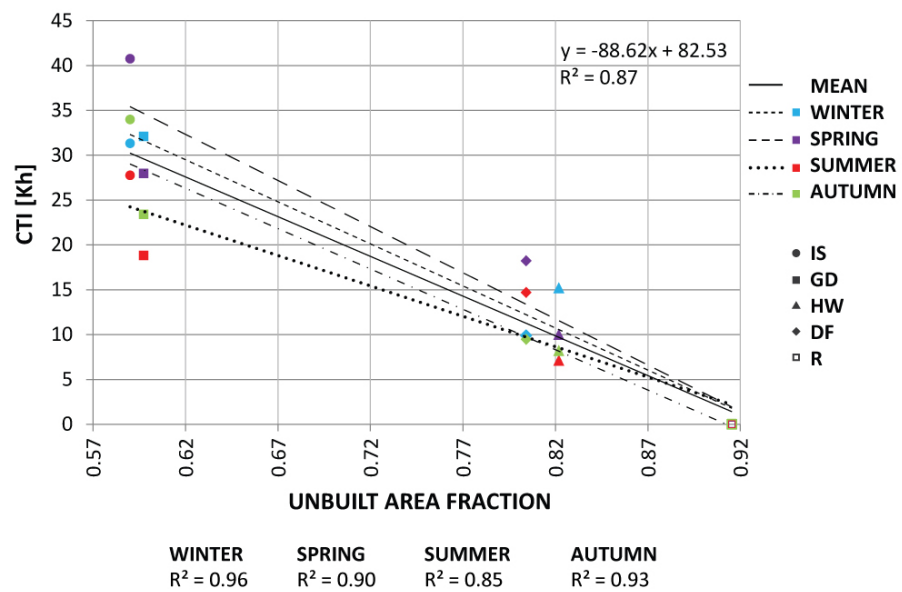
Figure 67. CTI as a function of Unbuilt Area Fraction
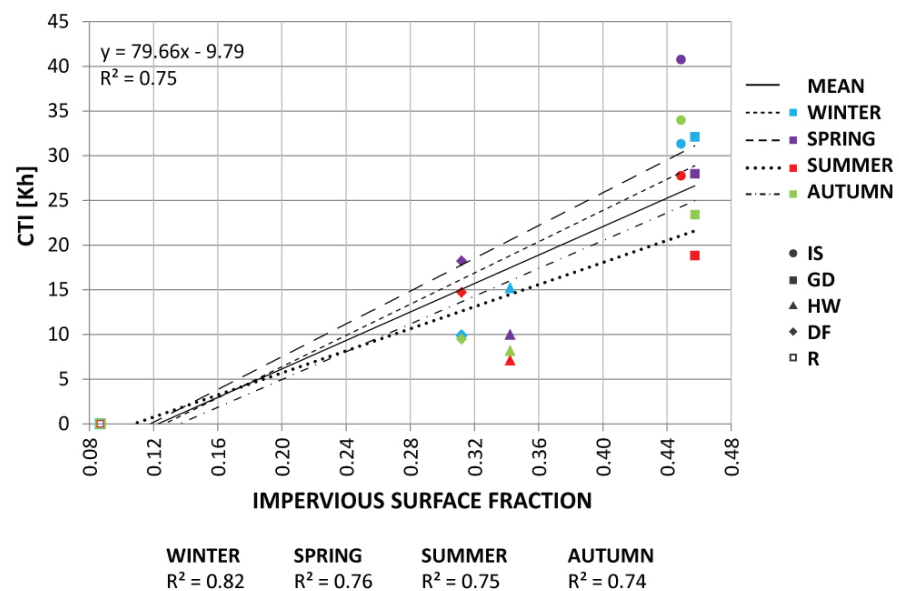
Figure 68. CTI as a function of Impervious Surface Fraction
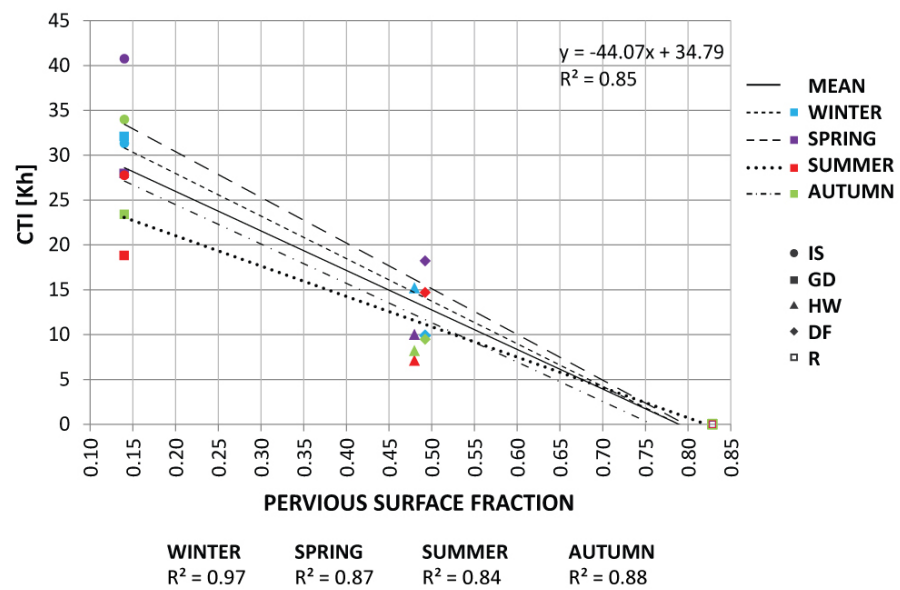
Figure 69. CTI as a function of Pervious Surface Fraction
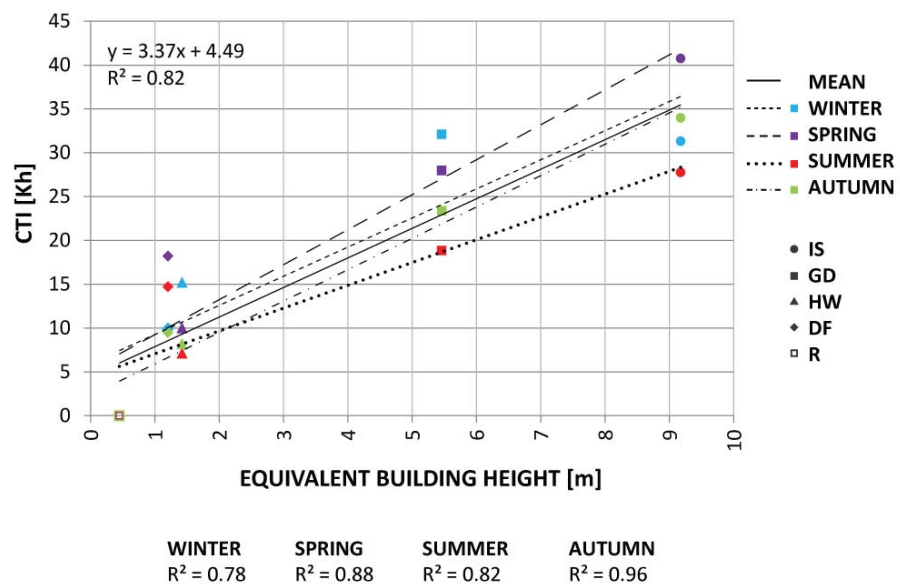
Figure 70. CTI as a function of Equivalent Building Height
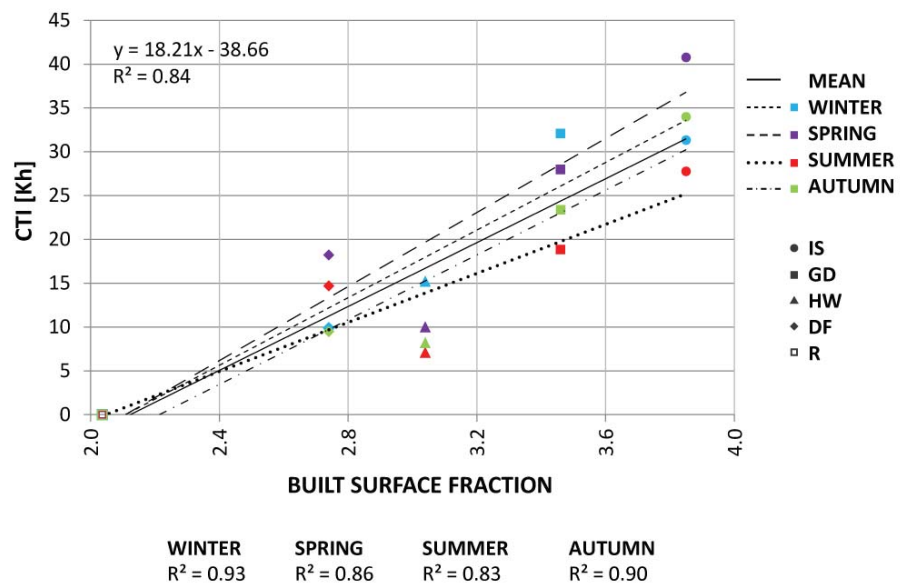
Figure 71. CTI as a function of Built Surface Fraction
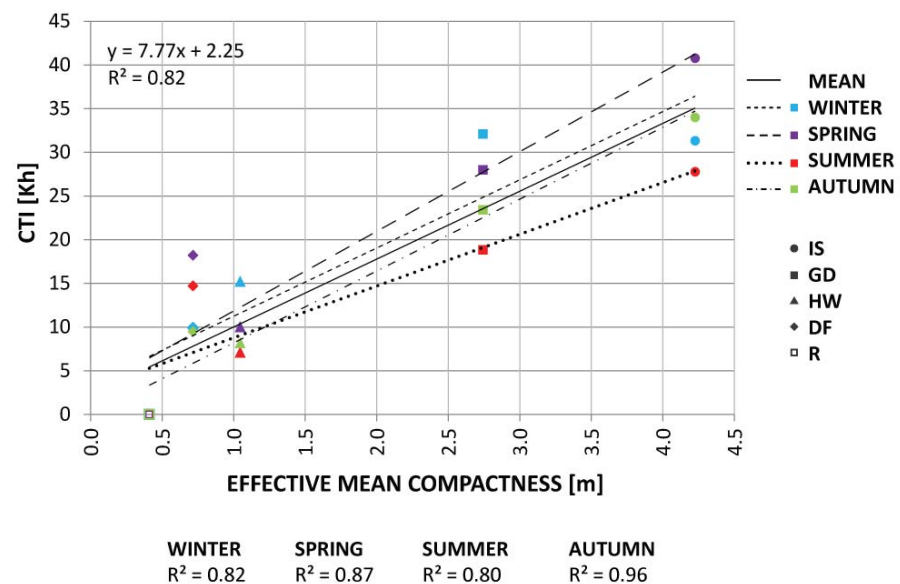
Figure 72. CTI as a function of Effective Mean Compactness
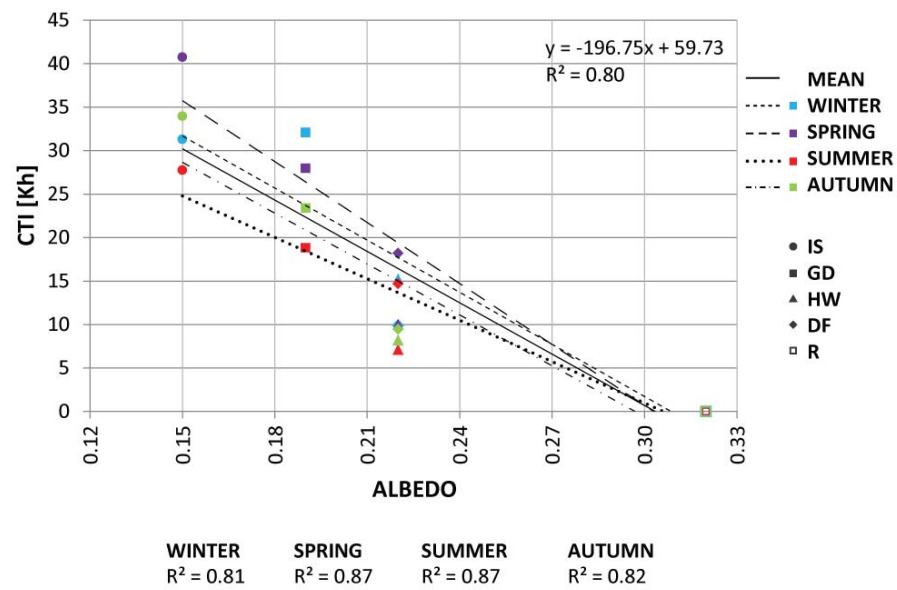
Figure 73. CTI as a function of Albedo

It should be noted that a number of U2O variables were omitted from correlation representation (especially emissivity, heat capacity, thermal conductivity, density and anthropogenic heat output). This is mainly due to a slight variation across the observed areas. Although, in the case of anthropogenic heat output, the main reason was the format of the input data, as the acquired data was representation of the mean annual and not seasonal distribution.

The results clearly illustrate that certain U2O variables positively correlate with CTIs (aspect ratio, built and unbuilt area fraction, impervious surface fraction, equivalent building height, built surface fraction, effective mean compactness), while others display a negative correlation (SVF, pervious surface fraction, albedo). In both cases the seasonal R-square value is relatively high, thus indicating high correlation between the computed CTIs and U2O variables. Although five data points might be considered insufficient to offer statistically meaningful correlations, the results presented in the Figure 64 to Figure 73 are consistent with previous research in this field and offer a solid base for further explorations.

4.5.2. Predictive model

Once the Least Squares statistical model between appropriate predictors (the U2O variables) and meteorological variables (CTIs) was constructed, the best fitted regression coefficients were obtained. The following equations illustrate the corresponding seasonal results from the Least Squares regression, from winter to autumn, respectively:

$$CTIw = 4.28 + 5.40 \cdot \psi_{sky} + 26.21 \cdot H/W + 2.71 \cdot ISF - 8.72 \cdot PSF -$$
$$3.59 \cdot h_e + 9.12 \cdot BSF - 6.53 \cdot l_c + 5.34 \cdot \alpha_{sw} \quad \text{[Kh]} \quad \text{Eq. 34}$$

$$CTIsp = 9.15 + 1.95 \cdot \psi_{sky} - 2.99 \cdot H/W + 14.34 \cdot ISF - 22.60 \cdot PSF +$$
$$22.31 \cdot h_e - 49.44 \cdot BSF + 9.71 \cdot l_c - 6.83 \cdot \alpha_{sw} \quad \text{[Kh]} \quad \text{Eq. 35}$$

$$CTIsu = -3.23 + 12.99 \cdot \psi_{sky} - 7.05 \cdot H/W + 11.58 \cdot ISF - 21.96 \cdot PSF +$$
$$15.46 \cdot h_e - 34.85 \cdot BSF + 10.76 \cdot l_c - 10.99 \cdot \alpha_{sw} \quad \text{[Kh]} \quad \text{Eq. 36}$$

$$CTIa = -1.15 + 4.51 \cdot \psi_{sky} + 1.22 \cdot H/W + 5.11 \cdot ISF - 10.41 \cdot PSF +$$
$$7.07 \cdot h_e - 11.57 \cdot BSF + 3.86 \cdot l_c - 3.88 \cdot \alpha_{sw} \quad \text{[Kh]} \quad \text{Eq. 37}$$

where CTIw, CTIsp, CTIsu, and CTIa represent the respective winter, spring, summer, and autumn CTI values.

As previously mentioned, the statistical significance of the computed model is calculated by the means of R-square (Coefficient of determination) and Root Mean Squared Error (RMSE). Following figure shows the strength of the relationship between the measured (expresses as the CTI) and predicted CTI values (expressed as the CTI').
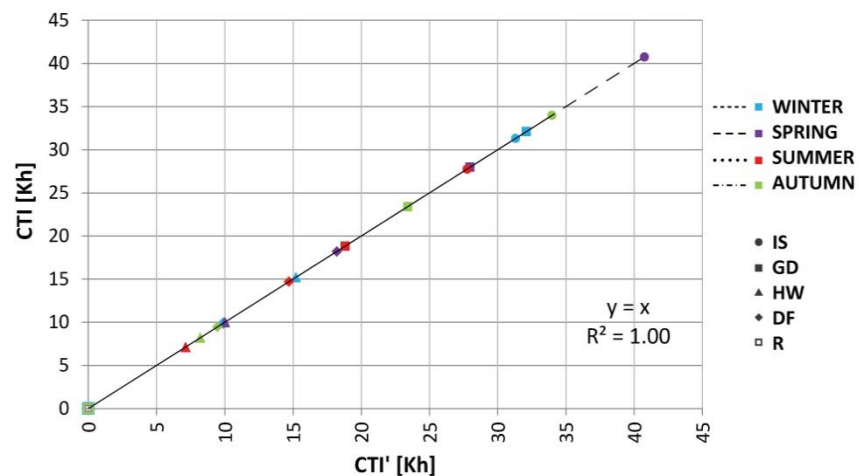
Figure 74. Correlation between the seasonal CTI and CTI' values

The following table gives an overview of the computed R-square and RMSE between measured and predicted CTI values for each season.

Table 17. Computed seasonal values of RMSE and R-square between measured and predicted CTI values

SEASON	RMSE	R^2
Winter	$0.1294\ e^{-08}$	1
Spring	$0.0474\ e^{-08}$	1
Summer	$0.0661\ e^{-08}$	1
Autumn	$0.0473\ e^{-08}$	1

The results reveal strong relationship between the observed and predicted values. Thus, in present analysis, the Least Squares model seems to fit perfectly. However, as mentioned before, five data points might be argued insufficient to yield any statistically valid relationships. Furthermore, the model cannot be evaluated using the same set of data that was used to derive it. Therefore, in order to test the model, the additional set of U2O variables was derived for a new location. The location in question, named AKH, represents central urban domain of mix-use development, with centrally positioned sparsely built hospital complex (Figure 75).
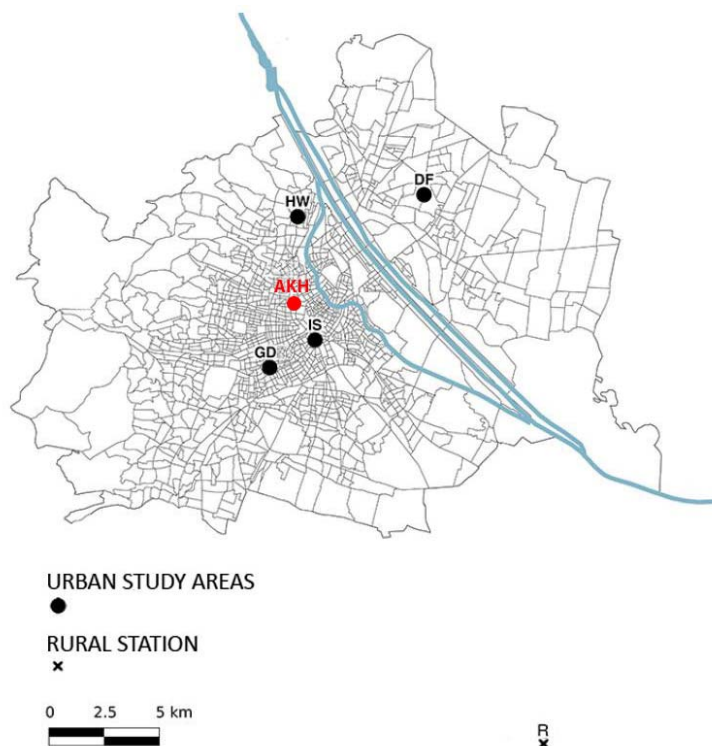
Figure 75. Position of the new location AKH (marked in red) in the city of Vienna

It should be noted that as the appropriate weather dataset cannot be obtained for this location, the model currently cannot be fully evaluated. Nonetheless, for the case of the city of Vienna, partial evaluation may be carried out based on previous findings.

Figure 76 illustrates the structured comparison of a selected set of the U2O variables for the location AKH compared to other study areas. It can be observed that the specific arrangement of the related scales is consistent with previous trends, thus stressing a more urban character. Detailed list of U2O variables for location AKH is provided within the Appendix.
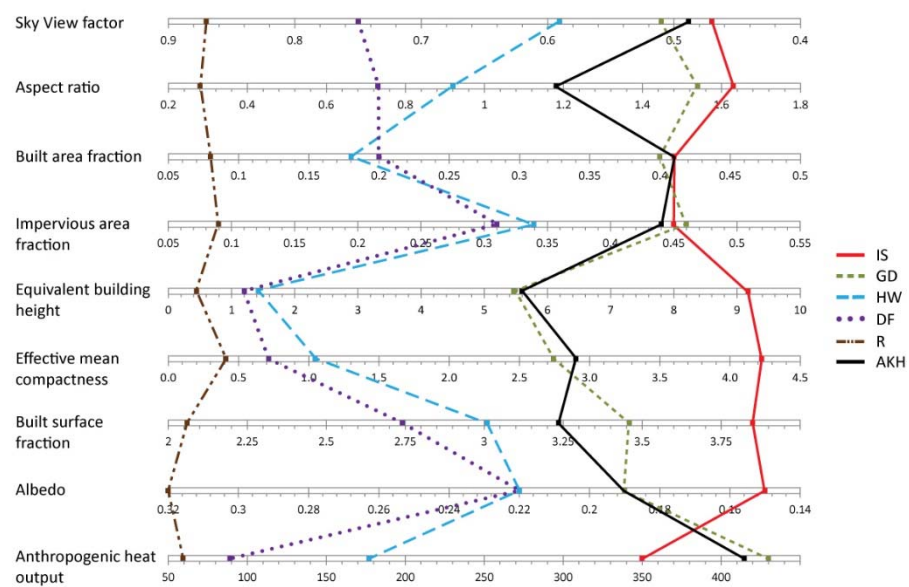
Figure 76. The computed values of a number of U2O variables for location AKH compared to other study areas

Given these results, and based on previous knowledge, there is a high probability to expect CTIs in range of those found in locations GD and HW. Once the AKH parameters are feed into the generated seasonal models, the predicted CTI values are obtained and analysed. The following table summarizes the modelling output.

Table 18. The predicted CTI values for the location AKH, along with GD and HW measured CTI data

SEASON	GD	AKH	HW
Winter	32.10	25.24	15.22
Spring	27.97	20.60	10.01
Summer	18.82	14.15	7.13
Autumn	23.40	20.67	8.20

While not statistically representative, the comprehensive analyses conducted within this study point to the potential of empirically-based models toward approximately predicting microclimatic conditions based on location specific attributes. As these results must be primarily read as initial and rough estimations, larger dataset is expected to significantly improve the reliability of model-based predictions.

5. Conclusion

5.1. Contribution

The main objective of the present dissertation has been to provide a better understanding of the complexity behind the microclimatic circumstances of urban settlements. Changes in urban microclimate, and corresponding higher air temperatures within urban domains, are believed to have cardinal consequences on the issues such as the thermal comfort of the city dwellers, mortality rate, local air quality, and energy demand of buildings. Thereby, the study of urban microclimate and related UHI phenomenon is highly relevant. However, literature-based review shows that there is a lack of practical assessment approaches focusing on the formation of UHI while considering a relatively wide range of factors of the built environment. This insight implies the need for more effective and comprehensive means of evaluating and analysing the UHI effect via advanced methods that thoroughly deal with the complexities of the urban climate systems.

In this context, this contribution introduced a systematic framework for a comprehensive UHI assessment with potential to effectively outline the influences of the morphological and physical features of urban settlements on the respective microclimatic circumstances. These morphological and physical features are believed to influence UHI and the urban microclimate variation. Using automated and semi-automated advanced data extraction methods and high-resolution and dynamic weather data streams, the above mentioned aspects were identified and computed for multiple locations in the city of Vienna. The initial hourly-based observations revealed distinct time-dependent (diurnal and nocturnal) patterns implying larger UHI intensities during the night hours. Additionally, the hourly based observations show a significant variation in UHI intensity in different urban areas, especially in terms of peak values. These results further illustrate UHI as a variable phenomenon over space and time. Furthermore, the specific arrangement of distinct morphological and physical features revealed an apparent trend that supports the notion of highly developed and denser urban areas toward less developed suburban and rural areas. The obtained data further allowed for an objective assessment of plausible correlations between location-based climatic conditions and distinct urban attributes. The findings showed good agreement with hypothesized correlations

between above mentioned aspects and offered a solid base for further explorations toward developing empirically-based predictive models. These models are expected to further support the understanding and prediction of local differences in the urban climate.

The underlying approach, which is based on systematic scientific assessment, has a potential to produce valuable information on the links between the urban microclimate, the design of urban spaces and the human wellbeing within the urban environment, and to suppress climatically-irresponsible urban design strategies.

5.2. Future research

As the initial results of the framework introduced in this research appeared to be quite promising, and in line with hypothesis set at the beginning of the research, they imply the need for further studies. Moreover, further explorations may gradually lead to more valid and statistically meaningful models. Specifically, a larger dataset is expected to provide better fitted model parameters with a potential for improved predictive performance. Furthermore, the model needs to be tested and validated in a new context, preferably on a broader geographical scale, thus supporting the development of general models for microclimate evaluation and prediction. In return, these future models are expected to provide a valuable feedback to the decision makers toward more sustainable urban environment design and maintenance practices.

Additionally, as the current challenge in the realm of microclimatic studies is aimed towards re-defining the very concept of the UHI intensity, which proved in some cases to be to some extent too generalizing, future efforts in this direction may yield a more site-specific climatic indicator. As the CTI indicator introduced in this research holds a great potential of illustrating the total overheating of an urban domain, additional measure that would account for the temporal nature of elevated urban temperatures would be more than beneficial. Moreover, the outcome of these explorations can in turn further the ongoing efforts towards the conception and evaluation of well-conceived urban intervention scenarios (e.g. mitigation measures pertaining to the UHI phenomena), thus identifying more effective solutions for a particular urban domain.

6. References

6.1. Literature

Akbari, H. 2002. Shade trees reduce building energy use and CO2 emissions from power plants. Environmental Pollution, Volume 116, pp. 119–126.

Akbari, H., Kurn, D.M., Bretz, S.E., Hanford J.W. 1997. Peak Power and Cooling Energy Savings of Shade Trees. Energy and Buildings, Volume 25, Issue 2, pp. 139-148.

Akbari, H. 2009. Cooling our Communities. A Guidebook on Tree Planting and Light-Colored Surfacing. EPA, United States Environmental Protection Agency.

Alcoforado, M. J., Matzarakis, A. 2010. Urban climate and planning in different climatic zones. Geographicalia, Volume 57, pp. 5-39.

Alexandri, E. 2008. Green cities of tomorrow?. Sustainable Construction, Materials and Practices, SB07, Lisbon, 12-14 September, pp. 710-717.

Ali-Toudert, F., Mayer, H. 2006. Numerical study on the effects of aspect ratio and orientation of an urban street canyon on outdoor thermal comfort in hot and dry climate. Buildings and Environment, Volume 41, pp. 94-108.

Alonso, M. S., Labajo, J. L., Fidalgo, M. R. 2003. Characteristics of the urban heat island in the city of Salamanca, Spain. Atmosfera, Volume 16, pp. 137-148.

Arnfield, A.J. 1982. An approach to the estimation of the surface radiative properties and radiation budgets of cities. Physical Geography, Volume 3, Issue 2, pp. 97–122.

Arnfield, A.J. 2003. Two decades of urban climate research: a review of turbulence, exchanges of energy and water, and the urban heat island. International Journal of Climatology, Volume 23, Issue 1, pp. 1-26.

ASHRAE 2009. Handbook – Fundamentals (SI Edition), Chapter 33, American Society of Heating, Refrigerating and Air-conditioning Engineers, Inc., Atlanta.

Bañuelos-Ruedas, F., Camacho, C.Á., Rios-Marcuello, S. 2011. Methodologies Used in the Extrapolation of Wind Speed Data at Different Heights and Its Impact in the Wind Energy Resource Assessment in a

Region. Wind Farm—Technical Regulations, Potential Estimation and Siting Assessment, InTech, pp. 246.

Basara, J. B., Hall Jr., P. K., Schroeder, A., Illston, B. G., Nemunaitis, K. L. 2008. Diurnal cycle of the Oklahoma City urban heat island. Journal of Geophysical Research, Volume 113, Issue D20, 16 pages.

Beckett, K. P., Freer-Smith, P., Taylor, G. 2000. Effective tree species for local air-quality management. Journal of Arboriculture, Volume 26, Issue 1, pp. 12-19.

Blazejczyk, K., Bakowska, M., Wieclaw, M. 2006. Urban heat island in large and small cities. 6th International Conference on Urban Climate, Göteborg, Sweden, June 12-16 2006, pp. 794-797.

Böhm, R. 1998. Urban Bias in Temperature Time Series – a Case Study for the City of Vienna, Austria. Climatic Change, Volume 38, Issue 1, pp. 113-128.

Bottyán, Z., Balázs, B., Gál, T. M., Zboray, Z. 2003. A statistical approach for estimating mean maximum urban temperature excess. Acta Climatologica et Chorologica, Volume 36-37. pp. 17-26.

Brown, M. J., Grimmond, C. S. B., Ratti, C. 2001. Comparison of Methodologies for Computing Sky View Factor in Urban Environments. The 2001 International Symposium on Environmental Hydraulics, ISEH 2001, Tempe, AZ, November 5-8.

Burian, S. J., Han, W. S., Brown, M. J. 2005. Morphological Analyses using 3D Building Databases: Oklahoma Citym Oklahoma. Los Alamos National Laboratory.

Campbell, J., Shin, M. 2011. Essentials of Geographic Information Systems. Saylor Foundation.

Corburn, J. 2009. Cities, Climate Change and Urban Heat Island Mitigation: Localising Global Environmental Science. Urban studies, Volume 46, Issue 2, pp. 413-427.

Chapman, L., Thornes, J. E., Bradley, A. V. 2001. Rapid determination of canyon geometry parameters for use in surface radiation budgets. Theoretical and applied climatology, Volume 69, pp. 81-89.

Chameides, W. L., Lindsay, R. W., Richardson, J., Kiang, C. S., 1988. The role of biogenic hydrocarbons in urban photochemical smog: Atlanta as a case study. Science, Volume 241, Issue 4872, pp. 1473-1475.

Chen, L., Xipo, A., Edward, N. 2010. Towards the use of a 3-D geo-database in investigating nocturnal urban temperature variation in Hong Kong. 1st International conference on sustainable urbanization, ICSU 2010, Hong Kong, China, December 15-17.

Chow, W. T. L., Svoma, B. M. 2011. Analyses of Nocturnal Temperature Cooling-Rate Response to Historical Local-Scale Urban Land-Use/Land Cover Change. Journal of Applied Meteorology and Climatology, Volume 50, Issue 9, pp. 1872–1883.

Donovan, R.G., Stewart, H.E., Owen, S.M., Mackenzie, A.R., Hewitt, C.N. 2005. Development and application of an urban tree air quality score for photo-chemical pollution episodes using the Birmingham, United Kingdom, area as a case study. Environmental Science and Technology, Volume 39, pp. 6730-6738.

Fanger, P.O. 1970. Thermal Comfort - Analysis and Applications in Environmental Engineering. Danish Technical Press, Copenhagen.

Frey, C. M., Rigo, G., Parlow, E. 2005. The cooling effect of cities in a hot and dry environment. Global developments in environmental earth observation from space, Proceedings of the 25th EARSeL Symposium, Porto, Portugal, 2005, pp. 169-174.

Gaffin, S. R., Rosenzweig, C., Khanbilvardi, R., Parshall, L., Mahani, S., Glickman, H., Goldberg, R., Blake, R., Slosberg, R. B., Hillel, D. 2008. Variations in New York city's urban heat island strength over time and space. Theoretical and applied climatology, Volume 94, pp. 1-11.

Gartland, L., 2008. Heat islands. Understanding and mitigating heat in urban areas, London, Earthscan.

Georgakis, C., Santamouris, M., Kaisarlis, G. 2010. The Vertical Stratification of Air Temperature in the Centre of Athens. Journal of Applied Meteorology and Climatology, Volume 49, pp. 1219–1232.

Giridharan, R., Ganesan, S., Lau, S. S. Y., 2005. Nocturnal heat island effect in urban residential developments of Hong Kong. Energy and Buildings, Volume 37. Issue 9, pp. 964-971.

Givoni, B. 1998. Climate Considerations in Building and Urban Design. Canada, John Wiley & Sons.

Glawischnig, S., Kiesel, K., Mahdavi, A. 2014a. Feasibility analysis of open-government data for the automated calculation of the micro-climatic attributes of Urban Units of Observation in the city of Vienna. 2nd ICAUD International Conference in Architecture and Urban Design, Epoka University, Tirana, Albania, May 08-10.

Glawischnig, S., Hammerberg, K., Vuckovic, M., Kiesel, K., Mahdavi, A. 2014b. A case study of geometry-based automated calculation of microclimatic attributes. 10th European Conference on Product and Process Modelling, Vienna, Austria, September 17-19.

Golden, J. 2004. The Built Environment Induced Urban Heat Island Effect in Rapidly Urbanizing Arid Regions - A Sustainable Urban Engineering Complexity. Journal of Integrative Environmental Sciences, Volume 1, Issue 4, pp. 321–349.

Grimmond, C. S. B. 1992. The suburban energy balance: Methodological considerations and results for a mid-latitude west coast city under winter and spring conditions. International Journal of Climatology, Volume 12, pp. 481-497.

Grimmond, C. S. B., Potter, S. K., Zutter, H. N., Souch, C. 2001. Rapid methods to estimate sky-view factors applied to urban areas. International Journal of Climatology, Volume 21, pp. 903-913.

Grimmond, S., Oke, T. 1998. Heat Storage in Urban Areas: Local-Scale Observations and Evaluation of a Simple Model. Journal of Applied Meteorology, Volume 38, pp. 922-940.

Grimmond, S., Oke, T. 1999. Aerodynamic properties of urban areas derived from analysis of surface form. Journal of Applied Meteorology, Volume 38, pp. 1262-1292.

Hammerberg, K. 2014. Accounting for the role of trees in urban energy balance modelling using GIS technologies. Master thesis, Vienna University of Technology.

Hammerberg, K., Mahdavi, A. 2014. GIS-based simulation of solar radiation in urban environments. 10th European Conference on Product & Process Modelling - ECPPM 2014, Vienna, Austria, September 17–19.

Hart, M., Sailor, D.J. 2007. Assessing causes in spatial variability in urban heat island magnitude. Seventh Symposium on the Urban Environment, San Diego, CA, 9 September 2007.

Hens, H. S. L. C. 2012. Building Physics - Heat, Air and Moisture: Fundamentals and Engineering Methods with Examples and Exercises. Wiley, pp. 284.

Hill, T., Lewicki, P. 2005. Statistics: Methods and Applications. USA, StatSoft, Inc.

Hoffman, P., Krueger, O., Schlünzen, K.H. 2012. A statistical model for the urban heat island and its application to a climate change scenario. International Journal of Climatology, Volume 32, pp. 1238–1248.

Howards, L. 1833. The Climate of London: Deduced from Meteorological Observations Made in the Metropolis and at Various Places Around it. London, Harvey and Darton.

Jamei, E., Ossen, D. R. 2012. Intra urban air temperature distributions in historic urban centre. American Journal of Environmental Science, Volume 8, Issue 5, pp. 503-509.

Jenerette, G. D., Harlan, S. L., Brazel, A., Jones, N., Larsen, L., Stefanov, W. L. 2007. Regional relationships between vegetation, surface temperature, and human settlement in a rapidly urbanizing ecosystem. Landscape Ecology, Volume 22, Issue 3, pp. 353–365.

Jauregui, E. 1997. Heat island development in Mexico City. Atmospheric Environment, Volume 31, Issue 22, pp. 3821–3831.

Johnson, G. T., Watson, I. D 1984. The Determination of View-Factors in Urban Canyons. Journal of Climate and Applied Meteorology, Volume 23, Issue 2, pp. 329-335.

Kalkstein, L. S., Green, J. 1997. An evaluation of climate/mortality relationships in large U.S. cities and the possible impact of a climate change. Environmental Health Perspectives, Volume 105, Issue 1, pp. 84–93.

Kanda, M., Moriwaki, R., Kimoto, Y. 2005. Temperature Profiles Within and Above an Urban Canopy. Boundary-Layer Meteorology, Volume 115, Issue 3, pp. 499-506.

Kleerekoper, L., van Esch, M., Salcedo, T. B. 2012. How to make a city climate-proof, addressing the urban heat island effect. Resources, Conservation and Recycling, Volume 64, pp. 30-38.

Koomen, E., Hettema, J., Oxenaar, S., Diogo, V. 2013. Analysing Urban Heat Island Patterns and simulating potential future changes. Impacts World 2013, International conference on climate change effects, Potsdam, May 27-30, pp. 7.

Kusaka, H., Kimura, F. 2004. Thermal Effects of Urban Canyon Structure on the Nocturnal Heat Island: Numerical Experiment Using a Mesoscale Model Coupled with an Urban Canopy Model. Journal of Applied Meteorology, Volume 43, Issue 12, pp. 1899–1910.

Landsberg, H. E. 1981. The Urban Climate. Academic Press, New York, pp. 275.

László, E., Szegedi, S. 2014. A multivariate linear regression model of mean maximum urban heat island: a case study of Beregszász (Berehove), Ukraine.
https://www.academia.edu/10270388/A_multivariate_linear_regression_model_of_mean_maximum_urban_heat_island_a_case_study_of_Beregsz%C3%A1sz_Berehove_Ukraine

Lee, D. O. 1979. Contrasts in warming and cooling rates at an urban and a rural site. Weather, Volume 34, Issue 2, pp. 60-66.

Li, W., Putra, S. Y., Yang, P. P. 2004. GIS Analysis for the Climatic Evaluation of 3D Urban Geometry - The Development of GIS Analytical Tools for Sky View Factor. GISDECO, Seventh International Seminar on GIS in developing countries, 10-12 May, Malaysia.

Lindberg F. 2005. Towards the use of local governmental 3-D data within urban climatology studies. Mapping and Image Science, Volume 2, pp. 32–37.

Lewis-Beck, M. S., Bryman, A. E., Liao, T. F. 2004. The SAGE Encyclopedia of Social Science Research Methods. SAGE Publications, Inc.

Mahdavi, A., Kiesel, K., Vuckovic, M. 2013. A framework for the evaluation of urban heat island mitigation measures. sb13 Munich, Implementing Sustainability - Barriers and Chances, München, Germany, April 24-26.

Mahdavi, A., Kiesel, K., Vuckovic, M. 2014a. Empirical and computational assessment of the urban heat island phenomenon and related mitigation measures. NSB 2014, 10th Nordic Symposium on Building Physics, Lund, Sweden, June 15-19.

Mahdavi, A., Kiesel, K., Vuckovic, M. 2014b. Empirical and computational assessment of the urban heat island phenomenon and related mitigation measures. Geographia Polonica, Volume 87, Issue 4, pp. 505-516.

Masson, V., Grimmond, C. S. B., Oke, T. R. 2002. Evaluation of the Town Energy Balance (TEB) Scheme with Direct Measurements from Dry Districts in Two Cities. Journal of Applied Meteorology, Volume 41, pp. 1011–1026.

MathWorks®: http://www.mathworks.com. Last accessed on 25.01.2015.

Memon, R. A., Leung, D. Y. C., Liu, C. 2008. A review on the generation, determination and mitigation of Urban Heat Island. Journal of Environmental Sciences, Volume 20, Issue 1, pp. 120-128.

Memon, R. A., Leung, D. Y. C., Liu, C. 2009. An investigation of urban heat island intensity (UHII) as an indicator of urban heating. Atmospheric Research, Volume 94, pp. 491-500.

Mills, G. 2011. Cubes and canyons: Different perspectives on the urban climate. City weathers: meteorology and urban design 1950-2010, Workshop, Manchester, 23-24 June.

Milojevic, A, Wilkinson, P, Armstrong, B, Davies, M, Mavrogianni, A, Bohnenstengel, S, Belcher, S. 2010. Impact of London's urban heat island on heat-related mortality. Annual Conference of the International Society for Environmental Epidemiology (ISEE), 22nd Annual Conference, Climate Change and Environmental Health, Seoul, South Korea.

Mirzaei, P. A., Haghighat, F. 2010. Approaches to study Urban Heat Island – Abilities and limitations. Building and Environment, Volume 45, pp. 2192-2201.

Moonen, P., Defraeye, T., Dorer, V., Blocken, B., Carmeliet, J. 2012. Urban Physics: Effect of the micro-climate on comfort, health and energy demand. Frontiers of Architectural Research, Volume 1, Issue 3, pp. 197–228.

Morris, C. J. G., Simmonds, I., Plummer, N. 2001. Quantification of the influences of wind and cloud on the nocturnal urban heat island of a large city. Journal of Applied Meteorology, Volume 40, pp. 169–82.

Musco, Francesco (Editor) 2015. Counteracting Urban Heat Island Effects in a Global Climate Change Scenario. Springer, pp. 295.

Ng, W. Y., Chau, C. K. 2011. Evaluation of the role of vegetation on the air quality in high dense urban areas. 14th Conference on Harmonization within Atmospheric Dispersion Modeling for Regulatory Purposes, 2-6 October, Kos, Greece.

NOAA, National Severe Storms Laboratory (NSSL): http://www.nssl.noaa.gov/. Last accessed on 04.07.2014.

Nowak, D. J. 2002. The effects of urban trees on air quality. USDA Forest Service, Syracuse, NY.

Nowak, D. J., Crane, D. E., Stevens, J. C. 2006. Air pollution removal by urban trees and shrubs in the United States. Urban Forestry and Urban Greening, Volume 4, pp. 11 5-123.

Nunez, M., Oke, T. R. 1977. The energy balance of an urban canyon. Journal of Applied Meteorology, Volume 16, pp. 11–19.

Oke, T. R. 1969. Towards a more rational understanding of the urban heat island. McGill University Climatological Bulletin, Volume 5, pp. 1-20.

Oke, T. R. 1973. City size and the urban heat island. Atmospheric Environment, Pergamon Press, Volume 7, Issue 8, pp. 769-77.

Oke, T. R. 1981. Canyon geometry and the nocturnal urban heat island comparison of scale model and field observations. Journal of Climatology, Volume 1, pp. 237–54.

Oke, T. R. 1981. Canyon Geometry and the nocturnal urban heat island: Comparison of scale model and field observations. Journal of Climatology, Volume 1, pp. 237-254.

Oke, T. R. 1982. The energetic basis of the urban heat island. Quarterly Journal of the Royal Meteorological Society, Volume 108, Issue 455, pp. 1-24.

Oke, T. R. 1987. Boundary layer climates. Methuen & Co. Ltd, USA.

Oke, T. R. 1989. The micrometeorology of the urban forest. Philosophical Transactions of the Royal Society of London, Series B, Volume 324, Issue 1223, pp.335-349.

Oke, T. R., Maxwell, G.B. 1975. Urban heat island dynamics in Montreal and Vancouver. Atmospheric Environment, Volume 9, Issue 2, pp. 191-200.

Oliviera, S., Andrade, H., Vaz, T. 2011. The cooling effect of urban green spaces as a contribution to mitigating urban heat: A case study in Lisbon. Building and Environment, Volume 46, Issue 11, pp. 2186-2194.

ONSET: http://www.onsetcomp.com/products/software. Last accessed on 04.07.2014.

Pandit, R., Laband, N. 2010. Energy savings from tree shade. Ecological Economics, Volume 69, pp. 1324–1329.

Pearlmuttera, D., Berlinera, P., Shaviv, E. 2005. Evaluation of Urban Surface Energy Fluxes Using an Open-Air Scale Model. Journal of Applied Meteorology and Climatology, Volume 44, Issue 4, pp. 532–545.

Piety, C. 2007. The relationship between urban tree cover and ground level ozone. Appendix G-13 to the Cecil County, Maryland 8-hour ozone State Implementation Plan.

Piringer, M., Grimmond, C. S. B., Joffre, S. M., Mestayer, P., Middleton, D. R., Rotach, M. W., Baklanov, A., De Ridder, K., Ferreira. J., Guilloteau, E., Karppinen, A., Martilli, A., Masson, V., Tombrou, M. 2002. Investigating the Surface Energy Balance in Urban Areas – Recent Advances and Future Needs. Water, Air and Soil Pollution: Focus, Volume 2, Issue 5-6, pp. 1-16.

QGIS: http://www.qgis.org/en/site/. Last accessed on 12/11/2014.

Ratti, C., Richens, P. 1999. Urban Texture Analysis with Image Processing Techniques. Proceedings CAADFutures99, Atlanta, GA.

Rawlings, J. O., Pantula, S. G., Dickey, D. A. 1998. Applied Regression Analysis: A Research Tool. New York, Springer, Second Edition, 1998.

Richens, P. 1997. Image processing for urban scale environmental modelling. 5th International IBPSA Conference: Building Simulation 97, Prague.

Rosenthal, J. K. 2010. Evaluating the impact of the urban heat island on public health: Spatial and social determinants of heat-related mortality in New York City. Dissertation. Columbia University.

Saaroni, H., Ben-Dor, E., Bitan, A., Potchter, A. 2000. Spatial distribution and microscale characteristics of the urban heat island in Tel-Aviv, Israel. Landscape and Urban Planning, Volume 48, Issues 1–2, pp. 1–18.

Sailor, D. J., Lu, L. 2004. A top–down methodology for developing diurnal and seasonal anthropogenic heating profiles for urban areas. Atmospheric Environment, Volume 38, pp. 2737–2748.

Sailor, D.J. 2006. Mitigation of Urban Heat Islands - Recent Progress and Future Prospects. Portland State University.

Şen, Z., Altunkaynak, A., Erdik, T. 2012. Wind Velocity Vertical Extrapolation by Extended Power Law. Advances in Meteorology, Volume 2012, pp. 6.

Shahmohamadi, P., Che-Ani, A.I., Maulud, K.N.A., Tawil, N.M., Abdullah, N.A.G. 2011. The Impact of Anthropogenic Heat on Formation of Urban Heat Island and Energy Consumption Balance. Urban Studies Research, Volume 2011, 9 pages.

Shishegar, N. 2013. Street Design and Urban Microclimate: Analysing the Effects of Street Geometry and Orientation on Airflow and Solar Access in Urban Canyons. Journal of Clean Energy Technologies, Volume 1, Issue 1, pp. 52-56.

Skelhorn, C., Lindley, S., Levermore, G. 2012. Development of a GIS Data Model for Urban Microclimate and Building Energy Estimations. GIS Research UK 20th Annual Conference, University of Lancaster, 11-13 April, pp. 325-329.

Smith, C., Lindley, S., Levermore, G. 2009. Estimating spatial and temporal patterns of urban anthropogenic heat fluxes for UK cities: the case of Manchester. Theoretical and Applied Climatology, Volume 98, Issue 1-2, pp. 19-35.

Spronken-Smith, R. A., Oke, T. R. 1998. The thermal regime of urban parks in two cities with different summer climates. International Journal of Remote Sensing, Volume 19, pp. 2085-2104.

Statistics Austria: http://www.statistik.at/web_en/. Last accessed on 07.07.2014.

Stewart, I. D. 2011. Redefining the urban heat island. Dissertation, University of British Columbia.

Stewart, I. D., Oke T. R. 2012. Local Climate Zones for Urban Temperature Studies. Bulletin of the American Meteorological Society, Volume 93, pp. 1879–1900.

Steyn, D. G. 1980. The calculation of view-factors from fisheye-lens photographs: Research note. Atmosphere-Ocean, Volume 18, Issue 3, pp. 254-258.

Sugawara, H., Narita, K. 2009. Roughness length for heat over an urban canopy. Theoretical and Applied Climatology, Volume 95, pp. 291–299.

Syrakova, M., Stefanova, M. 2009. Homogenization of Bulgarian temperature series. International Journal of Climatology, Volume 29, pp. 1835–1849.

Szegedi, S., Kircsi, A. 2003. Effects of the synoptic conditions on the development of the urban heat island in Debrecen, Hungary. Acta Climatologica et Chorologica, Volume 36-37, pp. 111-120.

Szymanowski, M., Kryza, M. 2012. Local regression models for spatial interpolation of urban heat island—an example from Wroclaw, SW Poland. Theoretical and Applied Climatology, Volume 108, pp. 53-71.

Taha, H., Akbari, H., Rosenfeld, A. 1988. Residential Cooling Loads and the Urban Heat Island: the Effects of Albedo. Building and Environment, Volume 23, Issue 4, pp. 271-283.

Taha, H. 1997. Urban climates and heat islands: albedo, evapotranspiration, and anthropogenic heat. Energy and Buildings, Volume 25, pp. 99-103.

Taha, H., Sailor, D.J., Akbari, H. 1992. High-albedo materials for reducing building cooling energy use. Technical Report, California Institute for Energy Efficiency, Berkeley, CA, United States.

Tomlinson, C. J., Chapman, L., Thornes, J. E., Baker, C. J. 2011. Including the urban heat island in spatial heat health risk assessment strategies: a case study for Birmingham, UK. International Journal of Health Geographics, Volume 10, pp. 42.

Unger, J., Bottyan, Z., Sumeghy, Z., Gulyas, A. 2000. Urban heat island development affected by urban surface factors. Quarterly Journal of the Hungarian Meteorological Service, Volume 104, Issue 4, pp. 253-268.

Urban, A., Kyselý, J. 2014. Comparison of UTCI with Other Thermal Indices in the Assessment of Heat and Cold Effects on Cardiovascular Mortality in the Czech Republic. International Journal of Environmental Research and Public Health 2014, Volume 11, pp. 952-967.

Van Hove, L. W . A., Steeneveld, G. J., Jacobs, C. M. J., Heusinkveld, B. G., Elbers, J. A., Moors, E. J., Holtslag, A. A. M. 2011. Exploring the urban heat island intensity of Dutch cities. City Weathers: Meteorology and Urban Design, 1950-2010, Manchester.

Vonkilch, A. 2009. Energieausweis in der Praxis: Technische und rechtliche Umsetzung in Österreich. ÖVI-Immobilien-Akademie, pp. 290.

Voogt, J. A., Oke, T. 1997. Complete urban surface temperatures. Journal of Applied Meteorology, Volume 36, pp. 1117-1132.

Voogt, J. A. 2002. Urban Heat Island. Encyclopedia of Global Environmental Change. Volume 3, pp. 660-666.

Voogt, J. A., Oke, T. 2003. Thermal remote sensing of urban climates. Remote Sensing of Environment, Volume 86, pp. 370–384.

Voogt, J. A. 2004. Urban heat islands: Hotter cities. ActionBioscience, http://www.actionbioscience.org/environment/voogt.html

Vuckovic, M., Kiesel, K., Mahdavi, A. 2014. The sources and implications of urban climate variance in Vienna. 3rd International Conference on Countermeasures to Urban Heat Island, Venice, Italy, October 13-15.

Wilby, R. L. 2008. Constructing climate change scenarios of urban heat island intensity and air quality. Environment and Planning B: Planning and Design, Volume 35, Issue 5, pp. 902 – 919.

Wilby, R. L., Jones, P. D., Lister, D. H. 2011. Decadal variations in the nocturnal heat island of London. Weather, Volume 66, Issue 3, pp. 59-64.

WHO 2007. Improving Public Health Responses to Extreme Weather/Heat-Waves – EuroHEAT. World Meteorological Organization, Meeting Report, Bonn, Germany, 22-23 March.

WMO 2008. Guide to Meteorological Instruments and Methods of Observation. World Meteorological Organization, Seventh edition, WMO-No. 8, Geneva, pp. 681.

WMO 2011. Guide to Climatological Practices. World Meteorological Organization, WMO-No.100, Geneva, pp. 117.

Yow, D. M., Carbone, G. J. 2006. The Urban Heat Island and Local Temperature Variations in Orlando, Florida. South-eastern Geographer, Volume 46, Number 2, pp. 297-321.

Zhao, X., Wang, K., Qiu, Q., Ye, H. 2010. Analysis of Urban Heat Island Seasonal Dynamics Using Landscape Metrics. 2010 Second IITA International Conference on Geoscience and Remote Sensing, pp. 72-75.

6.2. Project related publications

Dimitrova, B., Vuckovic, M., Kiesel, K., Mahdavi, A. 2014. Trees and the microclimate of the urban canyon: A case study, 2nd ICAUD International Conference in Architecture and Urban Design. Epoka University, Tirana, Albania, May 8-10.

Glawischnig, S., Kiesel, K., Mahdavi, A. 2014a. Feasibility analysis of open-government data for the automated calculation of the micro-climatic attributes of Urban Units of Observation in the city of Vienna. 2nd ICAUD International Conference in Architecture and Urban Design, Epoka University, Tirana, Albania, May 08-10.

Glawischnig, S., Hammerberg, K., Vuckovic, M., Kiesel, K., Mahdavi, A. 2014b. A case study of geometry-based automated calculation of microclimatic attributes. 10th European Conference on Product and Process Modelling, Vienna, Austria, September 17-19.

Lim, S. J., Vuckovic, M., Kiesel, K., Mahdavi, A. 2014. The variance of the urban microclimate in the city of Vienna, Austria. 2nd ICAUD International Conference in Architecture and Urban Design, Epoka University, Tirana, Albania, May 8-10.

Kiesel, K., Orehounig, K., Shoshtari, S., Mahdavi, A. 2012. Urban heat island phenomenon in Central Europe. 1st International Conference on Architecture & Urban Design, Epoka University, Tirana, Albania, April 19-21.

Kiesel, K., Vuckovic, M., Orehounig, K., Mahdavi, A. 2012. Analysis of micro climatic variations and the urban heat island phenomenon in the city of Vienna. EURA, Urban Europe – Challenges to Meet the Urban Future, Vienna, Austria, September 20-22.

Kiesel, K., Vuckovic, M., Mahdavi, A. 2013. Representation of weather conditions in building performance simulation: a case study of microclimatic variance in Central Europe. 13th Conference of International Building Performance Simulation Association, Chambéry, France, August 26-28.

Kiesel, K., Vuckovic, M., Mahdavi, A. 2013. The extent and implications of the urban heat island phenomenon in Central European region. CESBP, 2nd Central European Symposium on Building Physics, Vienna, Austria, September 9-11.

Maleki, A., Orehounig, K., Mahdavi, A. 2012. Monitoring and modeling of the urban micro-climate. 1st International Conference on Architecture & Urban Design, Epoka University, Tirana, Albania, April 19-21.

Mahdavi, A., Kiesel, K., Vuckovic, M. 2013. A framework for the evaluation of urban heat island mitigation measures. sb13 munich, Implementing Sustainability - Barriers and Chances, München, Deutschland, April 24-26.

Mahdavi, A., Kiesel, K., Vuckovic, M. 2014a. Empirical and computational assessment of the urban heat island phenomenon and related mitigation measures. NSB 2014, 10th Nordic Symposium on Building Physics, Lund, Sweden, June 15-19.

Maleki, A., Kiesel, K., Vuckovic, M., Mahdavi, A. 2014. Empirical and Computational Issues of Microclimate Simulation. ICT EurAsia 2014, Bali, Indonesia, April 14 – 17.

Mahdavi, A., Kiesel, K., Vuckovic, M. 2014b. Empirical and computational assessment of the urban heat island phenomenon and related mitigation measures. Geographia Polonica, Volume 87, Issue 4, pp. 505-516.

Orehounig, K., Kiesel, K., Mahdavi, A. 2012. Derivation of locally adjusted high-resolution weather information for building performance simulation. BauSIM 2012, Berlin, Deutschland, September 26-28.

Springer 2015. Counteracting Urban Heat Island Effects in a Global Climate Change Scenario. Springer, 2015, to be published, pp. 295.

Vuckovic, M., Kiesel, K., Mahdavi, A. 2014. The sources and implications of urban climate variance in Vienna. 3rd International Conference on Countermeasures to Urban Heat Island, Venice, Italy, October 13-15.

6.3. Tables

6.4. Figures

6.5. Equations

7. Appendix

7.1. Further results

7.1.1. Seasonal variation

Following figures illustrate the seasonal cumulative frequency distribution of UHI intensity for a one week period.
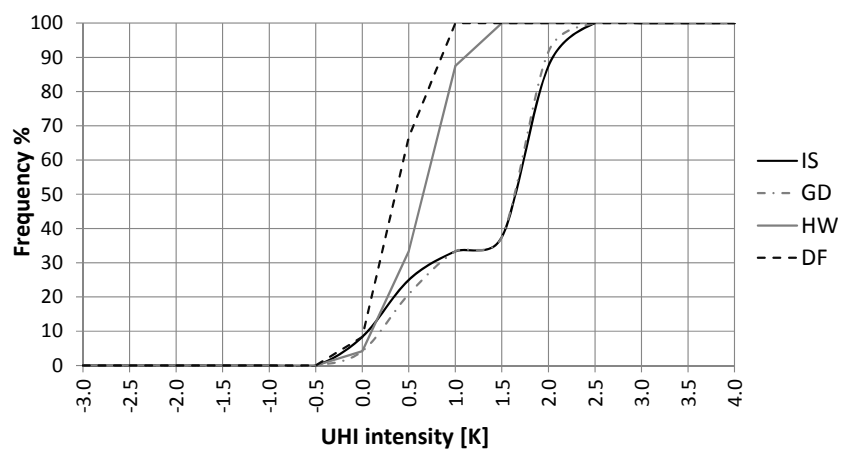
Figure A1. Cumulative frequency distribution of UHI intensity for a one week winter period
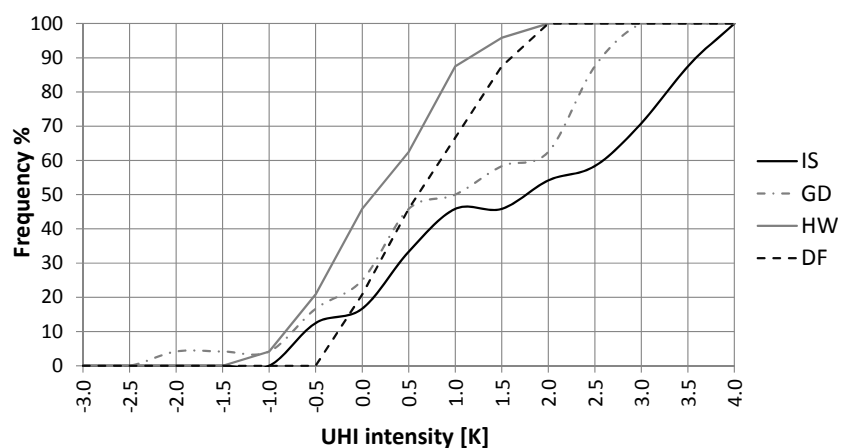
Figure A2. Cumulative frequency distribution of UHI intensity for a one week spring period
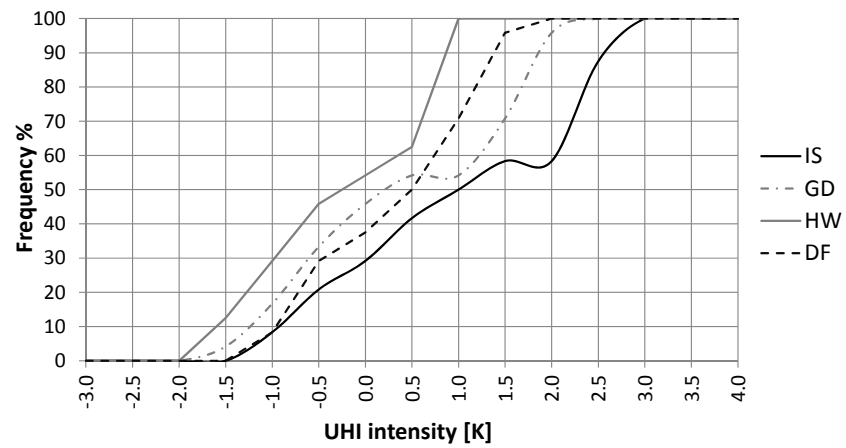
Figure A3. Cumulative frequency distribution of UHI intensity for a one week summer period
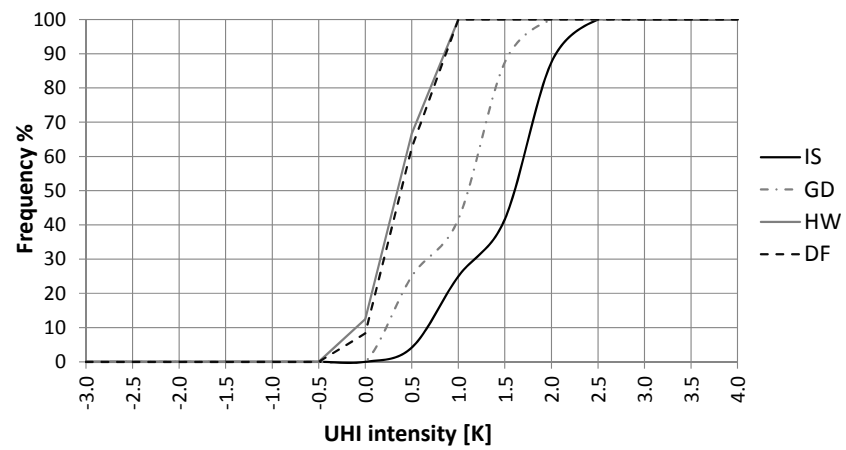
Figure A4. Cumulative frequency distribution of UHI intensity for a one week autumn period

7.1.2. Geometric features

Following tables provide a concise summary of derived geometric variables and respective input data for all study areas.

Table A1. Summary of the geometric properties for U2O Innere Stadt

GEOMETRIC PROPERTIES	VALUE	UNIT
Sky View Factor	0.47	-
Aspect ratio	1.63	-
Built area fraction	0.41	-
Building plan area	472586.30	m²
Total ground area	1150996.00	m²
Unbuilt area fraction	0.59	-
Unbuilt ground area	678409.70	m²
Impervious surface fraction	0.45	-
Impervious surface area	520537.94	m²
Pervious surface fraction	0.14	-
Pervious surface area	157871.76	m²
Bare soil fraction	0.00	-
Bare soil area	0.00	m²
Green area fraction	0.14	-
Green area	156109.59	m²
Water bodies fraction	0.00	-
Water bodies area	1762.17	m²
Equivalent building height	9.18	m
Built volume	10562303.73	m³
Built surface fraction	3.85	-
Total built surface area	1820844.32	m²
Wall fraction	2.85	-
Total wall area	1348258.03	m²
Roof fraction	1.00	-
Total roof area	472586.30	m²
Impervious roof fraction	0.99	-
Total impervious roof	470030.30	m²
Pervious roofs fraction	0.01	-
Total pervious roof area	2556.00	m²
Effective mean compactness	4.23	m
Mean sea level	169	m

Table A2. Summary of the geometric properties for U2O Gaudenzdorf

GEOMETRIC PROPERTIES	VALUE	UNIT
Sky View Factor	0.51	-
Aspect ratio	1.54	-
Built area fraction	0.40	-
Building plan area	662861.89	m²
Total ground area	1645954.00	m²
Unbuilt area fraction	0.60	-
Unbuilt ground area	983092.11	m²
Impervious surface fraction	0.46	-
Impervious surface area	752902.15	m²
Pervious surface fraction	0.14	-
Pervious surface area	230189.96	m²
Bare soil fraction	0.00	-
Bare soil area	0.00	m²
Green area fraction	0.14	-
Green area	223316.45	m²
Water bodies fraction	0.00	-
Water bodies area	6873.50	m²
Equivalent building height	5.46	m
Built volume	8988407.18	m³
Built surface fraction	3.46	-
Total built surface area	2293829.57	m²
Wall fraction	2.46	-
Total wall area	1630967.68	m²
Roof fraction	1.00	-
Total roof area	662861.89	m²
Impervious roof fraction	0.99	-
Total impervious roof	655557.95	m²
Pervious roofs fraction	0.01	-
Total pervious roof area	7303.94	m²
Effective mean compactness	2.74	m
Mean sea level	177	m

Table A3. Summary of the geometric properties for U2O Hohe Warte

GEOMETRIC PROPERTIES	VALUE	UNIT
Sky View Factor	0.59	-
Aspect ratio	0.92	-
Built area fraction	0.18	-
Building plan area	397306.43	m^2
Total ground area	2230367.00	m^2
Unbuilt area fraction	0.82	-
Unbuilt ground area	1833060.57	m^2
Impervious surface fraction	0.34	-
Impervious surface area	763186.98	m^2
Pervious surface fraction	0.48	-
Pervious surface area	1069873.59	m^2
Bare soil fraction	0.00	-
Bare soil area	0.00	m^2
Green area fraction	0.48	-
Green area	1064634.46	m^2
Water bodies fraction	0.00	-
Water bodies area	5239.13	m^2
Equivalent building height	1.43	m
Built volume	3178451.40	m^3
Built surface fraction	3.04	-
Total built surface area	1206987.10	m^2
Wall fraction	2.04	-
Total wall area	809680.68	m^2
Roof fraction	1.00	-
Total roof area	397306.43	m^2
Impervious roof fraction	0.99	-
Total impervious roof	393907.91	m^2
Pervious roofs fraction	0.01	-
Total pervious roof area	3398.52	m^2
Effective mean compactness	1.05	m
Mean sea level	202	m

Table A4. Summary of the geometric properties for U2O Donaufeld

GEOMETRIC PROPERTIES	VALUE	UNIT
Sky View Factor	0.75	-
Aspect ratio	0.73	-
Built area fraction	0.20	-
Building plan area	397887.49	m^2
Total ground area	2032309.00	m^2
Unbuilt area fraction	0.80	-
Unbuilt ground area	1634421.51	m^2
Impervious surface fraction	0.31	-
Impervious surface area	633956.44	m^2
Pervious surface fraction	0.49	-
Pervious surface area	1000465.07	m^2
Bare soil fraction	0.04	-
Bare soil area	82859.27	m^2
Green area fraction	0.45	-
Green area	913293.24	m^2
Water bodies fraction	0.00	-
Water bodies area	4312.56	m^2
Equivalent building height	1.20	m
Built volume	2447008.05	m^3
Built surface fraction	2.74	-
Total built surface area	1090381.83	m^2
Wall fraction	1.74	-
Total wall area	692494.34	m^2
Roof fraction	1.00	-
Total roof area	397887.49	m^2
Impervious roof fraction	1.00	-
Total impervious roof	396978.77	m^2
Pervious roofs fraction	0.00	-
Total pervious roof area	908.72	m^2
Effective mean compactness	0.72	m
Mean sea level	160	m

Table A5. Summary of the geometric properties for U2O Seibersdorf

GEOMETRIC PROPERTIES	VALUE	UNIT
Sky View Factor	0.87	-
Aspect ratio	0.28	-
Built area fraction	0.08	-
Building plan area	37139.74	m^2
Total ground area	439268.93	m^2
Unbuilt area fraction	0.92	-
Unbuilt ground area	402129.19	m^2
Impervious surface fraction	0.09	-
Impervious surface area	38121.82	m^2
Pervious surface fraction	0.83	-
Pervious surface area	364007.37	m^2
Bare soil fraction	0.00	-
Bare soil area	1256.00	m^2
Green area fraction	0.83	-
Green area	362751.37	m^2
Water bodies fraction	0.00	-
Water bodies area	0.00	m^2
Equivalent building height	0.45	m
Built volume	196840.62	m^3
Built surface fraction	2.04	-
Total built surface area	75640.99	m^2
Wall fraction	1.04	-
Total wall area	38501.25	m^2
Roof fraction	1.00	-
Total roof area	37139.74	m^2
Impervious roof fraction	1.00	-
Total impervious roof	37139.74	m^2
Pervious roofs fraction	0.00	-
Total pervious roof area	0.00	m^2
Effective mean compactness	0.41	m
Mean sea level	182	m

7.1.3. Correlation analysis

Following table provides a concise summary of derived linear equations pertaining to the individual correlations between U2O variables and respective CTIs, along with R-square values.

Table A6. Summary of seasonal linear equations

PROPERTY	EQUATION	R^2
Sky View Factor		
WINTER	y = -98.27x + 91.22	0.89
SPRING	y = -115.27x + 105.61	0.95
SUMMER	y = -50.92x + 46.17	0.64
AUTUMN	y = -70.94x + 60.27	0.78
Aspect Ratio		
WINTER	y = 24.45x − 7.23	0.99
SPRING	y = 25.79x − 6.92	0.86
SUMMER	y = 16.93x − 3.59	0.81
AUTUMN	y = 22.83x − 8.28	0.91
Built Area Fraction		
WINTER	y = 93.77x − 6.13	0.96
SPRING	y = 102.88x − 6.77	0.90
SUMMER	y = 67.80x − 3.56	0.85
AUTUMN	y = 90.00x − 7.87	0.93
Unbuilt Area Fraction		
WINTER	y = -93.77x + 6.13	0.96
SPRING	y = -102.88x + 6.77	0.90
SUMMER	y = -67.80x + 3.56	0.85
AUTUMN	y = -90.00x + 7.87	0.93
Impervious Surface Fraction		
WINTER	y = 87.45x − 11.10	0.89
SPRING	y = 91.74x − 10.83	0.76
SUMMER	y = 61.76x − 6.66	0.75
AUTUMN	y = 77.68x − 10.58	0.74
Pervious Surface Fraction		
WINTER	y = -47.47x + 37.46	0.97
SPRING	y = -50.98x + 40.60	0.87
SUMMER	y = -33.95x + 27.81	0.84
AUTUMN	y = -43.90x + 33.27	0.88
Equivalent building height		
WINTER	y = 3.32x + 5.93	0.78
SPRING	y = 3.99x + 5.24	0.88
SUMMER	y = 2.60x + 4.46	0.82
AUTUMN	y = 3.58x + 2.32	0.96
Built Surface Fraction		
WINTER	y = 19.28x − 40.62	0.93
SPRING	y = 21.12x − 44.50	0.86
SUMMER	y = 13.99x − 28.66	0.83
AUTUMN	y = 18.47x − 40.86	0.90

PROPERTY	EQUATION	R^2
Effective mean compactness		
WINTER	y = 7.80x + 3.44	0.82
SPRING	y = 9.11x + 2.73	0.87
SUMMER	y = 5.92x + 2.86	0.80
AUTUMN	y = 8.22x - 0.03	0.96
Albedo		
WINTER	y = -199.67x + 61.63	0.82
SPRING	y = -233.66x + 70.79	0.87
SUMMER	y = -158.72x + 48.60	0.87
AUTUMN	y = -194.95x + 57.90	0.82

7.1.4. Predictive model

Table A7. Input data for the MATLAB® model – U2O variables representing winter and spring – Xw (for locations IS, GD, HW, DF, R)

	ψ_{sky}	HW	ISF	PSF	h_e	l_c	BSF	α_{sw}
1	0.56	1.63	0.45	0.14	9.18	4.23	3.85	0.15
1	0.67	1.54	0.46	0.14	5.46	2.74	3.46	0.19
1	0.80	0.92	0.34	0.48	1.43	1.05	3.04	0.22
1	0.81	0.73	0.31	0.49	1.20	0.72	2.74	0.22
1	0.90	0.28	0.09	0.83	0.45	0.41	2.04	0.32

Table A8. Input data for the MATLAB® model – U2O variables representing summer and autumn – Xsu (for locations IS, GD, HW, DF, R)

	ψ_{sky}	HW	ISF	PSF	h_e	l_c	BSF	α_{sw}
1	0.47	1.63	0.45	0.14	9.18	4.23	3.85	0.15
1	0.51	1.54	0.46	0.14	5.46	2.74	3.46	0.19
1	0.59	0.92	0.34	0.48	1.43	1.05	3.04	0.22
1	0.75	0.73	0.31	0.49	1.20	0.72	2.74	0.22
1	0.87	0.28	0.09	0.83	0.45	0.41	2.04	0.32

Table A9. Input data for the MATLAB® model – CTI values – CTI

	IS	GD	HW	DF	R
winter	31.31	32.10	15.22	9.90	0.00
spring	40.75	27.97	10.01	18.21	0.00
summer	27.76	18.82	7.13	14.70	0.00
autumn	33.98	23.40	8.20	9.47	0.00

Table A10. Input data for the MATLAB® model – U2O variables representing winter and spring – AKH_w (for location AKH)

	ψ_{sky}	HW	ISF	PSF	h_e	l_c	BSF	α_{sw}
1	0.61	1.20	0.44	0.15	5.54	2.89	3.24	0.19

Table A11. Input data for the MATLAB® model – U2O variables representing summer and autumn – AKH_su (for location AKH)

	ψ_{sky}	HW	ISF	PSF	h_e	l_c	BSF	α_{sw}
1	0.49	1.20	0.44	0.15	5.54	2.89	3.24	0.19

Following code represents the least square model developed with MATLAB® software.

```matlab
load DATA

l_w = lsqr(Xw,CTI(:,1),[],100);
l_sp = lsqr(Xw,CTI(:,2),[],100);
l_su = lsqr(Xsu,CTI(:,3),[],100);
l_a = lsqr(Xsu,CTI(:,4),[],100);

lsqr = [l_w l_sp l_su l_a];
Eq = zeros(5,4);
Eq_AKH = zeros(1,4);
R2 = zeros(1,16);
c = 0;

for k = lsqr(:,1:2);
    c = c+1;
    Eq(:,c) = k(1)+k(2).*Xw(:,2)+k(3).*Xw(:,3)+k(4).*Xw(:,4)+k(5).*Xw(:,5)+k(6).*Xw(:,↙
6)+k(7).*Xw(:,7)+k(8).*Xw(:,8)+k(9).*Xw(:,9);
    Eq_AKH(:,c) = k(1)+k(2).*AKH_w(:,2)+k(3).*AKH_w(:,3)+k(4).*AKH_w(:,4)+k(5).*AKH_w↙
(:,5)+k(6).*AKH_w(:,6)+k(7).*AKH_w(:,7)+k(8).*AKH_w(:,8)+k(9).*AKH_w(:,9);
end

for l = lsqr(:,3:4);
    c = c+1;
    Eq(:,c) = l(1)+l(2).*Xsu(:,2)+l(3).*Xsu(:,3)+l(4).*Xsu(:,4)+l(5).*Xsu(:,5)+l(6).↙
*Xsu(:,6)+l(7).*Xsu(:,7)+l(8).*Xsu(:,8)+l(9).*Xsu(:,9);
    Eq_AKH(:,c) = l(1)+l(2).*AKH_su(:,2)+l(3).*AKH_su(:,3)+l(4).*AKH_su(:,4)+l(5).↙
*AKH_su(:,5)+l(6).*AKH_su(:,6)+l(7).*AKH_su(:,7)+l(8).*AKH_su(:,8)+l(9).*AKH_su(:,9);
end

display(CTI)
display(Eq)
display(Eq_AKH)

for i = Eq(:,1:4);
    for m = CTI(:,1:4);
        c = c+1;
        R = corrcoef(i,m);
        R2(:,c) = R(1,2)^2;
    end
end

R2_Eq_CTI = [R2(1,5) R2(1,10) R2(1,15) R2(1,20)]

RMSE1 = sqrt(sum((CTI(:,1)-Eq(:,1)).^2)/numel(CTI(:,1)));
RMSE2 = sqrt(sum((CTI(:,2)-Eq(:,2)).^2)/numel(CTI(:,1)));
RMSE3 = sqrt(sum((CTI(:,3)-Eq(:,3)).^2)/numel(CTI(:,1)));
RMSE4 = sqrt(sum((CTI(:,4)-Eq(:,4)).^2)/numel(CTI(:,1)));

RMSE = [RMSE1 RMSE2 RMSE3 RMSE4]

plot(CTI(:,1),Eq(:,1),'ks','MarkerSize',4,'MarkerFaceColor','w')
hold on
plot(CTI(:,2),Eq(:,2),'m+','MarkerSize',4,'MarkerFaceColor','w')
plot(CTI(:,3),Eq(:,3),'gd','MarkerSize',4,'MarkerFaceColor','w')
plot(CTI(:,4),Eq(:,4),'ro','MarkerSize',4,'MarkerFaceColor','w')

xlabel('Eq')
ylabel('CTI[Kh]')

coeff = polyfit(CTI,Eq,1);
trendline = polyval(coeff,Eq);
hold on
plot(Eq,trendline,'-r');
```

Table A13. Summary of the geometric properties for U2O AKH

GEOMETRIC PROPERTIES	VALUE	UNIT
Sky View Factor	0.49	-
Aspect ratio	1.20	-
Built area fraction	0.41	-
Building plan area	631922.88	m^2
Total ground area	1539383.00	m^2
Unbuilt area fraction	0.59	-
Unbuilt ground area	907460.12	m^2
Impervious surface fraction	0.44	-
Impervious surface area	679269.68	m^2
Pervious surface fraction	0.15	-
Pervious surface area	228190.44	m^2
Bare soil fraction	0.00	-
Bare soil area	0.00	m^2
Green area fraction	0.15	-
Green area	227948.75	m^2
Water bodies fraction	0.00	-
Water bodies area	241.68	m^2
Equivalent building height	5.54	m
Built volume	8530958.87	m^3
Built surface fraction	3.24	-
Total built surface area	2049531.20	m^2
Wall fraction	2.24	-
Total wall area	1417608.32	m^2
Roof fraction	1.00	-
Total roof area	631922.88	m^2
Impervious roof fraction	0.99	-
Total impervious roof	626844.75	m^2
Pervious roofs fraction	0.01	-
Total pervious roof area	5078.13	m^2
Effective mean compactness	2.89	m
Mean sea level	195	m

MILENA VUCKOVIC

TUWIEN | Vienna, Austria | milena.vuckovic@tuwien.ac.at |

EDUCATION

- Faculty of Architecture, University of Belgrade, Serbia   2001-2007

- Reconstruction work of Local Architectural heritage, working practice in Syria, Al-Baath University in Homs   2005

- Phd candidate at Vienna University of Technology   since 2011

WORK EXPERIENCE

ARCO PROJECT
Belgrade, Serbia

- Architectural Assistant   2007-2011

Vienna University of Technology
Department for building physics and building ecology, Vienna, Austria

- Project Assistant - UHI   2012-2013
- University Assistant   2013-2014
- Project Assistant - UHI   2014-aug 2014
- Researcher   nov 2014 - present

RESEARCH AREAS

- Human Ecology, Building Ecology, Building Simulation, Environmental Design

- Urban Microclimate, Urban Heat Island

PARTICIPATION IN RESEARCH PROJECTS

- UHI (Central Europe / 3CE292P3)   2012-2014